RATIONAL DESIGN AND SYNTHESIS OF FUNCTIONAL POLYMERS WITH COMPLEX ARCHITECTURES BY LIVING/CONTROLLED POLYMERIZATION

A Dissertation
Presented to
The Academic Faculty

by

Chaowei Feng

In Partial Fulfillment
of the Requirements for the Degree
Doctor of Philosophy in the
School of Materials Science and Engineering

Georgia Institute of Technology
May, 2015

RATIONAL DESIGN AND SYNTHESIS OF FUNCTIONAL POLYMERS WITH COMPLEX ARCHITECTURES BY LIVING/CONTROLLED POLYMERIZATION

Approved by:

Dr. Zhiqun Lin, Advisor
School of Materials Science and Engineering
Georgia Institute of Technology

Dr. John Reynolds
School of Materials Science and Engineering
Georgia Institute of Technology

Dr. Anselm C. Griffin
School of Materials Science and Engineering
Georgia Institute of Technology

Dr. Vladimir V Tsukruk
Materials Science and Engineering
Georgia Institute of Technology

Dr. Seth Marder
School of Chemistry and Biochemistry
Georgia Institute of Technology

Date Approved: April 02, 2015

Dedicated to my loving family

ACKNOWLEDGEMENTS

I wish to thank my advisor Prof. Zhiqun Lin for his constant support, motivation, and generosity. His passion about science highly motivates me to conduct my research passionately through my Ph.D. He placed tremendous trust in me for generating ideas, solving problems, and accomplishing projects. I would also like to thank all my dissertation committees, Prof. Seth Marder, Prof. John Reynolds, Prof. Anselm Griffin, and Prof. Vladimir Tsukruk for their kind willingness to take part in my dissertation committee, and specially for providing me with valuable comments and feedbacks to guide me through my research and successfully achieve the thesis goal.

My PhD tenure has been a memorable one, only because of the congenial and supportive culture of the NanoFM research group. Particularly, I would like to thank Prof. Xinchang Pang and Dr. Lei Zhao for providing me with tremendous support and guidance on my research in the junior years. I would specially like to thank Yanjie He and Yijie Tao for being kind and supportive companions. I would also like to thank current and former NanoFM lab members, Prof. S. Li, Prof. Y. Yang, Prof. Y. Ren, Prof. H. Ma, Prof. R. Wu, Prof. D. Yang, Prof. S. Wu, Dr. M. He, Dr. X. Xin, Dr. W. Han, Dr. M. Ye, Dr. Y. Xu, Dr. S. Wannapop, C. Zhang, C. Wan, B. Li, J. Jung, C. Han, Y. Chen, X. Liu, B. Jiang, J. Iocozzia, Young J. Yoon, A. Song, Z. Wang, J. Findley, D. Gottschalk, M. Wang, H. Tang, H. Xu, D. Zheng, W. Liao, and N. Tipcompor for their constant help and support.

I am extremely grateful to my dear parent and family for their unconditional love and constant support, without whom I would not be here. Sincere gratitude goes to all my friends, Rui Ding, Liyi Li, Zhuo Li, Hongzhi Wang, Siyuan Zhang, Zhishuai Geng, Xin Dong, and Pan Zhang for their mental support over the years.

TABLE OF CONTENTS

LIST OF TABLES

Page

LIST OF FIGURES AND SCHEMES

LIST OF SYMBOLS AND ABBREVIATIONS

CRP	Controlled radical polymerization
ATRP	Atom transfer radical polymerization
RAFT	Reversible addition–fragmentation chain transfer polymerization
NMP	Nitroxide-mediated polymerization
ROP	Ring opening polymerization
ROMP	Ring opening metathesis polymerization
GRIM	Grignard metathesis method
NMR	Nuclear Magnetic Resonance
GPC	Gel Permeation Chromatography
FT-IR	Fourier Transform Infrared Spectroscopy
AFM	Atomic Force Microscope
TEM	Transmission Electron Microscopy
MALDI-TOF	Matrix-Assisted Laser Desorption/Ionization – Time of Flight
DLS	Dynamic Light Scattering
UV-Vis	UV−Vis Spectrophotometer
PL	Photoluminescence Spectroscopy
PCL	Polycaprolactone
ε-CL	ε-Caprolactone
$Sn(Oct)_2$	Stannous octoate
RuO_4	Ruthenium (VIII) oxide
DMF	N,N-dimethylformamide
TC	2-(dodecylthiocarbonothioylthio)-2-methylpropionic acid
P(S-Cl)	Poly(4-chloromethyl styrene)

P(S-N_3)	Poly(4-(azidemethyl)styrene)
RhB	Rhodamine B
TMSPMA	3-(trimethoxysilyl)-propyl methacrylate
PTMSPMA	Poly(3-(trimethoxysilyl)-propyl methacrylate)
PMDETA	*N,N,N′,N″,N″*-pentamethyldiethylene triamine
β-CD	β-cyclodextrin
St.	Styrene
PS	Polystyrene
DCM	Dichloromethane
21 Br-β-CD	Heptakis[2,3,6-tri-O-(2-bromo-2-methylpropionyl]-β-cyclodextrin)
NMP	1-Methyl-2-pyrrolidone
TsOH	*p*-toluene sulfonic acid
KOH	Potassium hydroxide
TsCl	*p*-toluenesulfonyl chloride
EEGE	2,3-epoxypropyl-1-ethoxyethyl ether
PEEGE	Poly(2,3-epoxypropyl-1-ethoxyethyl ether)
DPMNa	Diphenylmethyl sodium
P3HT	Poly(3-hexylthiophene)
DPMNa	Diphenylmethyl sodium
Ni(dppp)Cl_2	[1,3-bis(diphenylphosphino)propane]dichloronickel-(II), ethynylmagnesium bromide

SUMMARY

Significant progress has been made in the field of living/controlled polymerizations over the past decades. The advance in living/controlled polymerizations has enabled the design and tailoring of structurally well-defined macromolecules with complex architectures. Polymers with complex molecular architectures often exhibit properties that are distinct from their linear counterparts. This dissertation aims to exploit the unique properties of rationally designed complex polymer structures to ***address the challenges*** related to the preparation of polymeric and hybrid nanostructures, as well as to ***explore and fundamentally understand*** the morphology or properties of new macromolecular architecture.

The studies presented in this dissertation addressed the challenges (e.g., poor size uniformity, limited accessible compositions) in the formation of polymeric or hybrid nanostructured materials based on the self-assembled polymer micelle approach via rational design of complex spherical star polymer architectures with tailor-made compositions and functionalities through living/controlled polymerizations, as well as investigated the morphology and self-assembly behavior of a newly designed cyclic brush copolymer grafted with P3HT as the side chains. Specifically, the uniqueness of this study can be summarized through the following novel and critical findings:

1. Uniform core-shell polymer nanoparticles can be formed by photo-crosslinking the shell layer of a monodisperse core-shell star block copolymer with azide moieties attached in the shell block. The dimensions of nanoparticles including the core size and the overall diameter are governed by the molecular weights of constituent blocks (i.e. inner and shell block) in the core-shell star diblock copolymer template.

2. Uniform hollow polymer nanoparticles with retained structural integrity can be produced by etching the degradable inner core of the unimolecular shell-crosslinked nanoparticles.

3. Organo-silica hybrid nanostructures can be crafted if the sol-gel chemistry of trimethylsilyl groups attached to the star polymer templates is employed as the crosslinking mechanism. Nanoparticles were yielded when the trimethylsilyl groups were incorporated in the inner block of star polymers, while nanocapsules with an interior cavity were produced when trimethylsilyl moieties were integrated in the shell block.

4. The novel cyclic brush copolymer composed of PEG as the backbone and P3HT as the side chains self-assembled into an interesting and unique macro-ring morphology in selective solvent.

The novel and robust star macromolecular templating strategy developed in this study will open the access to a wide range of structurally and functionally well-defined polymeric and hybrid nanostructured materials with tailor-made compositions and shapes. The findings presented in the work will provide fundamental insights or practical strategies for rational design of polymers with complex macromolecular architectures via living/controlled polymerizations.

CHAPTER 1

INTRODUCTION

1.1 Background

1.1.1. Recent Progress in Living/Controlled Polymerization

Anionic polymerization has been discovered as a living polymerization process about half a century ago by Szwarc.[1] Since its discovery, polymers with well-defined structure, chain end functionality[2-4] and narrow molecular weight distribution have been realized. Anionic polymerization proceeds with either carbanion or oxanion as reactive intermediate, and molecular weight of the macromolecules can be tuned by altering the feeding ratio of the monomer and the initiator concentration.[5,6] Anionic polymerization is a truly living process since the chain doesn't terminate without adding termination agent. It continues to grow when additional monomer is added. The living characteristics of anionic polymerization make it a sophisticated approach to construct well-defined polymer possessing complex macromolecular architecture.

Significant development and advance in living polymerization have been made in the last decade since the discovery of controlled free radical polymerization, particularly, Atomic Transfer Radical Polymerization (ATRP).[7] Except for anionic polymerization, molecular weight can also be precisely engineered and controlled by other living polymerization including controlled radical polymerization,[8] living ring opening polymerization of esters,[9-12] living polycondensation,[13] Ring Opening Metathesis Polymerization (ROMP),[14] etc. Clearly, narrow molecular weight distribution and well-defined structure can be achieved with living/controlled polymerization techniques.

The last decade has witnessed significant development in the field of controlled free radical polymerization or reversible-deactivation radical polymerization (RDRP)

since the discovery and understanding of ATRP. ATRP was first discovered by Matyjaszewski et al.[15] It was demonstrated to be a very successful controlled radical polymerization that is compatible with a variety of monomers to produce well defined polymers. After its discovery, enormous research has been done over the past decades in understanding the mechanism of ATRP,[16,17] the use of ATRP to produce polymer with complicated and sophisticated architecture, including star, bottlebrush polymers,[18-22] and industrialization of ATRP process by reducing the catalyst to true catalytic amount through the development of Initiators for Continuous Activator Regeneration (ICAR) and Activator ReGenerated by Electron Transfer (ARGET) ATRP[23-26] processes. More recently, Hawker *et al*. have pioneered a novel metal-free ATRP to overcome the metal catalyst contamination challenge encountered in traditional ATRP systems. The new polymerization process is catalyzed by organic-based photoredox catalysts and mediated via Ultraviolet (UV) light (**Figure 1.1**).[27] This newly developed metal-free ATRP process follows the first order polymerization kinetics. Polydispersity, molecular weights, and chain end functionalities of the resulting polymers can be elegantly controlled, which resemble the characteristics of traditional ATRP. Molecular weight increases linearly with respect to monomer conversion, and PDI of product remains low. The polymerization can be efficiently initiated or paused through "on−off" of UV light. In addition, chain end functionality is well preserved, which allows chain extension in sequential manner or combination with other living/controlled polymerizations to prepare block copolymers. Almost at the same time, another metal-free ATRP process with perylene as an organic photocatalyst, but mediated by visible light, was also discovered (**Figure 1.2**).[28] It was demonstrated that methyl methacrylate (MMA) and other functionalized vinyl monomers can be polymerized through this process, and block copolymer can also be produced by reinitiation. Significantly, polymer propagation can be controlled simply through pulsed visible-light sequences. These photo-mediated metal-free ATRP systems are free of metal contamination, easy to operate and purify, and

thus allow the fabrication of various functional materials, which will inspire more scientists and drive the field of living/controlled polymerizations to a new era. For example, almost immediately after the report of metal-free ATRP, a metal-free ring-opening metathesis polymerization (ROMP) process was also discovered by Boydston and co-workers.[29]

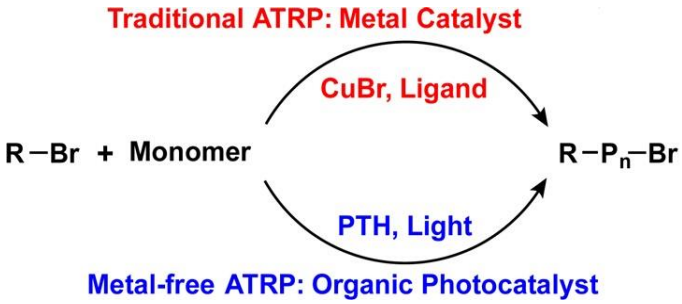

Figure 1.1. Mechanism of metal-free ATRP compared to traditional ATRP.[27]
Reprinted with permission from Ref. [27]. Copyright 2014, American Chemical Society.

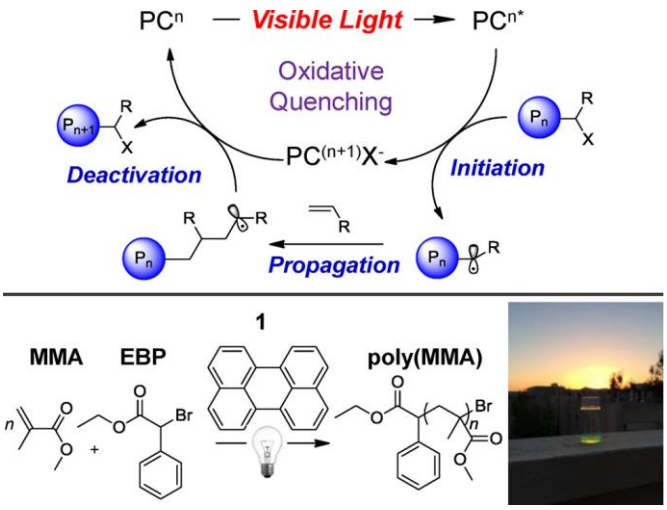

Figure 1.2. Proposed mechanism of visible-light mediated metal-free ATRP.[28]
Reprinted with permission from Ref. [28]. Copyright 2014, American Chemical Society.

In the meantime, other areas in living/controlled free radical polymerization have also achieved significant development. Reversible addition–fragmentation chain transfer (RAFT)[30-37] has been discovered as an even sophisticated process because of the high compatibility with a variety of functionalities, monomers, and ease of purification due to the absence of catalyst. Moreover, nitroxide-mediated polymerization (NMP)[8,38] has been developed and extended to be applicable to monomers, such as methyl methacrylate rather than only styrene and its derivatives by introducing new nitroxides mediating agent.

Controlled radical polymerization is not a true living process as chain terminating reactions, including the chain transfer and termination, are still present in the system.[39] However, these unfavorable termination reactions are minimized due to significant decrease in free radical concentration, as compared to traditional free radical polymerization, by introducing dormant species in fast exchange with reactive radical species. The fast dynamic exchange between propagating free radicals and various end-capped dormant species enables the apparent simultaneous growth of all polymer chains[8] and it is the art of controlled radical polymerizations. Halide-capped polymer chain serves as dormant species in ATRP and in RAFT dithioester-capped dormant chain is in fast dynamic exchange with propagating radicals. In NMP alkoxyamines is the dormant counterpart with free radicals.

In addition to controlled radical polymerization, significant advance has also been made in other fields of living/controlled polymerization, such as living ROMP and polycondensation. The development of living/controlled polymerization provides versatile tool to construct polymers with complex architectures.

1.1.2. Polymers with Complex Architectures

As shown in **Figure 1.3**, a variety of complex polymer topologies, including star-shaped,[40] bottlebrush-like and cyclic polymers, as well as other sophisticated structures synthesized by living/controlled polymerization techniques have been widely investigated.[41,42] Symmetrical/unsymmetrical star-shaped homopolymers, block copolymers and miktoarm star polymers have been designed and synthesized by a series of living polymerization techniques via either core-first method or arm-first approach.[22,43-46] In the arm-first method, linear monofunctional macromolecules are produced by living polymerization and subsequently cross-linked either by a difunctional comonomer during propagation[47] or by terminating with a multifunctional agent.[22,48] On the other hand, in the core-first approach,[49] star-like polymers are synthesized with a multifunctional initiator, and the resulting polymer possesses well-defined structure with number of arms being precisely controlled.

Bottlebrush-like polymers or cylindrical polymer brush[50,51] composed of a main polymer chain grafted with side chains along the backbone, and bottlebrush-like homo- and co-polymers with a large variety of chemical compositions have been prepared in the past decade via living/controlled polymerizations.[52-56] There are commonly three strategies documented in the literature for preparing bottlebrush-like copolymers. The first one is ‘‘grafting from’’ approach,[19,58] in which a linear multifunctional initiator with initiating sites along the backbone is utilized to initiate polymerization of a second monomer to result in the graft copolymers. The second one is ‘‘grafting onto’’[18] method. In this method, an end-functionalized polymer is grafted onto a linear functional macromolecule which bears reactive counterpart moieties along the chain. The last one is ‘‘grafting through” strategy.[57] A polymer chain or oligomer that has polymerizable functionality at chain end is used as macromonomer for homo-polymerization to form a bottlebrush copolymer or copolymerization with a second monomer to produce graft copolymers.

Cyclic polymers can be produced by intramolecular cyclization of either homotelechelic or heterotelechelic polymers[60] or ROMP of cyclic monomers.[61] The well-defined linear precursors are prepared by living polymerizations. Alternatively, cyclic brush copolymers can be synthesized by grafting side chains on cyclic backbone with functionalities. Notably, limited work has been reported on cyclic polymers due to their synthetic difficulty. Schappacher et al. reported successful synthesis of large macrocyclic polymers grafted with polystyrene or polyisoprene branches via a combination of sequential living cationic polymerization and anionic polymerization. Its morphology was directly visualized under AFM and the mean average diameter for the central backbone was estimated to be about 65-70 nm.[62]

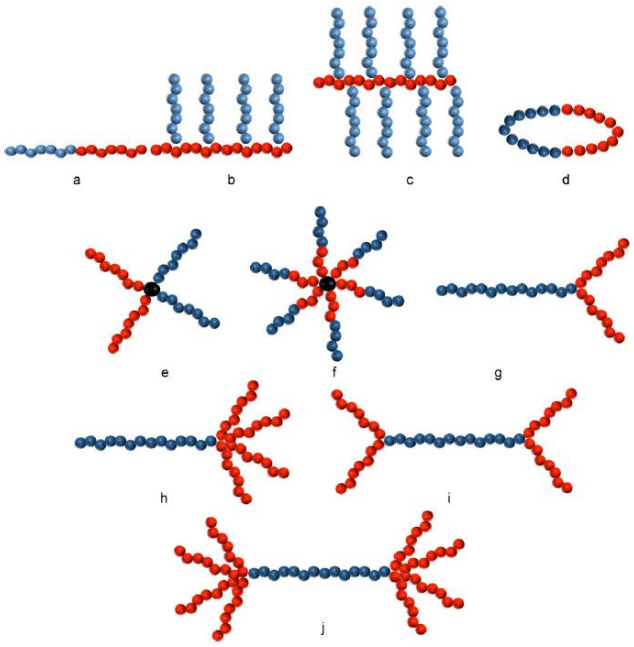

Figure 1.3. A variety of polymers with complex topologies.[41]
Reprinted with permission from Ref. [41]. Copyright 2012, Elsevier.

Polymers with complex architectures often exhibit unique properties that are distinctive from their linear counterparts.[63-66] For example, star polymers or linear brush

copolymers are regularly branched macromolecules and possess compact molecular structures with smaller radius of gyration.[22] As a result, their hydrodynamic volume and viscosities are lower compared to the linear counterparts that possess identical molecular weights with them. In addition, cyclic brush copolymer decorated with certain side chains, due to its unique ring-like structure, is capable of self-assembling into supramolecular cylindrical tubes in a selective solvent for the branch.[62] Significantly, properties of the polymers constructed through controlled radical polymerization (CRP) can be finely adjusted by independently selecting constituent blocks in macromolecules with desired compositions to accomplish specific functions. As a result, polymeric materials with a spectrum of properties can be designed based on living/controlled polymerizations for the final applications.

To date, a variety of polymer topologies have been made possible due to the development of versatile polymer synthetic tools. In the meantime, polymers with complex architectures have already found applications as template to fabricate a variety of organic and inorganic nanostructures[67] in nanotechnology (**Scheme 1.1**). Wang et al. have reported the preparation of polymer/silica hybrid nanowires and nanotubes that are stabilized by surface PEG ligand and soluble in water with bottlebrush copolymers as templates. The linear brush copolymers were grafted with either diblock copolymer or triblock copolymer as side chains which are synthesized through ATRP technique.[68,69] Kun et al. reported the fabrication of organic nanotubes with well-defined dimensions and pore sizes by exploiting multicomponent cylindrical brush copolymers as macromolecular precursors. The polymer templates were synthesized via combining RAFT and ROP polymerizations.[70-72] Especially, Pang et al. recently reported preparation of a variety of nanoparticles with either hollow or core-shell nanostructures by employing star-shaped block copolymers prepared via ATRP as template. However, further efforts are required to develop functional polymers with complex yet intriguing structures and explore their unique properties. Polymers with such sophisticated structures may

facilitate the fundamental research in polymer science and engineering and render advanced applications in many technological areas.

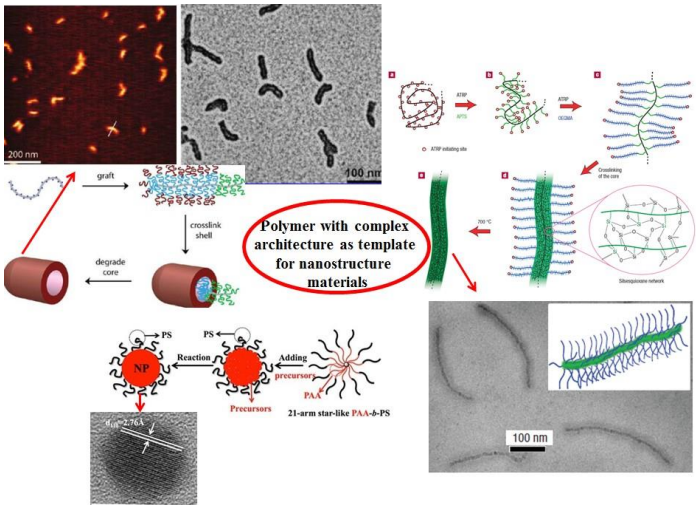

Scheme 1.1. Polymers with complex topologies as template to form organic or inorganic nanomaterials.

1.1.3. Core-shell and Hollow Polymeric Nanoparticles

1.1.3.1. Self-assembled Polymeric Nanostructures

Block copolymers are a class of copolymers where two or more chemically distinct constituent blocks are linked through covalent bonds.[73,74] The advance in living/controlled polymerization has enabled the design and synthesis of block copolymers with a variety of chemical compositions, controlled molecular weights and low polydispersity in the past decades.[75,76] As such, block copolymers with tailored compositions and molecular weights have been one of the crucial elements for crafting supramolecular nanostructures via bottom-up approach.[77] It is widely known that block amphiphilic macromolecules consisted of polymer blocks that have distinct affinities to a selective solvent will phase-separate on microscopic scale and self-assemble into micellar nanostructures.[78,79] The self-assembly process takes place in a selective solvent when

concentration of the unimers is above the critical micelle concentration (CMC) and temperature is higher than the critical micelle temoeratute (CMT).[80] The core of micelle is composed of the solvophobic block, which is stabilized and shielded from solvent by a shell comprising the solovphilic block. Conventionally, the micellar structures that can be formed include spherical, cylindrical micelles, and double-layered vesicles, which are interchangeable depending on the surrounding experimental conditions.[77] For example, remarkably, it was discovered that a polymeric micotubule produced by self-assembly of a air-responsive copolymer can "breathe" CO_2 to transform morphology from cylindrical microtubule form through spherical vesicle shape to final micelle structure, as shown in **Figure 4**.[81] The structure transformation can be modulated by stimulation level of the gas.[82] Recently, other complex micellar architectures were also created, such as nanotubes,[83-85] helices,[86-88] and bowl shaped micelle.[89-91] The resulting morphologies are dictated by a number of parameters, including volume ratio of constituent blocks (hydrophobicity/hydrophilicity balance), temperature, solvent nature, polydispersity of copolymer, concentration of macromolecules, thermodynamic interaction between polymer blocks with solvent, etc.[77,92] Quantitatively, the nanostructures formed can be predicted and tailored based on the following dimensionless parameter which is called "packing parameter"[92]:

$$p = v/(a_h l_c)$$

where l_c was hydrophobic tail length, a_h was optimized area of the side functional group, and v was volume of hydrophobic chain.[92] When $p \leq 1/3$, spherical micelle morphology is favored. While cylindrical micelle is usually formed when $1/3 \leq p \leq 1/2$. In addition, vesicle (polymersome) is resulted when $1/2 \leq p \leq 1$.[92]

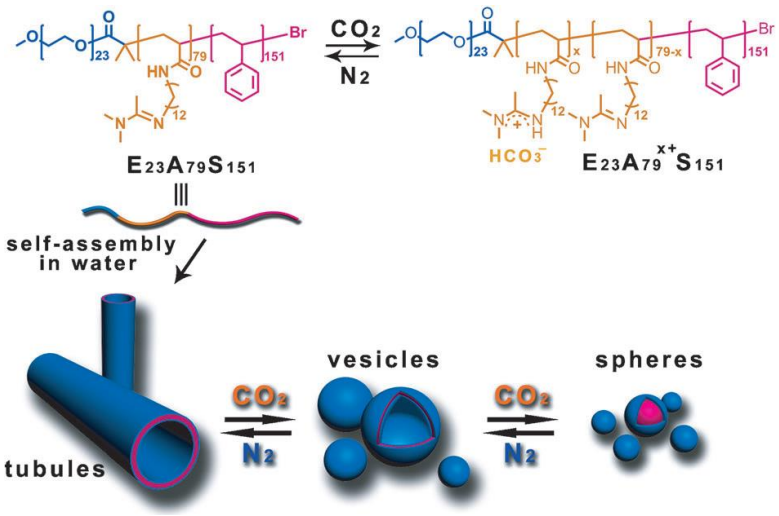

Figure 1.4. Morphology exchange of self-assembled supramolecular nanostructures by tuning surrounding conditions.[81]
Reprinted with permission from Ref. [81]. Copyright 2013, Wiley.

Among the various supermolecular structures formed, spherical core-shell[93-96] or core-shell-corona[97] type micelles (**Figure 1.5**) have drawn considerable academic attention because of their prospective as promising nanocarriers for drug/gene delivery or other applications, and this topic has been subjected to numerous studies. A variety of polymers have been selected as the hydrophobic core such as polycaprolactone, PS, PMMA, PMA, and their derivatives, while plenty of hydrophilic polymers have been examined as the shell materials, including PVP, PEG, polyelectrolytes (e.g. PAA) etc. Biocompatible and biodegradable polymers such as PCL, PLA, PLGA and PBLG are among the most interesting materials to construct the hydrophobic inner core and have been widely studied because their interaction with hydrophobic drugs allows the drugs to be preferentially encapsulated in the spherical micelles.[98-100] The enclosed bioactive compounds are stabilized and protected against scavenging by the reticuloendothelial system (RES), enabling them prolonged circulation half-life. When the drugs are delivered to target sites *in vivo*, degradation of the core materials under specific body environment would enable controlled release of the cargos from the micelles. On the

other hand, core-shell micelles composed of the inert and biocompatible PEG as the shell layer would be endowed with reduced systematic clearance rate and prolonged circulating time *in vivo*, which renders them stealth systems for drug delivery.[101-104]

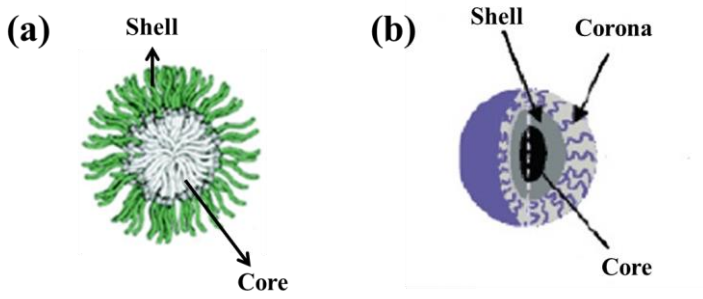

Figure 1.5. Illustration of (a) core-shell polymer micelles, (b) core-shell-corona polymer micelles.

Stimuli-responsive polymers are a class of "smart" macromolecules that can respond to external stimuli and change their physical/chemical properties (e.g. shape, conductivity, and color) in response to slight change in the environment.[105,106] They have been used in enormous applications across diverse fields such as electronics, pharmaceutics, optics, cosmetics, and biomedicine. Stimuli-responsive micelles are constructed using the stimuli-responsive polymers as constituent materials.[107-109] They have recently received considerable attention due to their distinct response to the external stimuli in the environment, which is manifested in the deformation or change in shape (i.e. spherical or cylindrical).[110] Especially, the reversibility of micelles bestowed by constituent responsive block can realize the controlled release of the loaded cargos by changing the local environment (e.g. temperature) that the micelles are subjected to. The external signals that can induce change of the responsive polymers or micelles include temperature,[110,111] pH,[112-114] light,[115-117] humidity, magnetic,[118,119] electric field[120] etc. A variety of thermo-responsive polymers such as poly(dimethylaminoethyl methacrylate)

(PDMAEMA), poly(*N*-(*2*-acryloyloxyethyl) pyrrolidone) (PNMP), poly(ethyl methacrylate) (PEMA), poly (*n*-acryloyl-*l*-proline ester) (P(Pro-oMe)), and poly(N-isopropylacrylamide) (PNIPAM) have been employed as one of the constituent blocks to build the responsive micelles, and PNIPAM is a widely investigated polymer among them that can respond to temperature.[121] The thermo-induced self-assembly behavior of block copolymers with PNIPAM as one fixed block and various hydrophilic or hydrophobic polymers as another tunable consistent were examined and reported. For instance, PDMA-*b*-PNIPAM-*b*-PDMA (ABA) and PNIPAM-*b*-PDMA (AB) were synthesized with varied thermal-responsive PNIPAM molecular weights and fixed PDMA block length for systematic self-assembly study in the aqueous solution.[110] Size (D_h) of the copolymer $PNIPAM_{460}$-*b*-$PDMA_{100}$ aggregates (C = 1.00 g/L) was examined at either 25 °C (temperature below LCST of PNIPAM) or 45 °C (temperature above LCST of PNIPAM) using DLS. D_h was approximately 10 nm at 25 °C, which is consistently close to the size of unimers dissolved on the molecular level, while D_h was about 80 nm at 45 °C, indicating the aggregation of copolymers above LCST of PNIPAM and the formation of micelles (**Figure 1.6**). The self-assembly process is reversible. For pH-responsive micelle systems, a series of pH-responsive polymers including polyacrylic acid (PAA), poly(4-vinylpyridine) (P4VP), poly(N,N-diethylaminoethyl methacrylate) (PDEAEMA), and poly(2-dimethylamino-ethylmethacrylate) (PDMAEMA) have been integrated into amphiphilic block copolymers and their pH triggered micellization behaviors were investigated. A series of PDMVBA-*b*-PVBTMAC were prepared with varied PDMVBA block length (DP = 11 to 50) and fixed PVBTMAC molecular weight.[122] Their micellization behaviors were subsequently investigated under varying solution pH. PDMVBA is fully protonated when pH is below 5.5, and the block copolymers are double hydrophilic. However, the PDMVBA became hydrophobic due to the deprotonation when pH increased to above 7. As a result, self-assembly of amphiphilic block copolymers will occur. Interestingly, the

micellization behavior was affected by molecular weight of PDMVBA block. At pH = 10.0 as DP of PDMVBA block was elevated from 11 to 50, the aggregation number of micelles (i.e. N_{agg}) determined by SLS increased from 3 to 12. In addition, copolymers that respond to other stimuli, such as light, chemical stimulations,[123] and electrical field, as well as dually responsive copolymers[124] in which constituent blocks are sensitive to different stimuli were prepared and examined for micelle formation. Dually responsive copolymers can display "schizophrenic" type assembly behavior.

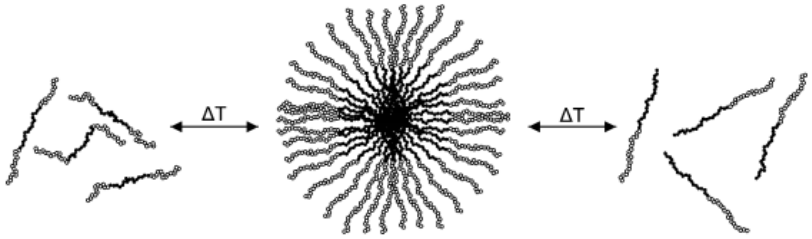

Figure 1.6. Self-assembly and reversible dissociation of PNIPAM-*b*-PDMA.[125]
Reprinted with permission from Ref. [125]. Copyright 2006, American Chemical Society.

In addition to linear block copolymers such as AB diblock copolymer, and ABA or ABC type triblock copolymer, self-assembly of polymers with complex macromolecular architectures including star-like block copolymers, molecular bottlebrushes, etc. and their formation of micelles were also studied. Copolymers with complex structures give us access to micelles with more sophisticated nanostructures, such as multicompartmental micelles[126-129] (**Figure 1.7**).

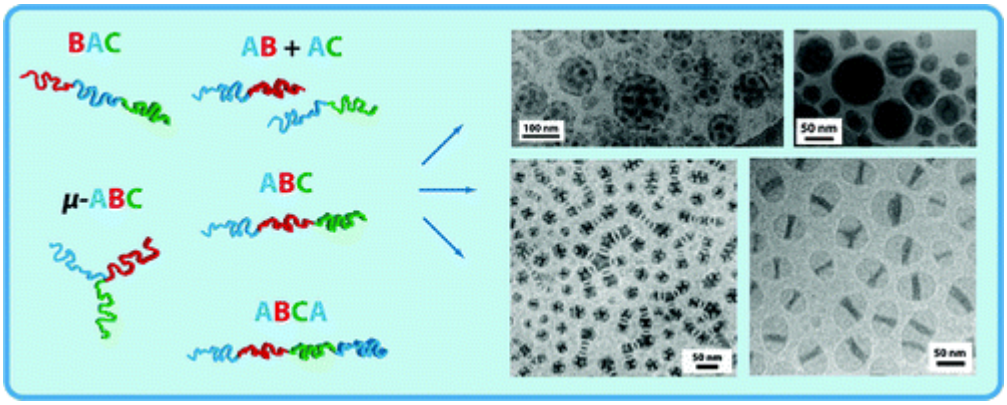

Figure 1.7. Multicompartmental micelles produced from polymers with complex macromolecular architectures.[126]
Reprinted with permission from Ref. [126]. Copyright 2011, American Chemical Society.

1.1.3.2. Core-shell Polymeric Nanoparticles

As mentioned above, self-assembly of copolymers which are comprised of one solvophobic block and another solvophilic block in selective solvents has produced a large variety of micelles with complex shape and will continuously enrich our library of intriguing supramolecular nanostructures. Spherical micelles have been paid special attention due to its promising application in drug delivery. However, the nanoscale micelles are kinetically trapped in non-equilibrium states and unstable. Their characteristics and shapes for a given system depend sensitively on concentration, solvent properties, temperature, pH, etc.,[92] and are subjected to vary in response to changes in these experimental conditions.[130] The self-assembly process is reversible, and dissociation of nanoscale assemblies into individual linear polymer chains can occur when the solution concentration is diluted to below the critical micelle concentration (CMC)[131,132] or triggered by other factors (e.g. pH[133]). Particularly, when the micelles were loaded with drug/gene for delivery application, concentration of the copolymers will be highly diluted under physiological conditions to below CMC after their administration to a patient. The dilution induced dissociation will occur, and the active compounds will be

released from the micelles prematurely before they reach the target.[134-136] In 1996, Wooley and coworkers reported, for the first time, the crosslinking of a core-shell micelle composed of the solvophobic PS inner domain and a solvophilic PVP outer layer using shell-crosslinking (SCL) approach, leading to a structurally stable core-shell polymeric nanoparticle (**Figure 1.8**).[137] The stability of micelle was enhanced significantly upon crosslinking with an essentially locked structure. Following her work, numerous studies were reported concerning the synthesis of core-shell nanoparticles with various compositions or functionalities via crosslinking of different micelles.[138-141] For example, a copolymer PAA_{90}-*b*-PMA_{240} with PAA as the solvophilic segment and PMA as the solvophobic constituent was prepared and reported. The macromolecule self-assembled in selective solvent to produce core-shell nanostructures consisted of PMA as the hydrophobic core. Subsequently, the core-shell nanoparticle was produced by crosslinking the hydrophilic PAA shell with 2,2'-(ethylenedioxy)bis(ethylamine). Crosslinking density of the shell was dictated and can be controlled by the stoichiometric ratio between amine and carboxylic acid. In addition, stimuli-responsive micelles were also cross-linked to form core-shell polymeric nanoparticles that can respond to external stimuli.[141-146] For instance, temperature-responsive micelles with PNIPAM as inner domain and PAAL as outer layer were prepared by micellization of PNIPAM-*b*-PDMA-*b*-PAAL copolymer. Responsive core-shell polymer nanoparticles were subsequently created through interpolyelectrolyte complex (IPEC) formation between the anionic carboxylate moieties on PAAL shell and the equal amount of cationic PVBTAC, as shown in **Figure 1.9**.[147] It was found that the core-shell nanoparticles responded to temperature stimulus by changing their size, which decreased slightly upon cooling to room temperature.

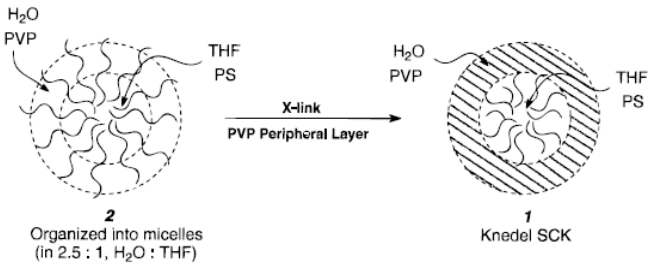

Figure 1.8. Core-shell polymeric nanoparticles with PS as inner domain and PVP as outer layer prepared through SCL approach.[137]
Reprinted with permission from Ref. [137]. Copyright 1996, American Chemical Society.

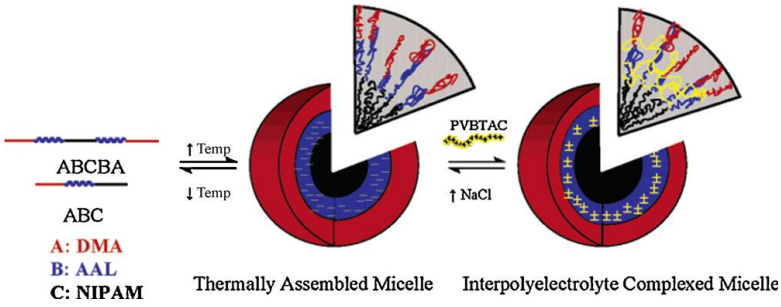

Figure 1.9. Temperature-responsive core-shell polymeric nanoparticles.[147]
Reprinted with permission from Ref. [147]. Copyright 2006, American Chemical Society.

In addition to shell-crosslinking (SCL) approach described above, crosslinking can also be carried out in the core domain of self-assembled micelles to stabilize their structures.[148-152] For instance, Kataoka *et al.* constructed a polyion complex (PIC) micelle from association of cationic PEG-*b*-P(Lys) copolymer and anionic P(Asp) homopolymer, driven by electrostatic interaction between the oppositely charged polymer pair. Inner domain of micelle is consisted of P(Lys), P(Asp), as well as deliberately introduced thiol moieties. Subsequently, the core was cross-linked via the oxidation of thiols into labile disulfide bond to stabilize the micelle (**Figure 1.10**).[93] Furthermore, the disulfide linkage can be cleaved in response to a chemical reducing agent, resulting in the dissociation of nanoparticles.

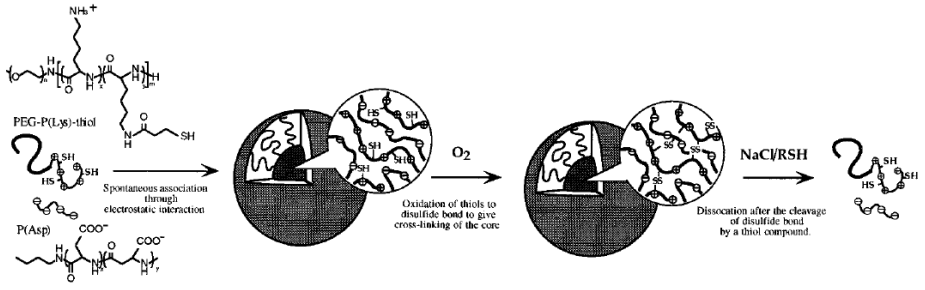

Figure 1.10. Core cross-linked organic core-shell nanoparticles.[93]
Reprinted with permission from Ref. [93]. Copyright 1999, American Chemical Society.

Different crosslinking mechanisms can be applied, and the crosslinking reactions reported in the larger body of literature can be grouped into two main categories: chemical crosslinking[79,150,153,154] and photo-crosslinking.[155-159] For chemical crosslinking, various chemical reactions were employed and investigated with respect to their feasibility, efficiency, kinetic rate, etc. A good example would be the reaction between activated ester group and difunctional amine, which allows the crosslinking to proceed efficiently. A micelle with nacryloxysuccinimide (NAS) functionalities located in the shell domain was prepared by thermo-induced self-assembly of PEO-*b*-P(DMA-*s*-NAS)-*b*-PNIPAM triblock copolymer, which is subsequently cross-linked in shell by ethylene diamine.[160] The crosslinking was about 95% completed in 2h, which is very fast. In addition, click chemistry, a quick and reliable way to join small units, was also employed to efficiently crosslink micelles for the preparation of stabilized nanoparticles.[151] Photo-crosslinking was recently brought to the attention of scientists due to their typical mild reaction conditions, no need for additional crosslinking agent, ease of reaction and purification, etc. The photochemistry that has been utilized for crosslinking micelles includes thymine,[161,162] coumarin,[159,161,163] diacrylated pluronic,[164,165] azide groups, etc. In particular, azido functionality possesses high latent reactivity and easy activation by

either heat or UV irradiation.[166,167] In the latter context, the crosslinking density can be easily controlled by simply varying the intensity of UV irradiation or the irradiation time.

Crosslinking can indeed benefit the micelles by providing them with excellent structural integrity, however, the stabilized structure will also render it difficult for the encapsulated cargos to release from nanoparticles when demanded.[136] In addition to irreversible crosslinking that was widely reported, reversible cross-linked systems were also developed.[79,93,140,168-171] In reversible crosslinking, a cleavable functionality was incorporated during the crosslinking of micelles. Subsequently, the crosslinkers can be cleaved either chemically or triggered by light to break down the nanoparticle, leading to their reversible dissociation into unimers. For example, the micelle formed from PEO_{45}-*b*-P(DMA_{98}-*s*-NAS_{30})-*b*-$PNIPAM_{87}$ triblock copolymer above LCST of PNIPAM was cross-linked by cystamine, a diamine that contains liable disulfide functionality.[168] The resulting core-shell nanoparticles can be disintegrated into unimers by cleaving the disulfide crosslinks through chemical reduction using tris(2-carboxyethyl)phosphine hydrochloride (TCEP) or dithiothreitol (DTT). Reversibly crosslinked micelles are particularly attractive because de-crosslinking process can facilitate the release of guest molecules that are loaded in the micelles ahead of time. Zhao *et al.* prepared a core cross-linked nanoparticles composed of poly(coumarin methacrylate) (PCMA) as inner component with PEO as hydrophilic outer layer through photodimerization of coumarin moieties in the core domain (**Figure 1.11**), which was subsequently loaded with hydrophobic Nile Red (NR).[136] Their study shows that the disruption of nanoparticles by photo-de-crosslinking allows the release rate of encapsulated cargos to increase. It is worth mentioning that reversible crosslinking can also be realized by either chemical crosslinking or photo-crosslinking.

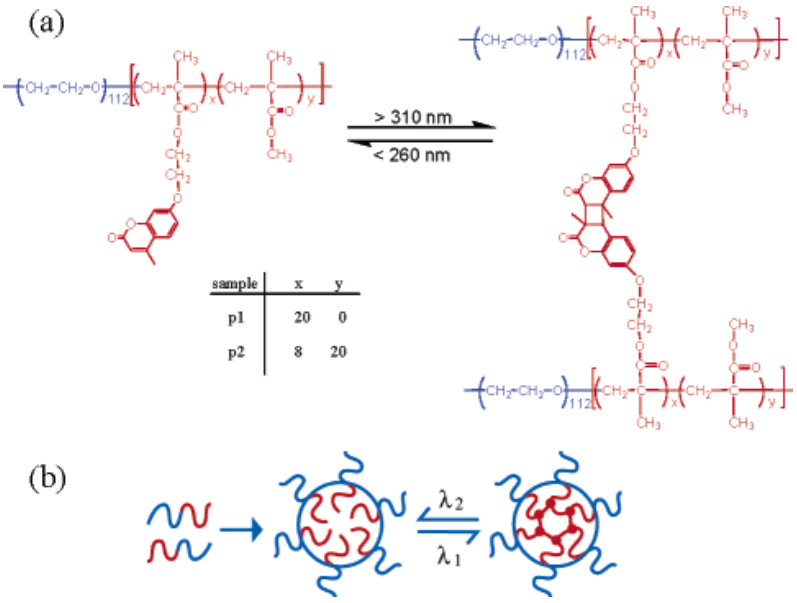

Figure 1.11. Reversibly photo-cross-linked spherical micelles.[136]
Reprinted with permission from Ref. [28]. Copyright 2007, American Chemical Society.

Clearly, core-shell polymeric nanoparticles can be fabricated through crosslinking either inner domain or the outer layer of self-assembled core-shell or core-shell-corona type micelles. Other than the crosslinked polymer micelle approach, other methods were also developed to prepare core-shell polymer nanoparticles such as seed/two-stage emulsion polymerization,[172] surface-initiated polymerization,[173] successive solvent displacements,[174] and photo-emulsion polymerization[175] etc.

The core-shell polymeric nanoparticles have wide potential applications, including drug delivery, solvation, biomedical applications, catalysis, coatings, phase transfer reactions, chromatography, fillers for plastics, nanoreactors, host for removing hydrophobic contaminants from aqueous solutions, etc.[137] For instance, Mann *et al.* synthesized a core-shell organic nanoparticle consisted of polyisoprene (PI) as the inner core by crosslinking the hydrophilic poly(acrylic acid) (PAA) shell via amidation reactions. The micelle was prepared by self-assembly of poly(acrylic acid-*b*-isoprene) (PAA_{78}-*b*-PI_{97}) in aqueous solution. Cross-linked PAA nanocapsules were also created by

ozonolysis of the PI core. Subsequently, both the core-shell nanoparticles and PAA nanocages were utilized as nanoreactors or templates to produce calcium phosphate-polymer hybrid nanostructures, which are shown in **Figure 1.12**.[176] In this context, the crosslinked PAA shell served as nucleation site for amorphous calcium phosphate.

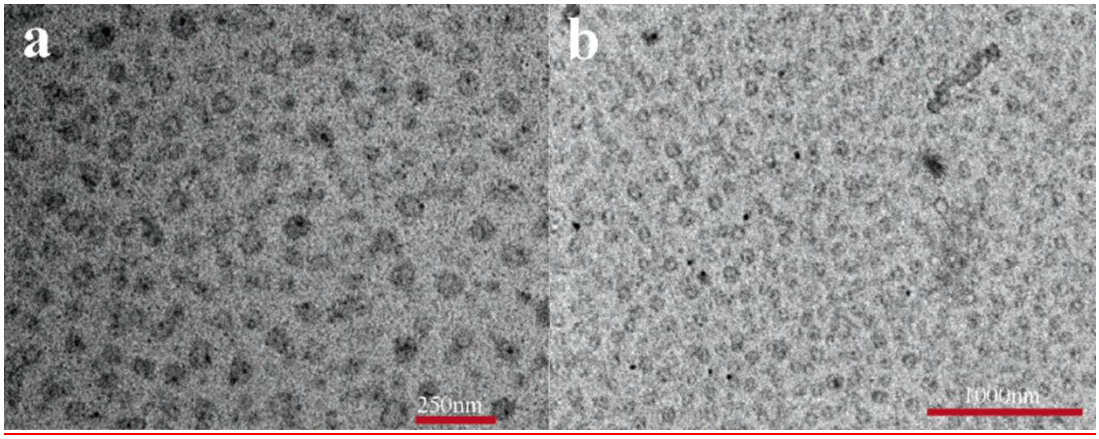

Figure 1.12. Application of core-shell polymer nanoparticles as nanoreactors to fabricate calcium phosphate-polymer hybrid nanostructures.[176]
Reprinted with permission from Ref. [28]. Copyright 2005, American Chemical Society.

1.1.3.3. Hollow Polymeric Nanoparticles

If the shell of a core-shell micelle is crosslinked and the core block is consisted of a degradable polymer, the inner core can then be subsequently etched following the shell crosslinking reaction to yield a hollow polymeric framework.[152,177,178] For example, a graft copolymer PONBDM-*b*-P(NBE-*co*-BNBE)-*g*-PBS was prepared by combining two living polymerization techniques, namely ROMP and ATRP, and selectively self-assembled in toluene into a core-shell micelle composed of solvophobic PONBDM core and P(NBE-co-BNBE)-g-PBS shell. The micelle was subsequently stably locked by crosslinking the butenyl functionalities from PBS brushes which are located in the shell. Finally, core of the cross-linked framework was degraded by hydrolytic etching of the ester bonds using acid, yielding hollow polymeric nanoparticles (**Figure 1.13**).[179]

Structural integrity of the spherical hollow nanostructure was preserved after core degradation due to the stable cross-linked shell. The shape and size of hollow nanoparticles are determined by the dimension of the cross-linked core-shell precursor. More recently, Lewis *et al*. reported a core-shell-corona type micelle with PMPC as inner core, PDMA as outer shell, and PEO as surface ligand from self-assembly of the PEO-*b*-PDMA-*b*-PMPC copolymer in alcohol aqueous solution. Subsequent crosslinking of the PDMA shell led to a cross-linked core-shell-corona type nanoparticle. Interestingly, with a low crosslinking density in the shell, the hydrophilic PMPC blocks can migrate through the shell layer into the corona to join the PEO block, forming a hollow polymeric nanoparticle possessing mixed polymer surface ligands.[180]

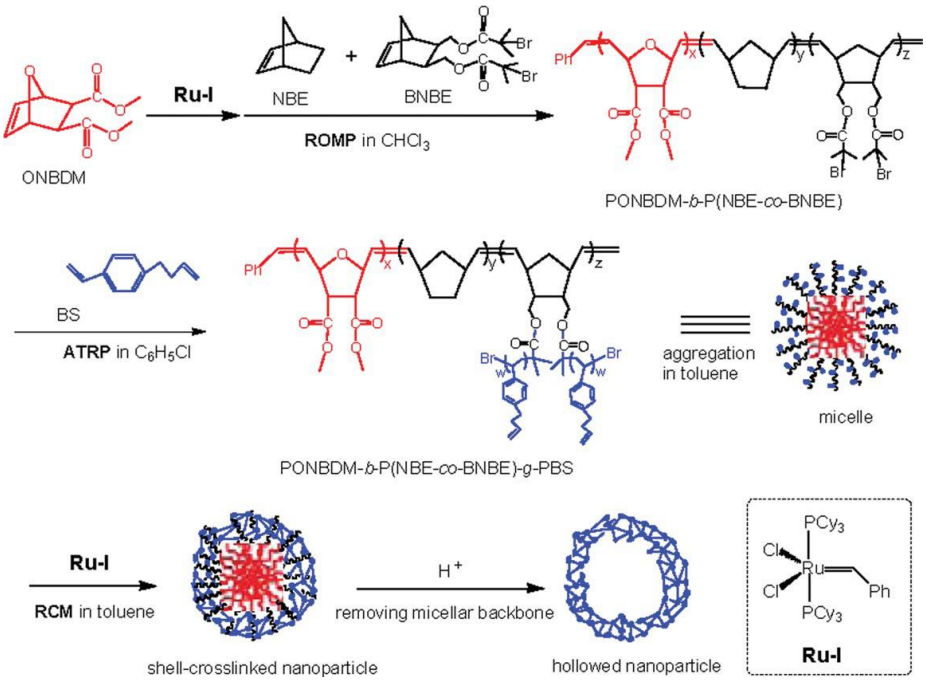

Figure 1.13. Templating synthesis of polymeric hollow nanoparticle.[179]
Reprinted with permission from Ref. [179]. Copyright 2011, Wiley.

Notably, the hollow polymeric nanoparticles may find applications in hydraulic fluids, recording materials, drug/gene delivery and controlled release.[137]

1.1.4. Polymer/silica Hybrid Nanostructured Materials

Organic/inorganic hybrid nanoparticles represent an important class of multifunctional nanomaterials that exhibit fascinating optical, electronic, magnetic, and biological properties in single nano-objects.[181-183] The chemical properties (e.g., solubility and photo-crosslinking) of such hybrid nanoparticles are mainly imparted by organic constituent, while the physical properties are often dictated by the synergy of inorganic nanoparticle and organic component.[184-186] Among various organic/inorganic hybrid nanostructures developed, silica/polymer hybrids, including polymer-functionalized silica nanoparticles and organo-silica structures, have garner much attention due largely to their ease of preparation and a wide range of applications for polymer matrix nanocomposites,[187,188] biomedical engineering,[189-191] and fluorescent thermometers.[192] Moreover, they have also been utilized as model colloids for evaluating the steric stabilization theory.[193,194] The commonly used approaches to produce silica/polymer hybrid_nanoparticles include physical adsorption,[195,196] grafting from,[197-202] grafting onto,[203] self-assembly,[204-207] etc.

In the "grafting from" approach, initiators are immobilized onto the surface of silica nanoparticles. Subsequently, using the functionalized particle as initiator, surface-initiated (SI) polymerization was conducted by controlled radical polymerization (e.g., ATRP) or other polymerization techniques to grow polymer chains from the nanoparticle surface, leading to the formation of particle brush. For example, Liu *et al*. reported the preparation of polymer/silica hybrids with thermo-responsive PNIPAM ligands densely grafted on the surface of nanoparticles via grafting from strategy (**Figure 1.14**).[197] Surface-initiated ATRP (SI-ATRP) was employed to polymerize PNIPAM from the surface of initiators functionalized silica particles using $CuCl/CuCl_2/Me_6TREN$ as catalytic system to fabricate the particle brush. The polymerization kinetics was well

controlled, as demonstrated by low polydispersities of grafted PNIPAM brushes and the linear evolution of PNIPAM molecular weight (M_n) with monomer conversion, resulting in PNIPAM surface grafts with tunable thickness. Due to the thermal-responsiveness of PNIPAM, thermal phase transition of the PNIPAM surface ligands was further studied, and an interesting and unique two-stage phase transition was found over a broad temperature range. For the "grafting onto" method, surface of nanoparticles is functionalized with reactive compounds. Polymers containing functional groups are prepared and then grafted onto the particle surface through certain coupling reaction, such as click chemistry. For instance, Hamaide *et al* prepared azido surface-functionalized silica nanoparticles by sol-gel process in reverse W/O emulsion. Polyethylene glycol (PEG) with ethynyl functionality was synthesized, and subsequently grafted onto silica particle surface by 1,3 dipolar cycloaddition (click reaction) between azido and ethynyl groups, leading to multifunctional hybrid nanoparticles coated with a PEG layer.[203] Whereas in the "self-assembly" approach, amphiphilic block copolymers with one constituent segment containing trimethoxysilyl moieties form spherical micelles in aqueous solution. Organo-silica hybrid nanoparticles grafted with polymer ligand on particle surface were then produced by intra-micellar crosslinking through hydrolysis and polycondensation of the trimethoxysilyl groups,[204,205,207] as shown in **Figure 1.15**.

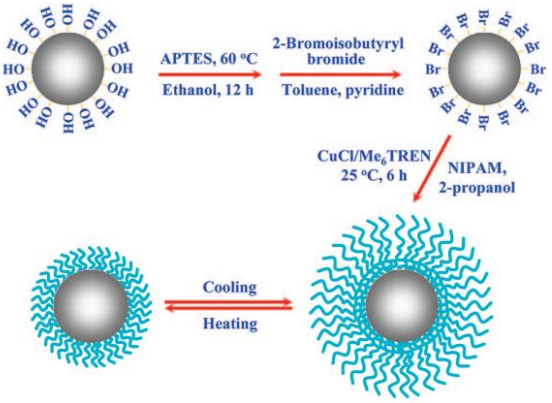

Figure 1.14. Organic/inorganic hybrid nanostructures prepared through "grafting from" strategy.[197]
Reprinted with permission from Ref. [197]. Copyright 2007, American Chemical Society.

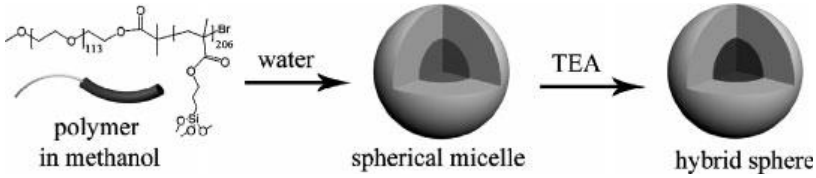

Figure 1.15. Polymer/silica hybrid nanostructures synthesized via "self-assembly" approach.[205]
Reprinted with permission from Ref. [28]. Copyright 2005, Wiley.

On the other hand, organo-silica hybrid nanocapsules with a well-controlled cavity are of particular interest as the hollow interior offers peculiar advantages, such as the ability to load guest molecules for delivery or act as nanoscale reactor by encapsulating reactive compounds.[208] However, the effective methods to form organo-silica hybrid nanocapsules are comparatively few and limited in scope. The preparation of hybrid nanocapsules primarily involves the use of self-assembled polymer micelles or vesicles.[208-211] For example, Schmidt *et al*. prepared a polymeric vesicle from amphiphilic PEO-*b*-PTMSPMA diblock copolymer where trimethoxysilyl functionalities were located in the hydrophobic PTMSPMA layer stabilized by PEO at inner and outer surface. Crosslinking or gelation of the trimethoxysilyl groups then proceeds within the inner hydrophobic layer of the vesicles to form polymer/silica hybrid vesicles which possess an interior cavity (**Figure 1.16**).[211]

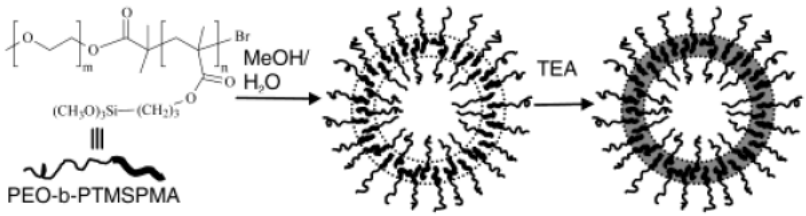

Figure 1.16. Approach to Hollow Hybrid Polymer Particles.[211]
Reprinted with permission from Ref. [211]. Copyright 2003, American Chemical Society.

It is worth noting that the "self-assembly" approach provides access to organo-silica hybrid nanoparticles and nanocapsules, depending on the morphology of self-assembled nanostructures.[207,208,211] Amphiphilic block copolymers incorporated with trimethoxysilyl groups can self-assemble into either core-shell micelle or vesicle in selective solvents by carefully tuning the solution conditions. If a core-shell micelle is formed, gelation can occur either in the core or shell of the micelle to obtain hybrid nanoparticles or hybrid nanocapsules, respectively, depending on the location of trimethoxysilyl moieties.[207,211] For example, Fukuda *et al*. prepared a spherical core-shell micelle with MOPS moieties distributed preferentially near the peripheral surface by micellization of PMMA-*b*-PPEGMA-*b*-poly(PEGMA-*r*-MOPS) copolymer in DMF/acetone/water mixture. Subsequently, hydrolysis and polycondensation of trimethoxysilyl functionalities in PMOPS segments occurred at the peripheral surface within individual micelle, producing organo-silica hybrid nanocapsules (**Figure 1.17**).[208] On the other hand, if a vesicle is yielded, inter-vesicular crosslinking of trimethoxysilyl groups will lead to polymer/silica hybrid vesicles or nanocapsules.

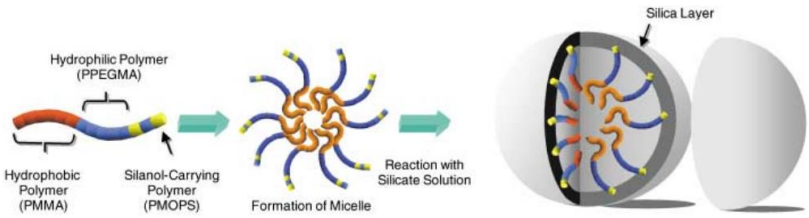

Figure 1.17. Polymer/silica hybrid nanocapsule via intra-micellar gelation within the shell of a spherical micelle.[208]
Reprinted with permission from Ref. [208]. Copyright 2003, Wiley.

1.1.5. Polymer based Drug Delivery and Controlled Release System

Drug delivery and controlled release technologies have made a pronounced impact on the medical field.[212] Loading guest chemotherapeutic agents in nanocarriers can result in improved drug solubility, stability, reduced clearance, and long circulating half-life.[212,213] In this context, a variety of nanoscale delivery vehicles have been developed for potential use in drug delivery, including liposomes, polymer-drug conjugates,[214] polymer micelle nanoparticles,[215,216] polymersome,[217-219] dendrimers,[220,221] and unimolecular micelles.[222,223] Among them, polymer micelle nanoparticles[224] have received attention due to highly enhanced drug solubility and long circulating half-life. For example, the long circulating PLGA-PEG nanoparticle has been approved by Food and Drug Administration (FDA) for the clinical use. However, two challenges associated with the polymer micelle systems limit their clinical applications. First, polymer micelle will dissociate into unimers under the high dilute psychological conditions *in vivo*, which will cause premature drug release. Crosslinking can be conducted in the micelles to enhance their stability. Second, it is challenging to produce polymer micelles in uniform shape and predictable size. On the other hand, unimolecular polymer micelles exhibit improved stability compared to self-assembled micelles. However, they are still unstable above the critical aggregation concentration (CAC) and the aggregation is often observed.[225-227] It is worth noting that the instability would trigger premature drug release and potentially harm healthy tissue.[222,225] A well-controlled size is particularly important for tumor-targeted drug delivery as the effective size of nanocarriers falls in the range of 20-100 nm.[228,229]

In this context, it is highly desirable yet challenging to create structurally well-defined nanostructures with good stability, monodispersity, and precise size controllability as a new type of drug vehicle.

1.2 Motivation

1.2.1. Challenges in Fabrication of Polymeric and Organic/Inorganic Hybrid Nanostructured Materials from Self-Assembled Polymer Micelles

Block copolymers with complex architectures (e.g., linear block copolymers, star-like block copolymers, molecular bottlebrushes, and cyclic brush copolymers etc.) that are composed of polymer blocks exhibiting distinct affinities to a selective solvent are capable of self-assembling into a wide variety of supramolecular nanostructures with complex shapes, such as spherical micelles, cylindrical micelles, double-layered vesicles, nanotubes, and helices. By carefully designing the macromolecules and tuning the solution conditions, spherical core-shell or core-shell-corona type micelles can be formed. They are particularly interesting because of their promising applications in delivery of active compounds. However, the micelles kinetically trapped in non-equilibrium states are unstable and sensitive to conditions of the surrounding environment.[130] The nanoscale assemblies can reversibly dissociate into unimers when the copolymer concentration is diluted to below the CMC, which is particularly undesirable when the micelles are utilized for drug delivery because the dilution induced dissociation *in vivo* will cause the premature release of bioactive compounds.

To address the challenge of instability, crosslinking was conducted in either core or shell domain of the spherical core-shell micelles to lock their structures,[33,93,136] which

led to structurally stable core-shell polymeric nanoparticles. Different crosslinking mechanisms including chemical crosslinking (e.g. activated ester group and difunctional amine) and photo-crosslinking (e.g. coumarin, and azide groups) were applied and investigated with respect to their feasibility, efficiency, and kinetic rate. Crosslinking can be reversible, depending on the mechanism employed, if a cleavable moiety is incorporated during the crosslinking of micelles. Chemical or light triggered de-crosslinking of nanoparticles by cleaving the crosslinkers will lead to their reversible dissociation into unimers, facilitating the release of loaded cargos. Plenty of core-shell type polymeric nanoparticles consisted of different solvophobic core materials (e.g. PS, PMA, PMMA, PCL, and their derivatives) and various solvophilic shell components (e.g. PEG, PVP, PAA, and their derivatives etc.) were prepared and reported via the crosslinking of spherical micelles. Among them, biocompatible polymers such as PCL, PLA, PLGA and PBLG are interesting candidate materials to construct the inner core because their interaction with hydrophobic drugs would facilitate loading of the compounds in the nanoparticles, while the inert PEG has attracted considerable interest as the shell material due to its beneficial stealth characteristics. In addition, stimuli-responsive core-shell nanoparticles that can respond to external stimuli by changing their physical or chemical properties (e.g., size) were also developed by crosslinking the micelles composed of stimuli-responsive polymers as constituent materials.

In particular, if the shell of a core-shell micelle is cross-linked and the core block is consisted of a degradable polymer, the inner core can be subsequently etched following the shell crosslinking reaction to prepare a hollow polymeric framework. Furthermore, organic/inorganic hybrid core-shell and hollow nanoparticles can also be prepared if metal elements are integrated during crosslinking of micelles. For example, amphiphilic block copolymers incorporated with trimethoxysilyl groups can self-assemble into either core-shell micelle or vesicle in selective solvents by deliberately tuning the solution conditions. Inter-micellar gelation can occur either in the core domain or shell layer of

the micelle to obtain organo-silica hybrid nanoparticles or nanocapsules, respectively, depending on the location of trimethoxysilyl moieties.[207,211]

Clearly, both core-shell and hollow nanostructured materials, which are consisted of polymers as the exclusive constituent elements or both organic and inorganic materials as the hybrid components, can be created from self-assembled polymer micelle systems, depending primarily on the materials that are selected and the crosslinking mechanism which is being employed. However, the access to polymeric or hybrid nanostructured materials which are dimensionally and functionally well-defined is limited due in part to the relatively poor size control and comparatively high polydispersity of nanostructures obtained via self-assembly of linear block copolymers.[230,231] More importantly, the common need for amphiphilic characteristics of block copolymers in order to impart self-assembly restricts the scope of selection on their chemical compositions and functionalities. Clearly, it is challenging to realize well-tailored polymeric and hybrid nanostructures (e.g., core-shell, hollow geometries) with a wider range of accessible compositions through the polymer micelle approach. In addition, the self-assembly process of polymers to form supramolecular structures can be tedious. As a result, a new synthetic strategy that can address the above challenges is in demand.

1.2.2. Interesting and Unique Properties of Polymers with Complex Architectures

Polymers with complex architectures often exhibit unique properties that are distinctive from their linear counterparts. For example, cyclic brush copolymer decorated with certain side chains, due to its unique ring-like structure, is capable of self-assembling into supramolecular cylindrical tubes in a selective solvent for the branch. As macromolecular architectures profoundly influence the physical or chemical properties of polymers, synthesis of polymers with complex topologies has drawn growing interest over the past decades. Their properties were examined for understanding the fundamental

structure-property relationship, and potential applications in diverse fields such as composite materials, nanotechnology, and biomedical engineering. The properties or morphologies of complex polymer architectures are largely documented in the literature. However, the library still needs to be enriched by exploring the behavior of new macromolecular structures and compositions.

Conjugated polymers (e.g. poly(3-alkylthiophenes) (P3AT)) has attracted considerable interest as promising semiconductor materials for electronic applications in LEDs, FETs, and organic photovoltaics. Regioregular poly(3-hexylthiophene) (*rr*-P3HT) is among the most important conjugated polymers owing to its ease of preparation, good solution processability, and excellent hole mobility. It is composed of a rigid conjugated backbone which allows for efficient π-π stacking, as well as pendant hexyl side chains for improving the solubility. While research effort on P3HT mainly involves linear P3HT or P3HT-based linear block copolymers, P3HT with other architectures have been recently prepared and discovered to exhibit unique properties. For example, a macrocyclic regioregular P3HT was prepared by intramolecular imperfect aldol reaction. Interestingly, the P3HT macrocycles self-assembled into a tubular nanostructure via effective π-π stacking interaction, which is different from the fibril morphology formed from linear P3HT chain. In addition, a P3HT linear brush copolymer was synthesized by ring opening metathesis polymerization (ROMP) of a conjugated macromonomer. The molecular bottlebrush grafted with P3HT side chains exhibits strong aggregation property attributed to the enhanced π-π interaction of P3HTs in bottlebrush architecture. However, to the best of our knowledge, cyclic brush copolymers grafted with P3HT conjugated side chains have not yet been prepared. The P3HT cyclic brush architecture may display interesting morphology or unique properties, which is the subject of our study in this dissertation.

CHAPTER 2

RESEARCH GOALS AND OBJECTIVES

2.1 Goals

The goal of this dissertation is to develop ***new approaches that may practically address the challenges in the preparation of polymeric and hybrid nanostructured materials*** from self-assembled polymer micelle systems via rational design of polymers with complex architectures (e.g., star-like block copolymers) and the utilization of their unique properties, and to ***explore and fundamentally understand the properties and morphology*** of P3HT-based copolymer with newly designed complex topology.

Thus, the dissertation can be divided into two parts. *In the first part*, we aim to address the challenges (i.e., poor size uniformity and controllability, and limited polymer composition/functionality) in preparing polymeric or hybrid nanostructured materials by developing new approaches. The key of the new methods is to replace the traditional self-assembled polymer micelle systems with a unimolecular micelle which can be formed from a stable spherical star-like polymer. In this case, the self-assembly process is eliminated, and polymer composition and functionality can be freely selected without any amphiphlicity constraint. In this strategy, the star-like block copolymers serve as unimolecular templates, which will be designed and synthesized via living/controlled polymerization techniques so the molecular weight can be controlled and the polydispersity of product remains low. This is crucial for realizing uniform shape and tailoring dimension of the resulting nanostructures. For polymeric nanoparticles, photo-crosslinking will be employed as the crosslinking mechanism in this study due to its mild reaction condition, ease of operation and purification. A degradable polymer will be selected as the inner block of star block copolymer because a shell-cross-linked hollow nanoparticle can be prepared by etching the core. For hybrid nanoparticles, sol-gel

chemistry of trimethoxysilyl groups will be utilized to synthesize polymer/silica hybrid nanostructures. Trimethoxysilyl functionalities can be integrated in either the inner block to prepare a solid nanoparticle, or the shell domain to form a hollow nanocapsule. *In the second part*, a cyclic brush copolymer grafted with P3HT as conjugated side chains will be synthesized. Morphology and properties of this new P3HT-based macromolecular architecture will be explored. The fundamental understanding between molecular structure of polymer and its properties will be established.

2.2 Objectives

In this dissertation, the two tasks will be accomplished through addressing the following **specific technical objectives:**

Part 1

For polymeric nanoparticles:

- Design and synthesize a structurally well-defined core-shell star-like block copolymer composed of a hydrophobic degradable polymer as the inner core and a hydrophobic photo-crosslinkable polymer as the shell material through living/controlled polymerization techniques, which can be employed as a unimolecular template to prepare polymeric nanoparticles;
- Synthesize and characterize a core-shell polymeric nanoparticle with the core-shell star block copolymer as spherical template by photo-crosslinking its shell block under high dilution conditions;
- Prepare and analyze a shell-crosslinked hollow nanoparticle by subsequently etching the core of the core-shell polymeric nanoparticle;
- Evaluate the unimolecular polymer nanoparticles developed in this study as nanocarriers for potential drug delivery application by loading dyes as model

compounds in the nanoparticles and studying the dye release behavior under varied crosslinking density.

For hybrid nanoparticles:

- Design and synthesize a structurally well-defined star-like homopolymer containing trimethoxysilyl functionalities through living/controlled polymerization techniques, which can be employed as a unimolecular template to prepare polymer/silica hybrid nanoparticles;
- Prepare and characterize an organo-silica hybrid nanoparticle with the star-like homopolymer as spherical template via intramolecular crosslinking or gelation of the trimethoxysilyl moieties under high dilution conditions;
- Design and synthesize a structurally well-defined core-shell star-like block copolymer with trimethoxysilyl groups incorporated in the shell domain through living/controlled polymerization techniques, which can be employed as a template to produce polymer/silica hybrid nanocapsules;
- Craft and analyze an organo-silica hybrid nanocapsule with an inner cavity by using the core-shell star-like block copolymer as nanoreactor via intramolecular gelation in the shell layer under high dilution conditions.

Part 2

- Design the synthetic route to preparing a well-defined cyclic backbone bearing azide functionalities through the end-to-end ring closure approach;
- Prepare ethynyl-terminated poly(3-hexylthiophene) (P3HT) with well-controlled molecular weights and low PDI via controlled polymerization technique;
- Synthesize and characterize the cyclic brush copolymer with P3HT as the side chains by grafting ethynyl-terminated P3HT onto the cyclic backbone;

- Study and understand the morphology, property and self-assembly behavior of the new P3HT-based macromolecular architecture.

The ***novelty*** of these studies are manifested in developing a state-of-art star-like macromolecular templating strategy for preparing polymeric and hybrid nanostructured materials (e.g., core-shell and hollow nanoparticles), and creating a new P3HT-based macromolecular architecture (i.e., cyclic brush copolymer). The ***significance*** of these studies is as follows. First, the new strategy is much simpler than the traditional self-assembled polymer micelle method for preparing polymeric and hybrid nanostructures as no self-assembly process is required. Second, a wide range of well-tailored unimolecular polymeric or hybrid nanostructured materials with different compositions and functionalities can be crafted based on this viable templating strategy, dispensing with the need for amphiphilic composition as in polymer micelle system. Finally, as the star polymer templates are built up by living/controlled polymerization techniques, their molecular weight can be well-controlled and molecular weight distributions are generally narrow. When these characteristics are transformed into the cross-linked frameworks, the resulting nanostructures exhibit excellent uniformity and well-tailored dimensions by tuning the molecular weights of constituent blocks in star-like polymer precursors.

2.3 Overview of Dissertation Content

Chapter 1 summarizes the recent progress and current status in the field of living/controlled polymerizations, polymers with complex molecular architectures, and provides a comprehensive review on the preparation of polymeric and hybrid nanostructured materials based on self-assembled polymer micelles. The challenges and problems in the preparation of polymeric and hybrid nanostructured materials through traditional polymer micelle systems is critically discussed.

Chapter 2 describes the goals and technical objectives of the studies in this dissertation. In addition, it briefly reviews the content of the thesis, with brief summaries on each chapter.

Chapter 3 includes the polymer synthetic and materials characterization techniques that are employed in the studies presented in this dissertation. Mechanisms and principles of a series of living/controlled polymerization techniques that are crucial for the synthetic work in this dissertation are presented, including anionic polymerizations, controlled radical polymerizations (CRP), ring opening polymerizations (ROP), and living polycondensation. Anionic polymerizations include anionic polymerization of olefins and anionic ring opening polymerization. Controlled radical polymerizations (CRP) include atom transfer radical polymerization (ATRP), reversible addition-fragmentation chain-transfer polymerization (RAFT), and nitroxide-mediated radical polymerization (NMP). Ring opening polymerizations (ROP) include coordination-insertion ring opening polymerization and ring opening metathesis polymerization (ROMP).

Chapter 4 reports on a novel and robust strategy that we have developed for crafting uniform unimolecular core-shell and hollow nanoparticles by exploiting star-like core-shell diblock copolymers comprising biodegradable inner blocks (i.e., core blocks) and photo-crosslinkable outer blocks (i.e., shell blocks containing photo-crosslinkable azido functionalities) as templates. Monodisperse and structurally stable star-like diblock copolymers composed of inner degradable core blocks and outer photo-crosslinkable shell blocks were synthesized via a combination of two living polymerizations, namely, coordination-insertion ring opening polymerization (ROP) followed by reversible addition-fragmentation chain-transfer polymerization (RAFT). Subsequently, uniform unimolecular core-shell nanoparticles were successfully produced by photo-crosslinking the shell blocks of star-like diblock copolymers. The core diameter and shell thickness of nanoparticles are determined by molecular weights of inner core block and outer shell

block, respectively, thereby rendering nanoparticles with tunable structural characteristics. The crosslinking density of nanoparticles can be readily controlled by varying the exposure time of star-like diblock copolymer templates to UV illumination. The selective degradation of inner core blocks yielded hollow polymer nanoparticles which retained structural integrity. The dye encapsulation and release studies revealed that unimolecular core-shell nanoparticles may be exploited as a new class of nanocarriers and promising drug nano-vehicles.

Chapter 5 presents a viable and versatile strategy that we have pioneered for preparing uniform organo-silica hybrid nanoparticles and nanocapsules. The key to our strategy is the implementation of spherical star-like homopolymer and diblock copolymer with well-controlled molecular weights that form unimolecular micelles in solution as nanoreactors. Organo-silica hybrid nanoparticles were crafted by introducing trimethoxysilyl functionalities to the arm of star-like homopolymer. Quite intriguingly, organo-silica hybrid nanocapsules with an interior cavity were created when the trimethoxysilyl moieties were incorporated in the outer block of star-like diblock copolymer. The diameter of hybrid nanoparticles and the shell thickness of hybrid nanocapsules can be readily tailored during the living polymerization of star-like homopolymer and diblock copolymer nanoreactors, respectively. These hybrid nanoparticles and nanocapsules may find promising applications in polymer nanocomposites, water purification, separation, catalysis, and drug delivery. We envision that the nanoreactor strategy is general and robust. By rationally designing nonlinear yet structurally regular polymers possessing metal-containing units, other exotic metal- and metal oxide-containing nanostructures can also be easily accessed for a variety of applications.

Chapter 6 discusses a novel cyclic brush-like copolymer, poly(ethylene oxide)-g-poly(3-hexyl thiophene) (PEO-g-P3HT), composed of conjugated polymer P3HT as side chains which is prepared by a combination of living anionic ring opening polymerization,

quasi-living Grignard metathesis (GRIM) method and click chemistry. A well-defined linear α, ω-dihydroxyl polymer with protected hydroxyl groups in each repeating unit (linear PEEGE) was synthesized via anionic ring opening polymerization. Subsequent cyclization of linear PEEGE was conducted to yield cyclic polymer. Cyclic PEEGE was hydrolyzed to recover hydroxyl functionalities along the cyclic backbone, which were then converted into azide functionalities via several transformation steps. Alkyne functionalized P3HT was synthesized by a quasi-living Grignard metathesis (GRIM) method. Subsequently, it was grafted onto cyclic backbone with azide groups via click chemistry to obtain the final product. The intermediate and final products were systematically characterized and confirmed by GPC, ^{1}HNMR, FT-IR and MALDI-TOF. Morphology and self-assembly behavior of the cyclic PEO-g-P3HT was also investigated by AFM.

Finally, **Chapter 7** describes general conclusions on the studies in this dissertation and proposes the outlook and future research directions.

CHAPTER 3

POLYMER SYNTHETIC AND CHARACTERIZATION TECHNIQUES

The following chapter is intended to provide a brief description of the mechanism and principles for polymer synthetic techniques used throughout the studies in this dissertation.

3.1 Living/Controlled Polymerization

3.1.1. Anionic Polymerization

3.1.1.1. Anionic Polymerization of Olefins

Anionic polymerization is a living chain growth polymerization discovered by Szwarc about half a century ago with carbanion or oxanion as reactive intermediate. Molecular weight can be tailored by varying $\frac{[M]_0}{[I]_0}$, and narrow molecular weight distribution with PDI below 1.1 can be obtained in anionic polymerization. Anionic polymerization is a truly living process since the chain doesn't terminate without purposely added termination agent, and it can continue to grow if additional monomer is added.[232] The living characteristics of anionic polymerization make it a sophisticated approach to construct polymers with well-defined structure.[232]

3.1.1.2. Anionic Ring Opening Polymerization

Similar to anionic polymerization of vinyl monomers, anionic ROP of ethylene oxide and its derivatives proceeds with oxanion as the reactive intermediate.[233-235] Fast

initiation and propagation ensure its living characteristic and low PDI can be achieved. Molecular weight can be tailored by controlling feeding ratio $\frac{[M]_0}{[I]_0}$, and initiator bearing hydroxyl group was deprotonated to initiate chain propagation.[234] Consequently, macromolecules synthesized through ring opening polymerization are always end capped by hydroxyl functional groups after terminating the oxanion with acid, and telechelic polymers can be obtained with initiators bearing either one or two hydroxyl groups. Furthermore, terminal hydroxyl groups can be readily converted to various functionalities by post-modification.

3.1.2. Controlled Radical Polymerization (CRP)

3.1.2.1. Atom Transfer Radical Polymerization (ATRP)

ATRP is a transition metal complexes mediated controlled radical polymerization (CRP). ATRP equilibrium is controlled by the persistent radical effect (PRE).[236] Alkyl halide is employed as initiator in ATRP and homolytically cleaved by transition metal complex activator (Mt^m/L) with activation constant (k_{act}) to generate free radical propagating species and metal complex with higher oxidation state (X-Mt^{m+1}/L).[237] The X-Mt^{m+1}/L species serve as persistent radicals or deactivators in the system. Active propagating radicals are rapidly deactivated (k_{deact}) to reform dormant halide-capped polymer chain intermittently by deactivators (i.e. X-Mt^{m+1}/L) after adding few monomers and the equilibrium is established by PRE with equilibrium constant defined as $K_{eq} = \frac{k_{act}}{k_{deact}}$ as shown in **Scheme 3.1**.[237] Deactivators are built up by termination of free radicals and the irreversible accumulation of deactivators shift ATRP equilibrium to dormant species side. After the equilibrium is established, the concentration of deactivator reaches nearly constant, and propagating radicals concentration is significantly diminished as compared to conventional radical polymerization.[236]

Termination and chain transfer reaction is thus minimized because of the diminished radical concentration in the system. Linear increase of molecular weight (MW) versus conversion is then achieved, which is important characteristic of living polymerization.[7] Fast initiation, fast dynamic exchange between radical propagating species and dormant species, and diminished chain termination reactions ensure essentially the simultaneous growth of all polymer chains and gives ATRP its "living" nature. The whole process in ATRP can be simply viewed as monomer insertion in alkyl halide initiator to obtain polymers end capped with halide group.

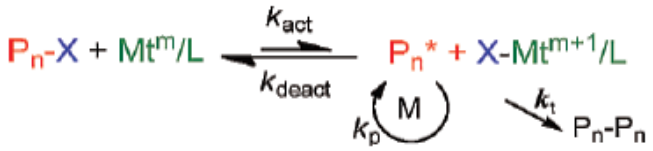

Scheme 3.1. Equilibrium in ATRP.[237]
Reprinted with permission from Ref. [237]. Copyright 2012, American Chemical Society.

Similar to conventional radical polymerization (RP) system, propagation rate in ATRP process is proportional to propagation rate constant, monomer concentration and free radical concentration in steady state. However, steady state propagating radical concentration is established by activation-deactivation equilibrium, rather than initiation-termination equivalence as in conventional radical polymerization as shown in **Equation 1**.[237] As can be shown from **Equation 1**, rate of propagation is affected by monomer, dormant species and activity of catalyst complex as well as reaction conditions such as temperature and solvent. Propagating radical concentration in steady state can be usually increased by enhancing activity of catalyst, and propagation rate will increase due to higher equilibrium constant K_{eq}. However, a relatively higher PDI will be resulted due to more termination reactions associated with higher radical concentration.

$$R_{\mathrm{p}} = k_{\mathrm{p}}[\mathrm{M}][\mathrm{P}_n^*] = k_{\mathrm{p}}K_{\mathrm{ATRP}}\left(\frac{[\mathrm{P}_n\mathrm{X}][\mathrm{Cu}^{\mathrm{I}}/\mathrm{L}][\mathrm{M}]}{[\mathrm{X}{-}\mathrm{Cu}^{\mathrm{II}}/\mathrm{L}]}\right)$$

Equation 1[237]

For a well-controlled ATRP process, MW of the product increases almost linearly with conversion, and can be precisely controlled and engineered based on **Equation 2** assuming apparent rate constant is known.[237] PDI of the macromolecules depends on the ratio of propagation and deactivation rate constants $\frac{k_p}{k_{deact}}$, monomer conversion, as well as concentration of deactivator and dormant species, which can be derived quantitatively from **Equation 3**.[238] The molecular weight distribution decreases as monomer is converted into polymers. Fast deactivation achieved either by large deactivation rate constant or higher deactivator concentration is very important to maintain low PDI. Alternatively, narrow molecular weight distribution can be obtained by reducing concentration of dormant species, yielding targeting higher molecular weight.[237]

$$MW = \frac{[M]_0}{[R-X]_0} * C$$

$$In\left(\frac{1}{1-C}\right) = k_{app}t$$

Where $k_{app} = \frac{k_p K_{ATRP}[P-X][Cu^{I}/L]}{[X-Cu^{II}/L]}$

Equation 2[237]

$$\frac{M_{\mathrm{w}}}{M_{\mathrm{n}}} = 1 + \frac{1}{\mathrm{DP}_n} + \left(\frac{k_{\mathrm{p}}[\mathrm{P}_n\mathrm{X}]}{k_{\mathrm{deact}}[\mathrm{X}{-}\mathrm{Cu}^{\mathrm{II}}/\mathrm{L}]}\right)\left(\frac{2}{p} - 1\right)$$

Equation 3[238]

To maintain narrow molecular weight distribution and achieve well-controlled ATRP system, alkyl halide initiator should be sufficiently reactive for specific selected monomer to ensure fast initiation compared to propagation ($k_{act} > k_p$). Activation rate constants (k_{act}) of various ATRP initiator systems with Cu^IX/PMDETA as catalyst are summarized in **Scheme 3.2** for comparison.[237]

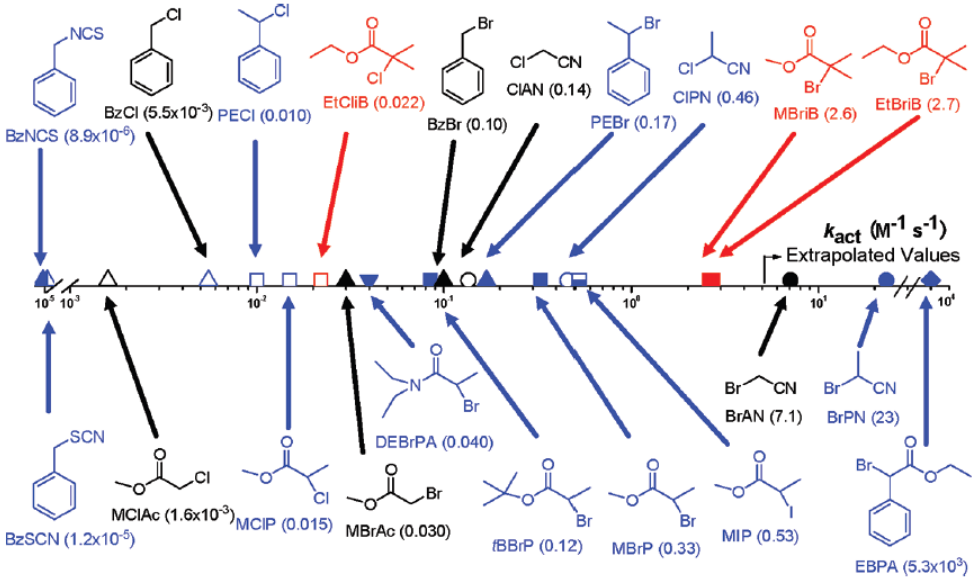

Scheme 3.2. Dependence of activation rate constant on various initiator systems.[237]
Reprinted with permission from Ref. [237]. Copyright 2012, American Chemical Society.

Equilibrium constant not only depends on alkyl halides, but also depends on structure of monomers and catalyst with k_{act} being more affected. In addition, block copolymer synthesized by ATRP technique should follow the order of monomer reactivity, otherwise $k_{act} < k_p$ will be resulted and broad PDI will be obtained. However, halogen exchange has been introduced in ATRP technique to decrease k_p as

well as maintaining a high activation constant, thus achieve comparable k_{act} and k_p. It is worth mentioning that copper complex has been widely used as ATRP catalyst. k_{act} for CuBr complex with various ligands using EtBriB as initiator are summarized in **Scheme 3.3**.[237]

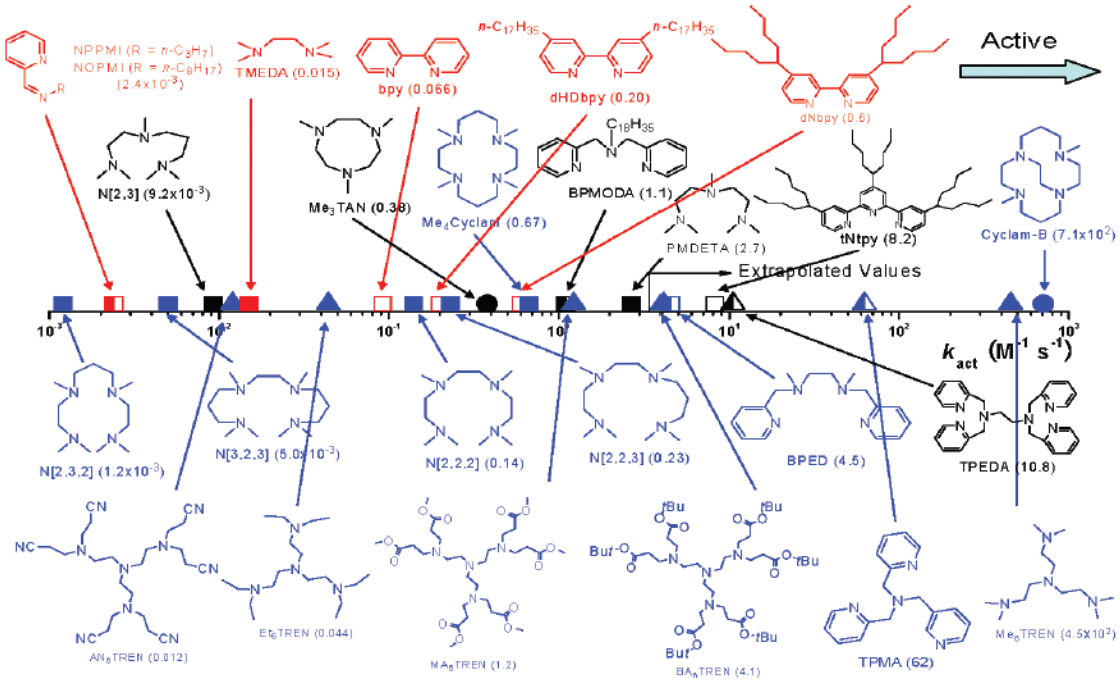

Scheme 3.3. Dependence of activation rate constant on various ligands.[237]
Reprinted with permission from Ref. [237]. Copyright 2012, American Chemical Society.

ATRP equilibrium constant controls the propagation rate and extent of termination side reaction by controlling steady state radical concentration. However, the dynamics of the exchange reaction between active radical species and dormant species is controlled by deactivation reaction, and k_{deact} should be as high as possible to maintain concurrent growth of all polymer chains and a low PDI. Consequently, appropriate catalyst should be chosen for each specific monomer to obtain well controlled system. For monomers with low reactivity, catalyst should be selected to possess high K_{ATRP} to

maintain reasonable polymerization rate and also preserve large k_{deact}. However, for highly reactive monomers such as methyacrylates, a catalyst with low reactivity should be selected to decrease the steady state radical concentration, thus minimizing termination and chain transfer side reactions. Alternatively, ATRP process is usually not compatible with some functional groups such as carboxyl or amine groups due to their coordination with transition metal competing with ligands, thus decreasing catalyst reactivity. Consequently, these functional groups need to be protected to maintain a well-controlled ATRP system and de-protected after polymerization.[238]

3.1.2.2. Reversible Addition–Fragmentation Chain Transfer Polymerization (RAFT)

RAFT polymerization is a system that is probably the closest to conventional free radical polymerization since only RAFT agent bearing high chain transfer constant was added to conventional radical polymerization system to mediate the polymerization. Its reaction kinetics follows traditional radical polymerization kinetics ideally. Chain transfer from propagating radical to RATF mediating agent or dithioester-capped dormant chain is reversible, fast and only at the chain end compared to irreversible and random chain transfer process in traditional radical polymerization system. The living characteristic is thus achieved by the fast dynamic exchange between propagating radical species and dithioester-capped dormant species.[239]

RAFT is a degenerative transfer (DT) process. It can be generalized and described by the addition-fragmentation equilibria (**Scheme 3.4)**.[239] During the pre-equilibrium, propagating radical (P_n) produced from conventional free radical initiator react with thiocarbonylthio group (RSC(Z)=S, compound **1**) to form the intermediate radical and its subsequent fragmentation gives one new free radical (R) together with one polymeric thiocarbonylthio group (PnSC(Z)=S, compound **3**), which is the dormant species in RAFT process. Re-initiation of the fragmented new radical produces a new propagating

radical Pm, which is subsequently added to thiocarbonylthio group (PnSC(Z)=S, compound **3**) to exchange with this dormant species. After the chain equilibrium is established, fast dynamic exchange between active propagating radicals and dormant thiocarbonylthio compound realize rapid transfer of small amount of radical active centers along all polymer chains, and thus ensures essentially concurrent growth of all polymer chains to produce materials with low polydispersity.

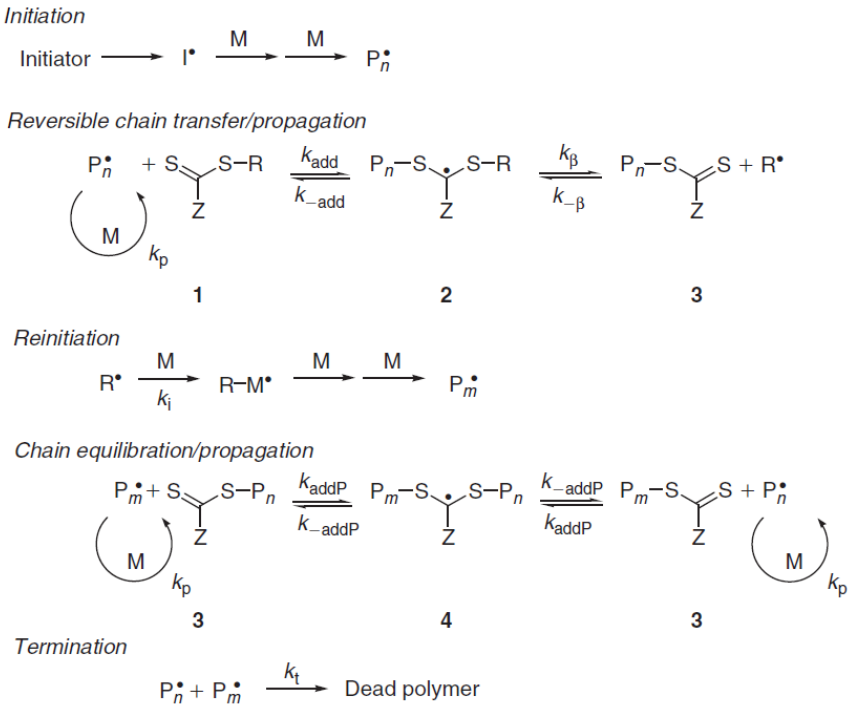

Scheme 3.4. Mechanism of RAFT Polymerization.[239]
Reprinted with permission from Ref. [239]. Copyright 2008, Elsevier.

Termination reaction still occurs in RAFT with the generation of "dead polymers", so it is not a true "living" process. Polymerization kinetics is not affected in an ideal RAFT process, and steady state radical concentration is established by initiation-termination equilibrium as in conventional RP. Propagation rate can be derived with steady state assumption as shown in **Equation 4**.[35] However, "living' characteristics can

be achieved in RAFT through rapid dynamic exchange between active radical and dormant thiocarbonylthio moiety-capped species, with MW increasing almost linearly versus conversion.[35] Thus, similar to ATRP process, molecular weight can be designed and engineered by controlling the feeding ratio between monomer and RAFT agent concentration as well as conversion which can be pre-determined if apparent rate constant is known, as derived in **Equation 5**.[35] It is noteworthy that RAFT produce polymers with smaller molecular weight than conventional RP.

$$R_p = (k_p/k_t^{1/2}) R_i^{1/2}[M]$$

Equation 4[35]

$$MW = \frac{[M]_0}{[RAFT]_0} * C$$

$$In\left(\frac{1}{1-C}\right) = k_{app} t$$

Where $k_{app} = (k_p/k_t^{1/2}) R_i^{1/2}$

Equation 5[35]

To ensure an efficient RAFT process and a well-controlled polymerization, transfer rate coefficient $k_{tr} = k_{add} \frac{k_\beta}{k_{\beta+}k_{-add}}$ and resulting chain transfer constant $C_{tr} = \frac{k_{tr}}{k_p}$ need to be sufficiently high to maintain a successful chain transfer process to RAFT compound in pre-equilibrium and fast dynamic exchange between active and dormant species in chain equilibrium is required with a high k_{addp}. Thus, RAFT agent and polymeric RAFT agent generated should possess a sufficiently reactive C=S double bond to provide high k_{add} and k_{addp}. Fragmentation rate (k_β) of the intermediate radicals formed (2 and 4) should be sufficiently high and intermediate 2 should fragment

in favor of product to give a high transfer constant C_{tr}. Alternatively, the expelled radical R should efficiently reinitiate chain propagation rather than reversibly added back to intermediate 2.[241] Consequently, appropriate RAFT agent should be carefully selected for a chosen monomer to impart a controlled RAFT process and the property of RAFT agent can be tailored by its R and Z groups.

Z group tailors chain transfer constant of selected RAFT agent by changing addition rate (k_{add} and k_{addp}) of radicals to C=S group.[241] On the other hand, R group tunes transfer constant by controlling fragmentation rate and partition of intermediate 2 between product and starting material ($\frac{k_\beta}{k_{\beta+}k_{-add}}$), which is dictated by leaving ability of R versus propagating radicals.[242] R with better leaving group ability imparts higher $\frac{k_\beta}{k_{\beta+}k_{-add}}$, and leaving ability of R is in turn determined by radical stability, steric and polar effects.[242] Furthermore, generated R should be able to effectively re-initiate propagation rather than adding back to polymeric RAFT agent.

The general guideline for selecting appropriate RAFT agent for various polymerization systems is shown in **Figure 3.1**.[239] For highly active monomers such as methyl methacrylate, due to its high propagation rate constant and high radical stability, more effective Z group with high addition rate and R with better leaving ability should be selected to ensure a sufficiently high transfer constant ($C_{tr} = \frac{k_{tr}}{k_p}$) for maintaining a well-controlled RAFT system. On the other hand, for less active monomers like vinyl acetate, less effective Z group with higher fragmentation rate should be selected to avoid retardation and a broader range of R group can be used. However, it is better to choose R group that's not too stable to re-initiate.

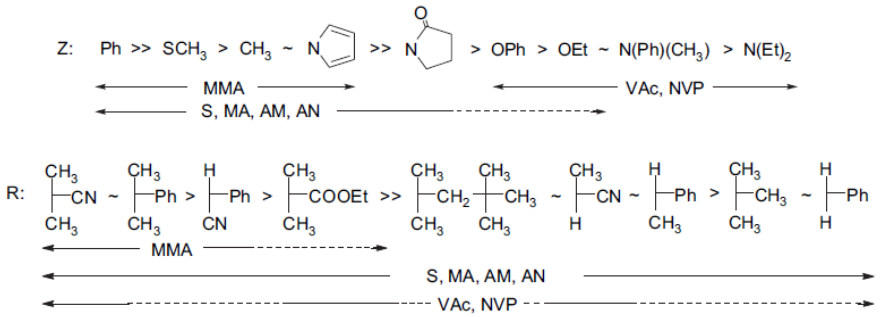

Figure 3.1. General guideline for selecting appropriate RAFT agent.[239]
Reprinted with permission from Ref. [239]. Copyright 2008, Elsevier.

RAFT has been recognized as one of the most efficient techniques among controlled radical polymerizations due to its high compatibility with a variety of monomers, functionalities, and reaction mediums such as water.

3.1.2.3. Nitroxide-Mediated Polymerization (NMP)

Similar to ATRP, NMP is also a reversible-deactivation radical polymerization that follows PRE operating principle. Nitroxides such as TEMPO serve as the persistent radical in NMP and reversibly deactivate propagating radical to form dormant alkoxyamine species. The mechanism of NMP is shown in **Scheme 3.5**.[8] It is the fast dynamic exchange between alkoxyamine and propagating radicals that achieved control and living characteristics in NMP process.

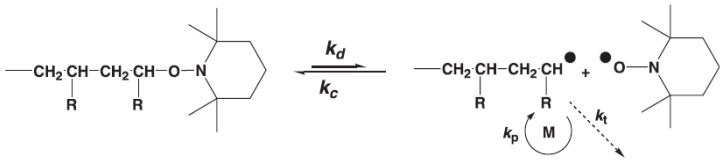

Scheme 3.5. Mechanism of NMP.[8]
Reprinted with permission from Ref. [8]. Copyright 2007, Elsevier.

3.1.3. Ring Opening Polymerization (ROP)

3.1.3.1. Coordination-insertion Ring Opening Polymerization

In ROP of ε-caprolactone, stannous(Ⅱ) 2-ethylhexanoate ($Sn(Oct)_2$) is commonly employed as the catalyst due to its versatility and high efficiency. The polymerization mechanism has been widely studied and the most accepted one is coordination-insertion process, in which compounds containing hydroxyl groups are assumed to be coordinated by catalyst to give tin(Ⅱ) alkoxide as actual initiator.[10] Polyester chain growth then proceeds from the metal alkoxide active specie via monomer insertion as shown in **Scheme 3.6**.[10] Stereoregular polyesters with low PDI can be produced from this process. In addition, MW can be tuned via controlling monomer to alcohol feeding ratio, i.e. $\frac{[M]_0}{[I]_0}$, and the resulting polymer possesses hydroxyl functional end groups which could be involved in a variety of further chemical transformations.

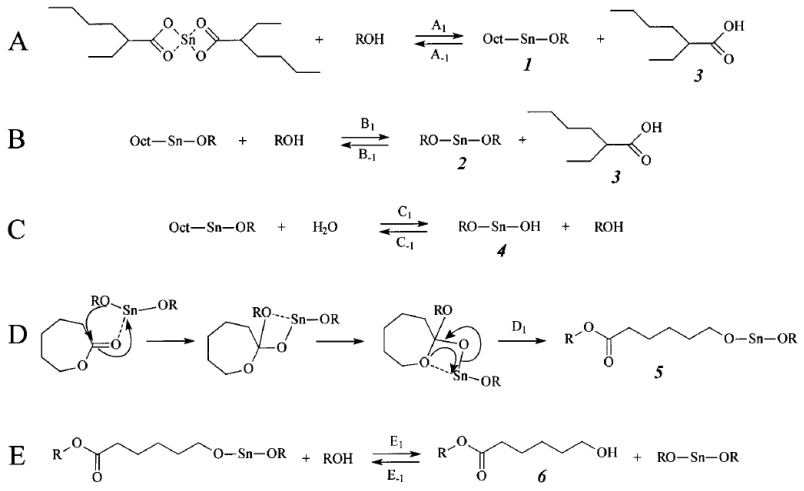

Scheme 3.6. Mechanism of $Sn(Oct)_2$ Catalyzed Ring Opening Polymerization.[10]
Reprinted with permission from Ref. [10]. Copyright 2002, American Chemical Society.

3.1.3.2. Ring Opening Metathesis Polymerization (ROMP)

ROMP is a chain growth polymerization of cyclic olefin monomers based on olefin metathesis with metal center as propagating species. Different from typical olefin addition reaction, unsaturation associated with the cyclic olefin monomers is conserved after ROMP. Importantly, ROMP reactions are usually reversible, and equilibrium between polymerization and de-polymerization exists. Consequently, ROMP is generally favored with temperature as low as possible (below ceiling temperature) and the highest possible monomer concentration. Living ROMP can be achieved by development and manipulation of a variety of metal catalyst, with ruthenium based catalyst being the most efficient and popular one. MW increased almost linearly versus C and low PDI was obtained in living ROMP. The catalyst is capable of fast and complete initiation in living ROMP and the propagating metal center can be efficiently quenched by functional terminating agent to produce end functionalized polymers. Thus, living ROMP provides another efficient tool for the preparation of well-defined polymers with complex architectures.[14]

3.1.4. Living Polycondensation

Polycondensation has been recently realized as a living polymerization process and living polycondensation proceeds with chain growth mechanism.[243] Four possible mechanisms are generally involved in realizing living polycondensation.

Regioregular P3HT is widely synthesized by a quasi-living Grignard metathesis (GRIM) method and its mechanism is shown in **Scheme 3.7**.[244,245] GRIM is essentially a living polycondensation technique achieved by activation of polymer chain end via transferring catalyst to its end.

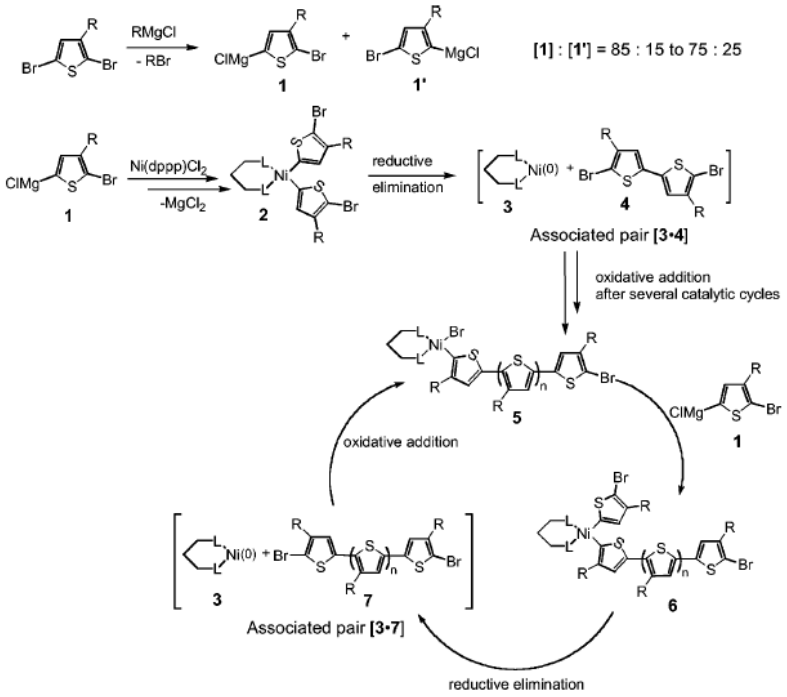

Scheme 3.7. Mechanism of GRIM.[245]
Reprinted with permission from Ref. [245]. Copyright 2009, American Chemical Society.

3.2 Characterization Techniques

The polymers with complex architectures, polymeric and hybrid nanostructures synthesized in this study have been characterized and analyzed using a series of materials characterization techniques. Specifically, NMR, GPC, FT-IR, and UV-Vis were used to analyze the topology, molecular weight, polydispersity, and functionalities of the non-linear polymers, while AFM, TEM, and DLS were mainly employed to probe the structure, morphology, and dimension of the polymeric and hybrid nanoparticles.

3.2.1. Nuclear Magnetic Resonance (NMR)

NMR is used to analyze the chemical composition, and estimate the real molecular weight of the macromolecules with complex architectures including star

polymers and cyclic polymers by end group analysis. The ^{1}H NMR spectra of the products were acquired using a Bruker 400MHz spectrometer with the solvent resonances as the internal standard. $CDCl_3$ was used as the deuterated solvent in most of the measurements, while for polar polymers that cannot be dissolved in $CDCl_3$, DMSO-d_6 was utilized for the characterizations in this study. The resonance from the polymer end group must be resolved in NMR spectra for estimating the molecular weight of the product. In order to integrate the peak and obtain data with higher accuracy in this study, the sensitivity of NMR can be enhanced by increasing the sample concentration, scanning time, or using the spectroscopy with higher magnetic strength. For high MW polymers with complicated macromolecular topologies, their real molecular weights are hard to be obtained by other analytical techniques such as GPC or MALDI-TOF. As a result, NMR provides an important tool in this work to estimate the real molecular weight and probe the structure of the macromolecules.

3.2.2. Gel Permeation Chromatography (GPC)

Molecular weights and PDI of the polymers were obtained by GPC (Shimadzu) equipped with a LC-20AD HPLC pump and a refractive index detector (RID-10A, 120V). THF was used as the mobile phase for the measurement at the flow rate of 1.0 mL/min at 35°C. One Phenogel 5u Linear column and one Phenogel 5u 10E4A mixed bed column were calibrated with 10 polystyrene standard samples with molecular weights ranging from 1.2×10^6 to 500 g/mol. The molecular weights acquired by GPC for polymers with complex compostions or non-linear structures are not real, which are relative compared to linear polystyrene standards. Thus, MWs acquired from GPC meausrements and their values estimated by NMR end group analysis were combined with the calculated theoretical molecular weights based on monomer conversion to analyze the imitation efficiency and topologies of the macromolecules synergistically.

3.2.3. Fourier Transform Infrared Spectroscopy (FT-IR)

Important functional groups on the macromolecules such as azide groups or trithioester moieties were probed via FT-IR analysis. FT-IR spectra of the products were collected on the Shimadzu IRAffinity1 spectrometer equipped with a Miracle Single Reflection Horizontal ATR Accessory (Pike Technologies).

3.2.4. UV−Vis Spectrophotometer (UV-Vis)

UV-Vis was mainly employed in this study to confirm the grafting of trithiocarbonate RAFT agent onto star polymers and loading of guest molecules in the core-shell nanoparticles. UV-visible spectra of absorption from thiocarbonylthio group or polymeric NPs encapsulated wity dye molecules were recorded using Shimadzu UV-2600 UV-VIS spectrophotometer.

3.2.5. Atomic Force Microscope (AFM)

The morphologies of core-shell/hollow polymeric nanoparticles as well as the self-assembled nanostructures from cyclic brush copolymers were examined by AFM. The nanostructures of the nanoparticles or supramolecular assemblies were directly visualized using AFM (Bruker Dimension Icon) which is operated in the tapping mode at 0.5Hz scanning rate. The samples for AFM measurements were prepared by spin-coating the dilute nanoparticle solution onto Si substrate at 3000 rpm for 1 min (Headway PWM32 spin coater). While for the cyclic brush copolymer, the samples were prepared by spin-coating the toluene solution of the macromolecule onto Si substrate at 2000 rpm for 1 min.

3.2.6. Transmission Electron Microscopy (TEM)

Core-shell/hollow polymeric nanoparticles and the polymer/silica hybrid nanostructures were studied by TEM. The images were acquired by JEOL TEM 100CX, which was operated at 100kv. TEM samples were prepared by drop-coating a dilute nanoparticle solution onto the 400 mesh carbon-coated copper TEM grid. Due to the low electron density of polymeric nanoparticles and low contrast of the results, prior to TEM imaging, the organic samples were stained with RuO_4 vapor for various periods of times to enhance the contrast. The core-shell structure of the polymeric nanoparticles and interior cavity of the hybrid nanocapsule prepared in this study were substantiated by direct TEM imaging. Thus TEM is an important analytical imaging tool for this work.

3.2.7. Dynamic Light Scattering (DLS)

Size of the star polymers and dimension of the nanoparticles were analyzed by DLS characterizaiton. DLS measurements were performed using laser light scattering spectrometer (Malvern Zetasizer Nano ZS) at 25°C.

3.2.8. Photoluminescence Spectroscopy (PL)

PL was utilized for the purpose of investigating the controlled release behavior of encapsulated guest molecules from the core-shell nanoparticles. The photoluminescence spectra were taken using a Shimadzu RF-5301 spectrofluorometer (equipped with a 150 W xenon lamp light source and a R928 photomultiplier), which covers a wavelength range of 220-900 nm with a resolution of 1.5 nm.

CHAPTER 4

DESIGN AND SYNTHESIS OF SPHERICAL STAR BLOCK COPOLYMER AS TEMPLATE TO DEVELOP UNIMOLECULAR CORE-SHELL AND HOLLOW POLYMER NANOPARTICLES

4.1 Introduction

Amphiphilic linear block copolymers possess the propensity to self-assemble into a large variety of complex nanoscale assemblies, including spherical micelles,[246] cylindrical or wormlike micelles,[247] and vesicles,[248] when dispersed in selective solvents.[249] These nanoscale micelles are, however, often kinetically trapped in non-equilibrium states. As a result, their characteristics and shapes for a given system depend sensitively on concentration, solvent properties, temperature, pH, etc.,[92] and are subjected to vary in response to changes in these experimental conditions.[130] For example, dissociation of nanoscale assemblies into individual linear polymer chains can occur when the solution concentration decreases below the critical micelle concentration (CMC). Thus, crosslinking of either the core or shell of self-assembled nanostructures is carried out to improve their stability by essentially locking in the structures.[33,93,136] However, the access to core-shell polymer nanoparticles that are dimensionally and functionally well-defined is still limited due in part to the relatively poor size control and comparatively high polydispersity of nanostructures obtained via self-assembly of linear block copolymers.[230,231] It is noteworthy that the common need for amphiphilic characteristics of block copolymers in order to impart self-assembly restricts the scope of selection on their chemical compositions and functionalities. Clearly, it is challenging to realize well-tailored core-shell or hollow polymer nanoparticles from self-assembled micelles.

In stark contrast to micelles comprising linear amphiphilic polymer chains that are dynamically stable as noted above, star-like polymers can readily form static unimolecular micelles in solution, that is, structurally stable spherical macromolecules. Star-like polymers are a class of branched macromolecules in which multiple linear chains or arms are covalently connected to a multifunctional core. A variety of star-shaped homopolymers and core-shell block copolymers as well as miktoarm star polymers have been synthesized by living polymerization techniques via either the core-first or arm-first approach.[22,43-46] Recent advances in living/controlled polymerization renders the preparation of star-like core-shell block copolymers with a precisely controllable topology. Intriguingly, they may be utilized as unimolecular micellar templates for creating core-shell and hollow polymer nanoparticles with controlled dimensions and compositions. This has yet to be explored.

Drug delivery and controlled release technologies have made a pronounced impact on the medical field.[212] Loading guest chemotherapeutic agents in nanocarriers can result in improved drug stability, reduced clearance, and long circulation time. In this context, a variety of nanocarriers have been developed for drug delivery applications, including liposome, polymer-drug conjugates,[214] polymer micelle nanoparticles,[215,216] and unimolecular micelles.[222,223] Among them, polymer micelle nanoparticles[224] have received attention due to highly enhanced drug solubility and long circulating half-life. Unimolecular micelles exhibit improved stability compared to self-assembled polymer micelles. However, they are still unstable above the critical aggregation concentration (CAC) and the aggregation is often observed.[225-227] It is worth noting that the instability would trigger premature drug release and potentially harm healthy tissue.[222,225] A well-controlled size is particularly important for tumor-targeted drug delivery as the effective size of nanocarriers falls in the range of 20-100 nm.[228,229] In this context, it is highly desirable yet challenging to create structurally well-defined nanostructures with good stability, monodispersity, and precise size controllability as a new type of drug vehicle.

Herein, we report a robust strategy for crafting monodisperse unimolecular core-shell and hollow nanoparticles by exploiting star-like core-shell diblock copolymers comprising biodegradable inner blocks (i.e., core blocks) and photo-crosslinkable outer blocks (i.e., shell blocks containing photo-crosslinkable azido functionalities) as templates. Star-like photo-crosslinkable core-shell diblock copolymers were synthesized by a combination of two consecutive living polymerization techniques, and adopted a spherical conformation. Photo-crosslinking of azido moieties in the shell blocks was chosen to yield uniform unimolecular core-shell nanoparticles as the photo-crosslinking proceeds under simple and mild UV irradiation and the crosslinking density can be facilely tuned by varying UV intensity and irradiation time.[166,167] By selectively removing the core blocks, hollow polymer nanoparticles can be formed, suggesting the in vitro degradability of inner blocks. The versatility of unimolecular core-shell nanoparticles as intriguing and effective nanocarriers for potential use as drug nano-vehicles was elaborated by loading dyes (e.g., rhodamine B) as model compounds in nanoparticles. Dye-loaded nanoparticles with controlled size and low polydispersity were obtained as a result of spherical shape and monodisperse characteristics of star-like core-shell diblock copolymer templates. More importantly, the release behavior of dyes within nanocarriers was tracked by fluorescence spectroscopy. It is interesting to note that the dimension of nanoparticles, that is, the diameter of the core and the thickness of the shell, can be readily controlled by simply tuning the molecular weights of the core block and the photo-crosslinkable shell block respectively. These rationally designed photo-crosslinkable core-shell star-like diblock copolymers hold promise for the construction of unimolecular polymer nanoparticles as nanocarriers and delivery vehicles.

4.2 Experimental Details

Materials. Stannous octoate ($Sn(Oct)_2$, 95%), oxalyl chloride (≥99%), 2-(dodecylthiocarbonothioylthio)-2-methylpropionic acid (TC; 98%, HPLC grade), Rhodamine B (RhB; 95%), sodium azide (≥99.5%), and anhydrous $MgSO_4$ were purchased from Sigma-Aldrich, and used as received. β-cyclodextrin (β-CD, Sigma-Aldrich) was dried at 80°C under reduced pressure overnight prior to use. ε-caprolactone (ε-CL, Sigma-Aldrich, 97%) and 4-chloromethyl styrene (Sigma-Aldrich, 90%) were distilled over CaH_2 under reduced pressure prior to use. Ruthenium (VIII) oxide (Strem Chemicals Inc., 0.5%) was used as received. Anhydrous dichloromethane (DCM) and N,N-dimethylformamide (DMF) were obtained from a commercial solvent purification system (MB-SPS, MBraun Inc.). Osmapentalyne was obtained from Xiamen University, China.[250] All other reagents were purified by common purification procedures.

Synthesis of star-like PCL. 21-arm star-like polycaprolactone (PCL) was synthesized via controlled ring opening polymerization of ε-CL using β-CD as multifunctional initiator and $Sn(Oct)_2$ as catalyst. To impart efficient initiation and homogeneous polymerization, DMF was used as solvent to solubilize β-CD. All polymerizations were performed under stringent anhydrous conditions to avoid initiation from water. Three samples with different molecular weights were synthesized by varying the $Sn(Oct)_2$ concentration or temperature (**Table S1**). It is clear that larger catalyst concentration and higher temperature resulted in faster polymerization rate and nearly complete monomer conversion (**Table S1**). As demonstrated elsewhere,[251,252] ring opening polymerization catalyzed by $Sn(Oct)_2$ proceeds with in situ metal alkoxide generated as the active center, and it is the fast dynamic exchange between dormant and reactive species that maintains living polymerization characteristics. Thus, the polymerization rate increased as a result of increased concentration of reactive center in an equilibrium with dormant –OH species at the [Sn]/[OH] ratio below 0.5. On the other hand, the increase in temperature led to faster reaction rate due to higher rate constant.

A typical polymerization procedure is described as follows: A flame-dried ampule was connected to a Schlenk-line where the exhausting-refilling processes were repeated for three times. β-CD (97.5mg) was dried at 80°C under reduced pressure overnight, which was subsequently dissolved in anhydrous DMF and transferred into a reaction ampule together with $Sn(Oct)_2$ (36.5mg) and dry ε-CL monomer (10ml) under argon atmosphere. The ampule was then immersed into an oil bath at 130°C. The polymerization was allowed to proceed for a desirable amount of time. After being cooled to room temperature, the crude polymer was diluted with chloroform and precipitated in cold methanol for three times, yielding the purified product. The pure homopolymer was finally dried in vacuum oven. Yield: 10 g (97.1%).

Synthesis of TC-end-functionalized star-like PCL (i.e., PCL-TC). A round bottom flask was connected to a Schlenk-line where exhausting-refilling processes were repeated for three times. Trithiocarbonate RAFT agent (TC; 0.12g) was dissolved in anhydrous CH_2Cl_2 (5mL) and then transferred to a flask under argon atmosphere, followed by the addition of oxalyl chloride (0.43mL). The reaction mixture was stirred at room temperature for 3h until the gas evolution stopped. The excess reagents were then removed via rotary evaporation. The residue was re-dissolved in anhydrous CH_2Cl_2 (5ml). Subsequently, star-like PCL solution (1g in 15mL CH_2Cl_2) was added. After stirring at room temperature for 19h, the content was precipitated in cold methanol for three times. The product was finally dried at 50°C in a vacuum oven. Yield = 0.92 g (90%). ^{1}H NMR: Conversion > 95%.

Synthesis of core-shell star-like PCL-b-(P(S-Cl)) via RAFT. Core-shell star-like polycaprolactone-block-poly(4-chloromethyl styrene) (denoted PCL-*b*-P(S-Cl)) was effectively prepared by reversible addition-fragmentation polymerization (RAFT) of 4-chloromethyl styrene in toluene in the presence of star-like PCL-TC as the mediating

chain transfer agent via thermal initiation. In a typical process, an ampoule charged with star-like PCL-TC (0.15g), 4-chloromethyl styrene monomer (1.67ml) and toluene (4.28ml) was degassed by three freeze-evacuate-thaw cycles in liquid N_2, and then sealed. The polymerization was conducted at 120°C without adding azobisisobutyronitrile (AIBN) initiator. After proceeding to a desirable time, the reaction was quenched by immersion in liquid N_2. The reaction mixture was then diluted with CH_2Cl_2 and precipitated in cold methanol to obtain crude product. To remove linear homopolymer produced during the RAFT process, the selective precipitation of crude product in a tetrahydrofuran (THF)/methanol mixture was performed three times to yield pure copolymers. The final product was dried to a constant weight under vacuum at 50°C.

Synthesis of crosslinkable copolymer template star-like PCL-b-P(S-N_3). The chlorine groups on P(S-Cl) shell blocks in PCL-*b*-P(S-Cl) were substituted by azido functionalities to produce star-like PCL-*b*-P(S-N_3) template. Specifically, star-like PCL-*b*-P(S-Cl) (50mg) and sodium azide (55 mg) were mixed in DMF (4mL). The reaction mixture was stirred at room temperature for 24 h, and then precipitated in cold methanol. The crude product was re-dissolved in CH_2Cl_2, and then washed with distilled water three times. The obtained organic layer was dried by anhydrous $MgSO_4$, and precipitated in cold methanol again after concentration. The final pure product was collected and then dried in vacuum oven at 40°C.

Preparation of unimolecular core-shell polymer nanoparticles via intramolecular crosslinking. Core-shell polymeric nanoparticles were formed by crosslinking pendant azido groups on the shell blocks of the star-like copolymer template via UV irradiation. It is worth noting that the dilute condition was invoked to ensure only intramolecular crosslinking. In a typical procedure, star-like PCL-*b*-P(S-N_3) template (2mg) was

dissolved in chloroform (4ml) and filtered using a 0.45μm PTFE filter. The solution was then exposed to UV irradiation at room temperature under stirring. The crosslinking was stopped at various exposure times to afford different degrees of crosslinking density. The mixture was then concentrated under vacuum and precipitated in methanol to yield final product.

Formation of hollow nanoparticles by degrading core blocks. Core-shell nanoparticles (7mg) were dissolved in 22 ml dioxane with the addition of 1 ml 10M HCl solution. The reaction mixture was placed in a constant temperature oil bath at 90°C and refluxed for 3 days. The solution was then concentrated and precipitated in methanol to yield final product.

Encapsulation of dye. Due to intrinsic spherical shape of star-like PCL-*b*-P(S-N_3) diblock copolymer and the stable characteristics of crosslinked core-shell nanoparticles, a simple yet versatile encapsulation technique using dye as a model compound was developed. Briefly, star-like diblock copolymer templates (1mg) were mixed with dyes (RhB (14mg) or osmapentalyne (10mg)) in $CHCl_3$ (2mL). The solution was filtered using 0.45μm PTFE filter. The mixture was then exposed to UV irradiation for various exposure times under stirring at room temperature to form dye-loaded nanoparticles. The organic solvent was removed under reduced pressure. To remove dyes that were not encapsulated within nanoparticles, nanoparticles were washed with methanol for a desirable amount of time and separated via centrifugation at 5000rpm for 5min. Final products (i.e., nanocarriers) were found to exhibit the same color as dyes.

Dye release study. For the dye release studies, RhB-loaded nanoparticles were re-dispersed in solvent (chloroform or THF). Subsequently, fluorescence emission spectra of solution were directly measured at predetermined times. The amount of RhB released

from nanoparticles into solution was tracked by monitoring the fluorescence intensity at the emission wavelength of 572 nm (excited at 559 nm).

Characterizations. Molecular weights of polymers were obtained by gel permeation chromatography (GPC; Shimadzu) equipped with a LC-20AD HPLC pump and a refractive index detector (RID-10A, 120V). THF was used as the mobile phase at the flow rate of 1.0 mL/min at 35°C. One Phenogel 5u Linear column and one Phenogel 5u 10E4A mixed bed column were calibrated with 10 polystyrene standard samples with molecular weights ranging from 1.2×10^6 to 500 g/mol. All ^{1}H nuclear magnetic resonance (NMR) spectra were obtained using a Bruker 400MHz spectrometer with the solvent resonances as the internal standard. $CDCl_3$ was used as the solvent in all measurements. The morphologies of core-shell and hollow nanoparticles were examined by atomic force microscope (AFM; Bruker Dimension Icon; operated in the tapping mode at 0.5Hz scanning rate). The samples for AFM measurements were prepared by spin-coating the dilute nanocapsule solution onto Si substrate at 3000 rpm for 1 min (Headway PWM32 spin coater). Core-shell and hollow nanoparticles were also imaged by transmission electron microscopy (TEM) (JEOL TEM 100CX; operated at 100kv). TEM samples were prepared by drop-coating a dilute nanocapsule solution onto the 400 mesh carbon-coated copper TEM grid. Prior to TEM imaging, samples were subsequently stained with RuO_4 vapor for various times. Dynamic light scattering (DLS) measurements were performed using laser light scattering spectrometer (Malvern Zetasizer Nano ZS) at 25°C. FTIR spectra were collected on the Shimadzu IRAffinity1 spectrometer equipped with a Miracle Single Reflection Horizontal ATR Accessory (Pike Technologies). UV-visible spectra were recorded using Shimadzu UV-2600 UV-VIS spectrophotometer. The photoluminescence spectra were taken using Shimadzu RF-5301 spectrofluorometer (equipped with a 150 W xenon lamp light source and a R928

photomultiplier), covering a wavelength range of 220-900 nm with a resolution of 1.5 nm.

4.3 Results and Discussion

4.3.1. Synthesis of Core−shell Star Diblock Copolymers

The synthetic route to unimolecular polymer nanoparticles based on core-shell star-like block copolymers is depicted in **Scheme 4.1a**. The core-first approach was employed to yield high initiation efficiency and a well-defined architecture of the resulting star-like block copolymers. Because of the hydrolytic and in vivo degradability of poly(ε-caprolactone) (PCL), star-like PCL with terminal hydroxyl functionalities was synthesized as the biodegradable core. Specifically, star-like PCL with narrow molecular weight distribution (i.e., polydispersity index, PDI < 1.1) was synthesized via coordination-insertion ring opening polymerization (ROP) of ε-caprolactone by using $Sn(Oct)_2$ as catalyst and β-cyclodextrin (β-CD) with 21 hydroxyl groups on its surface as initiator due to its biocompatibility (**Scheme 4.1a**). Three samples with different molecular weights were synthesized and summarized in **Table 4.1**. The methylene proton signal at 3.64 ppm in ^{1}H-NMR spectrum indicated that star-like PCL was terminated by hydroxyl end groups (**Figure 4.1a**). The molecular weights were calculated based on the integration ratio of H^e to H^f (I^e/I^f) (**Figure 4.1a**), assuming that each hydroxyl group on β-CD participated in the initiation. The consistency between $M_{n,th}$ and $M_{n,NMR}$ suggested that the initiation efficiency for polymerization of ε-caprolactone was nearly quantitative, leading to the formation of star-like PCL with 21 arms. In addition, GPC traces displayed mono-modal distribution in all samples (**Figure 4.2a**).

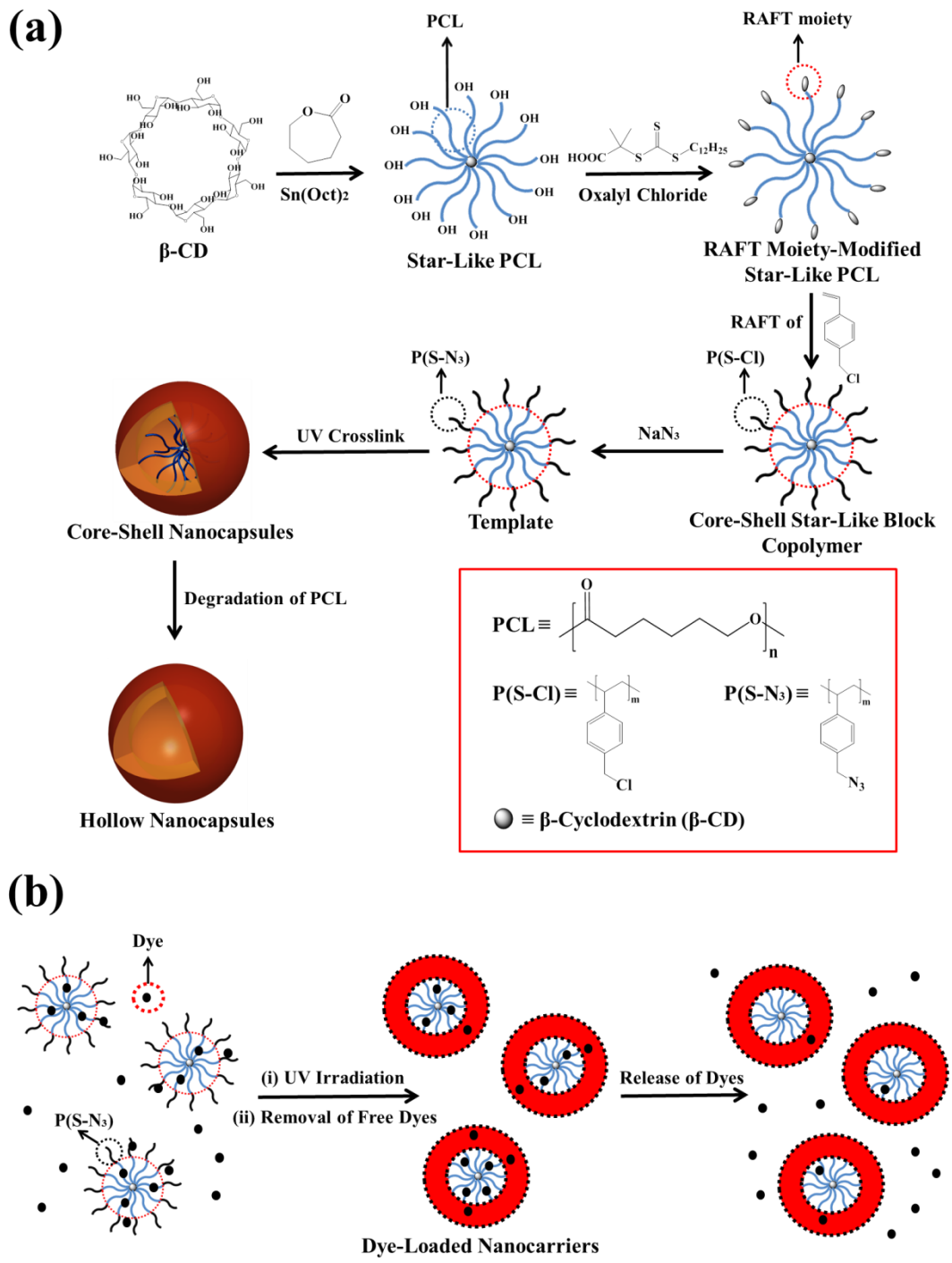

Scheme 4.1. (a) Synthetic strategy for unimolecular polymeric core-shell and hollow nancapsules. (b) The encapsulation and release of dyes.

Table 4.1. Summary of star-like PCL with different molecular weights synthesized under various reaction conditions

	T (°C)	[CL]/[OH]	[Sn]/[OH]	$M_{n,th}$[a] (kg/mol)	$M_{n,NMR}$[b] (kg/mol)	$M_{n,GPC}$[c] (kg/mol)	PDI[d]	Conversion[e]	N[f]
Sample 1	110	50	0.02	30	43	31	1.04	25%	18
Sample 2	110	50	0.2	85	82	44	1.05	71%	34
Sample 3	130	50	0.05	120	130	93	1.07	97%	53

[a]Calculated based on $M_{n,th} = \frac{[CL]}{[OH]} * Conversion * 114.14 * 21$. [b]Calculated from NMR according to $M_{n,NMR} = (\frac{A_e}{A_f} + 1) * 21 * 114.17$, where A_e and A_f represent the integral areas of the methylene protons in repeating unit of star-like PCL and at the chain end of star-like PCL in conjunction with the hydroxyl end groups, respectively. [c and d]Molecular weight and polydispersity obtained from GPC. [f]Determined by thermal gravimetry analysis. [f]The number of repeating unit and obtained from the NMR end group analysis.

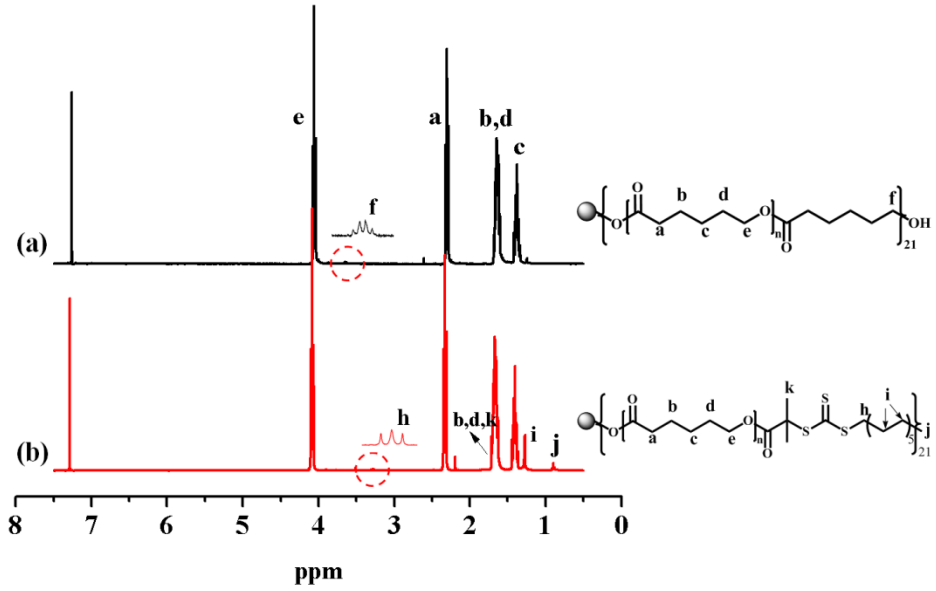

Figure 4.1. [1]H-NMR spectra of star-like homopolymer. (a) star-like PCL, (b) polymeric RAFT agent star-like trithiocarbonate-end-functionalized PCL (i.e., PCL-TC).

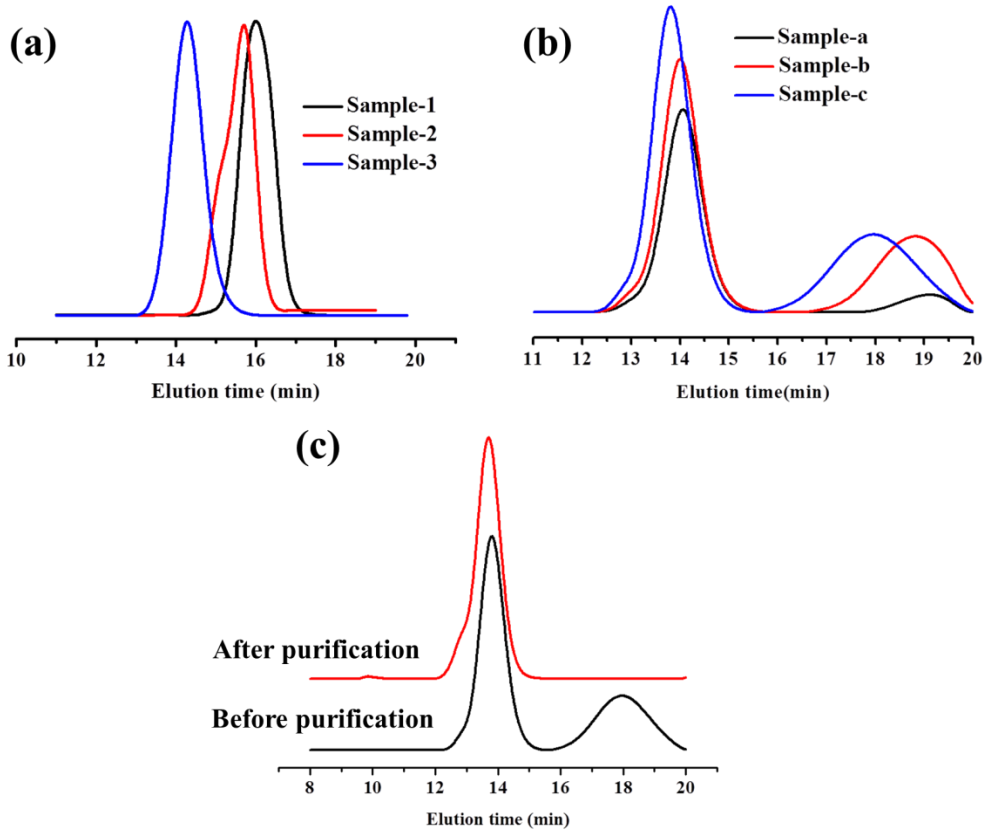

Figure 4.2. GPC traces of (a) star-like PCL with different molecular weights as summarized in **Table S1**, (b) star-like PCL-*b*-P(S-Cl) with different molecular weights as summarized in **Table 1**, (c) star-like PCL-*b*-P(S-Cl) before and after purification (i.e., sample-c as an example).

RAFT was selected to graft the second block poly(4-chloromethyl styrene) (P(S-Cl)) due to its high versatility and compatibility with 4-(chloromethyl)styrene monomer.[30,31] First, trithiocarbonate (TC)[70] was grafted onto star-like PCL (i.e., sample 3 in **Table 4.1**) by coupling with its end hydroxyl groups to form R-connected[41] polymeric RAFT agent (i.e., PCL-TC). The success in grafting was confirmed by NMR (**Figure 4.1b**) and UV-Vis spectroscopy measurements (a characteristic absorption peak of TC is at 308 nm, **Figure 4.3**). Subsequent chain extension from star-like PCL-TC by RAFT polymerization of 4-(chloromethyl)styrene was performed to yield star-like PCL-*b*-P(S-Cl) diblock copolymer with P(S-Cl) as shell. In the synthesis of star polymers by RAFT

using the R-group approach,[41] high radical flux and long reaction time would easily result in excess star-star coupling termination for slowly propagating monomers such as styrene and its derivatives.[41] Thus, thermal initiation was utilized in the chain extension step to avoid undesirable star-star coupling. Any additional initiator would lead to multi-modal molecular weight distribution due to high radical flux, and thus excess termination reactions in the system. We note that linear polymers including linear macro-RAFT agent and terminated chains may be inevitably generated during polymerization, as evidenced by the tail present in low molecular weight region in GPC traces (**Figure 4.2b**)[41] and were removed prior to further reaction in order to obtain pure star-like PCL-*b*-P(S-Cl) diblock copolymers (**Figure 4.2c**). We note that samples a-c (i.e., star-like PCL-*b*-P(S-Cl); **Table 4.2**) were prepared by grafting P(S-Cl) from sample 3 (i.e., star-like PCL; **Table 4.1**), and only sample c was subsequently used to produce core-shell and hollow polymer nanoparticles descried in the following two consecutive sections. The pendant chlorides on the shell block were then substituted by azido groups to introduce photo-crosslinkable moieties (i.e., N_3 groups) and yield photo-crosslinkable star-like PCL-*b*-P(S-N_3) diblock copolymer (**Table 4.2**). Complete shift of –CH_2- adjacent to –N_3 upfield to new position at 4.27 ppm in ^{1}H-NMR spectra was indicative of a nearly complete conversion of benzyl chlorides (**Figure 4.4**). ^{1}H-NMR spectra (**Figures 4.1 and 4.4**) and GPC traces (**Figure 4.2**) of intermediate and final products after each transformation step suggested the successful synthesis of well-defined core-shell star-like diblock copolymer with low polydispersity as summarized in **Table 4.2**. The molecular weights of polymers derived from ^{1}H-NMR are different from those obtained by GPC due to their different hydrodynamic volumes in comparison to linear PS standards. The molecular weight of each block in star-like diblock copolymers can be readily controlled by living polymerization techniques (i.e., ROP and RAFT), which is of key importance in yielding uniform sizes of both core and shell blocks for producing monodisperse polymeric nanoparticles.

Table 4.2. Structural parameters of polymer precursors and the prepared nanoparticles.

		$M_{n,NMR}$[a] (kg/mol)	$M_{n,GPC}$[b] (kg/mol)	$M_{n,theory}$[c] (kg/mol)	Core N[d]	Shell N[d]	Core size, D_{Core}[e] (nm)	Overall size, $D_{Overall}$[e] (nm)	PDI[f]
Star PCL-b-(P(S-Cl))	**(Sample a)**	180	110	170	53	15	-	-	1.10
	(Sample b)	190	120	220	53	19	-	-	1.12
	(Sample c)	240	150	280	53	32	-	-	1.14
Star PCL-b-(P(S-N_3))	**(Template)**	-	-	-	53	32	35	64	1.14
Nanoparticles		-	-	-	-	-	25	58	0.11

[a]Molecular weights calculated from NMR analysis based on molecular weights of precursors (i.e., PCL-TC). [b]Molecular weights determined by GPC using PS as the calibration standard. [c]Theoretical molecular weights calculated based on the monomer to initiator feeding ratio and conversion. [d]Number of repeating units obtained by NMR analysis. [e]Sizes obtained from DLS for star-like diblock copolymer template (i.e., the intensity hydrodynamic diameter D_h of star-like PCL for D_{core}, and the intensity hydrodynamic diameter D_h of star PCL-b-P(S-N_3) for $D_{overall}$ (Sample 3 in Table S1)), and from TEM image analysis for nanoparticles. [f]Polydispersity obtained from GPC for polymers (i.e., samples a-c and template) and DLS for nanoparticles, respectively. Note: all nanoparticles were produced using template derived from sample c.

It is also noteworthy that the grafting-from strategy employed in the present study enabled the crafting of diblock copolymers with well-tailored star-like architectures and high grafting density of arms.

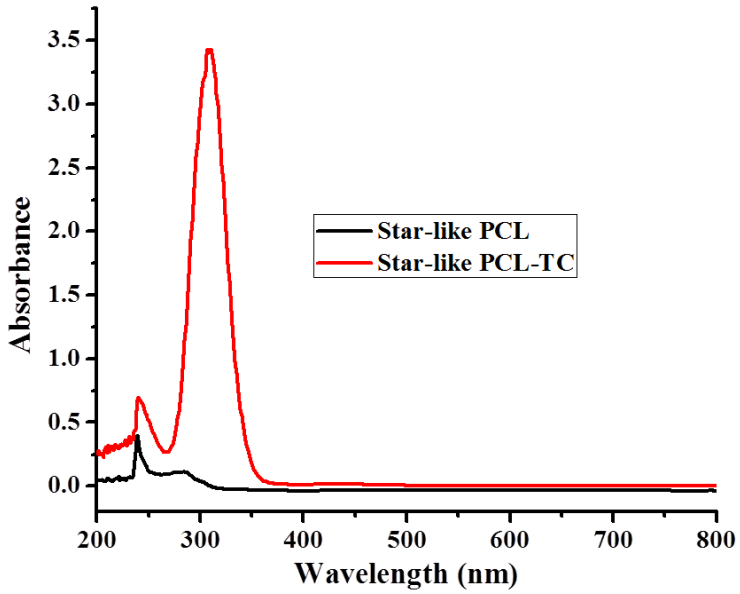

Figure 4.3. UV-vis spectra for star-like PCL (black curve) and trithiocarbonate-end-functionalized star-like PCL (i.e., PCL-TC; red curve).

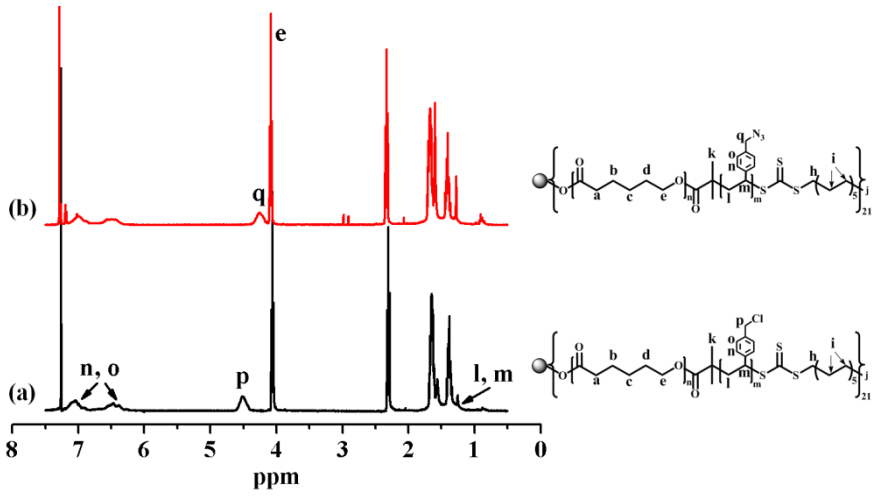

Figure 4.4. ^{1}H-NMR spectra of core-shell star-like diblock copolymers. (a) star-like PCL-*b*-P(S-Cl), and (b) star-like PCL-*b*-P(S-N_3).

4.3.2. Uniform Unimolecular Core−shell Nanoparticles

Photo-crosslinkable star-like PCL-*b*-(P(S-N_3)) diblock copolymers composed of azido groups incorporated into PS shell blocks were then exploited as spherically shaped unimolecular templates to form uniform core-shell polymer nanoparticles by UV exposure. In sharp contrast to the relatively tedious chemical crosslinking widely used for producing polymer nanostructures,[70,253] azido photochemistry allows for photo-crosslinking to occur under mild conditions and requires no additional crosslinking agents. Azido functionality possesses high latent reactivity and easy activation by either heat or UV irradiation.[166,167] In the latter context, the crosslinking density can be easily controlled by simply varying the intensity of UV irradiation or the irradiation time.

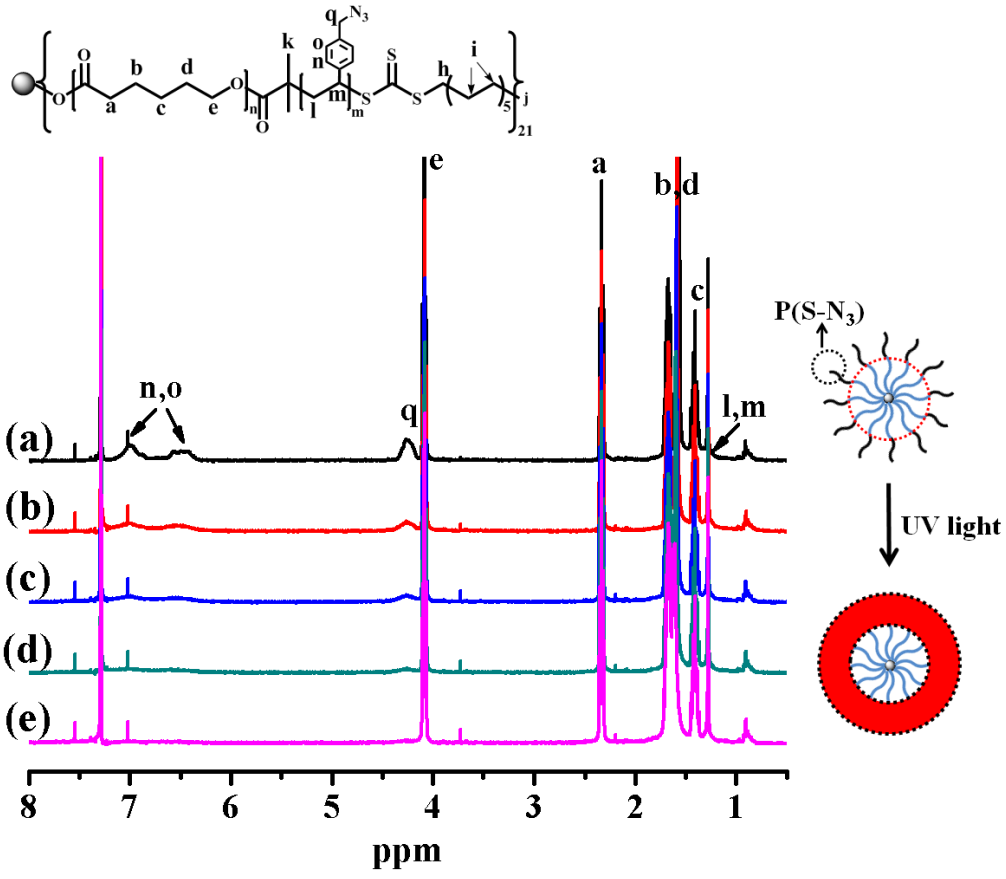

Figure 4.5. NMR spectra of star-like PCL-*b*-P(S-N_3) upon the exposure to UV irradiation for different times for crosslinking to yield unimolecular core-shell nanoparticles**.** (a) as-

prepared sample, (b) crosslinked for 10 min, (c) crosslinked for 20 min, (d) crosslinked for 40 min, and (e) crosslinked for 70 min.

The crosslinking reaction was performed by exposing star-like PCL-*b*-P(S-N_3) diblock copolymer in chloroform solution to UV irradiation. A dilute solution was used to avoid undesirable intermolecular crosslinking reaction. Successful crosslinking reaction and the formation of polymeric nanoparticles were confirmed by ^{1}H-NMR, FTIR, AFM and TEM. NMR spectroscopy was utilized to directly monitor the photo-crosslinking process. The intensity corresponding to P(S-N_3) segment at 4.27 ppm, 6.49 ppm and 7.02 ppm labelled as q, o and n, respectively, in ^{1}H-NMR gradually decreased upon increasing UV exposure time, and completely disappeared at 70 min (**Figure 4.5**). This implied the formation of nanoparticles with a crosslinked shell (i.e., core-shell nanoparticles).[33] The signals from PCL blocks were also observed in NMR spectra, suggesting the preservation of PCL as inner core in nanoparticles after UV exposure. Uniform core-shell nanoparticles started to form after crosslinking for 20 min as evidenced by AFM measurements (**Figure 4.6**). Prolonged UV exposure would increase the degree of crosslinking and thus the shell rigidity. Complete disappearance of the peak at 2098 cm^{-1} corresponding to azido group in FTIR measurement (**Figure 4.7**) suggested that the crosslinking of azido groups reached completion at 70min, which was consistent with NMR analysis (**Figure 4.5**). The crosslinked nanoparticles were thus obtained.

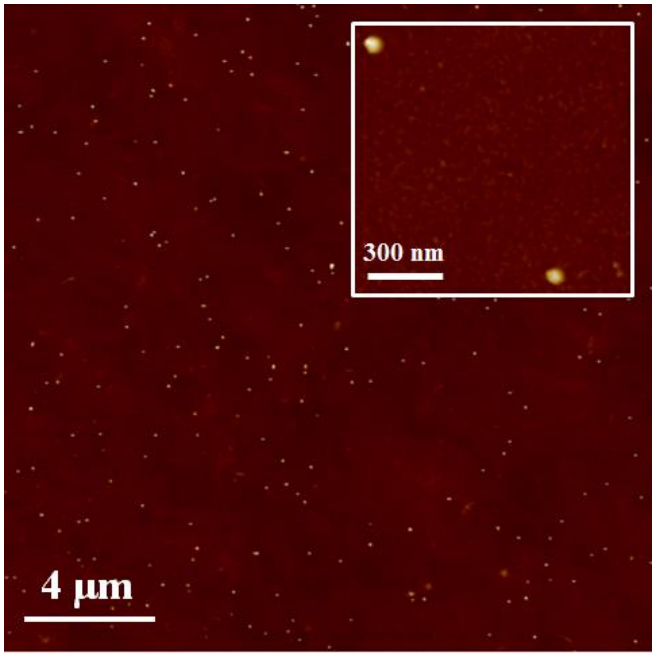

Figure 4.6. AFM height image of partially crosslinked core-shell nanoparticles after exposing to UV irradiation for 20 min. The close-up is shown as an inset.

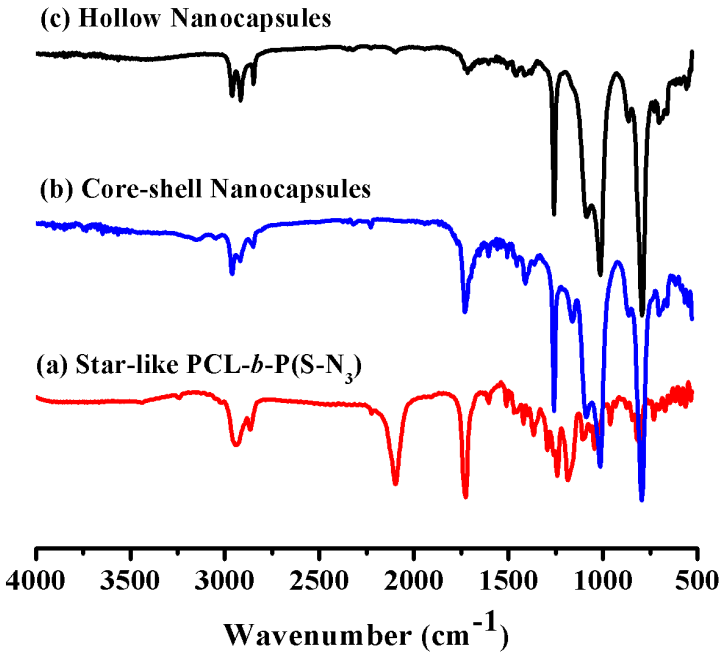

Figure 4.7. FTIR spectra of star-like diblock copolymer template and polymer nanoparticles. (a) star-like PCL-*b*-P(S-N_3) template, (b) core-shell nanoparticles, and (c) hollow nanoparticles.

Figure 4.8a shows fully crosslinked nanoparticles (i.e., crosslinked for 70 min) readily visualized by AFM, exhibiting their highly uniform structures upon deposition on Si substrate. A close-up of nanoparticles clearly showed their spherical shape and smooth surface (**Figure 4.8b**). The corresponding 3D profile also signified that the deposited nanoparticles on Si substrate were very uniform and of equal height (**Figure 4.8c**). Clearly, the spherical shape and monodisperse characteristics of star-like PCL-*b*-P(S-N_3) templates were retained after their transformation into unimolecular core-shell nanoparticles. The average height $h_{core\text{-}shell,\ AFM}$ and diameter $D_{core\text{-}shell,\ AFM}$ of fully crosslinked nanoparticles were 54.1 ± 2.3 nm and 95 ± 5.6 nm, respectively. The discrepancy between $h_{core\text{-}shell,\ AFM}$ and $D_{core\text{-}shell,\ AFM}$ is due to the AFM tip convolution of nanoparticles, leading to overestimate in lateral size (i.e., $D_{core\text{-}shell,\ AFM} > h_{core\text{-}shell,\ AFM}$). We note that star-like block copolymer template prior to crosslinking would tend to spread out when adsorbed on the substrate because of the chain flexibility. Thus the average height was less than 10 nm and the template size was not uniform (**Figure 4.9**). In contrast, a rigid shell was formed after crosslinking which prevented the collapse of nanoparticles. As a result, the height increased significantly upon crosslinking (i.e., 54.1 ± 2.3 nm) as compared to that of uncrosslinked template (< 10 nm). [70,254]

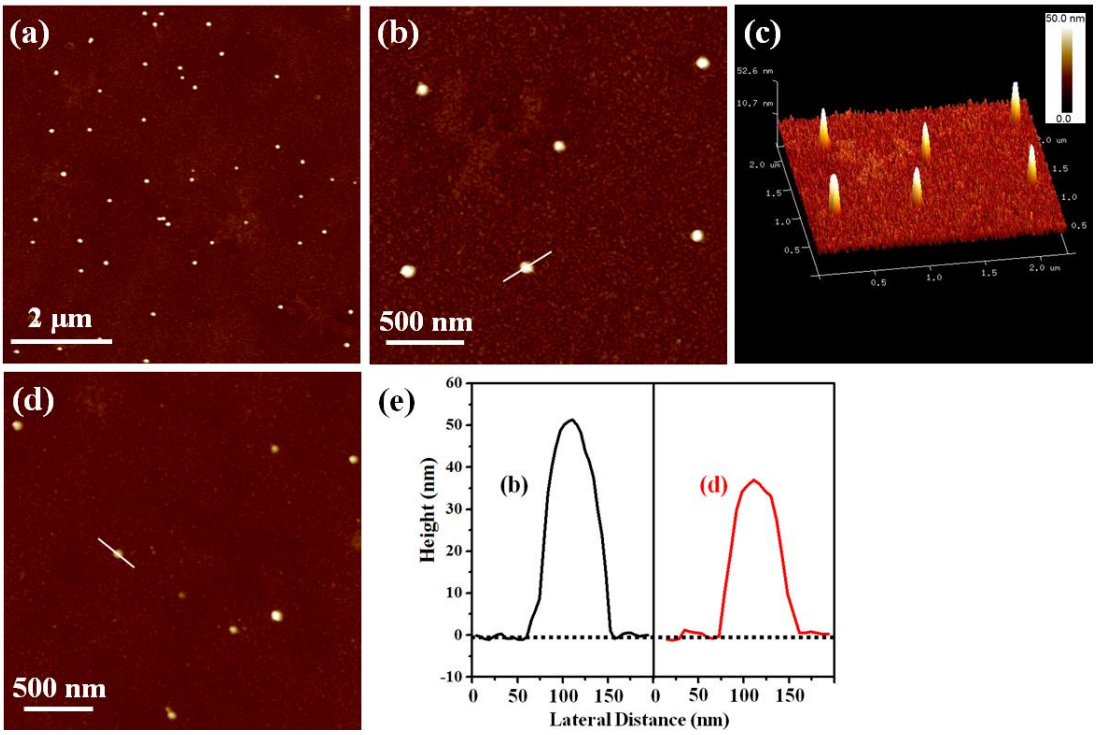

Figure 4.8. Core-shell nanoparticles obtained from crosslinking of star-like PCL-*b*-P(S-N_3) template in **Table 1**. (a) AFM height image of uniform fully crosslinked nanoparticles after exposure to UV irradiation for 70min, (c) Representative 3D height image of fully crosslinked nanoparticles, (b) and (d) AFM height images of fully crosslinked and partially crosslinked (after a 20-min UV exposure) nanoparticles, respectively, and (e) Cross-sectional profiles of fully crosslinked and partially crosslinked nanoparticles obtained from the corresponding AFM height images in (b) and (d), respectively (i.e., straight lines across nanoparticles in (b) and (d)).

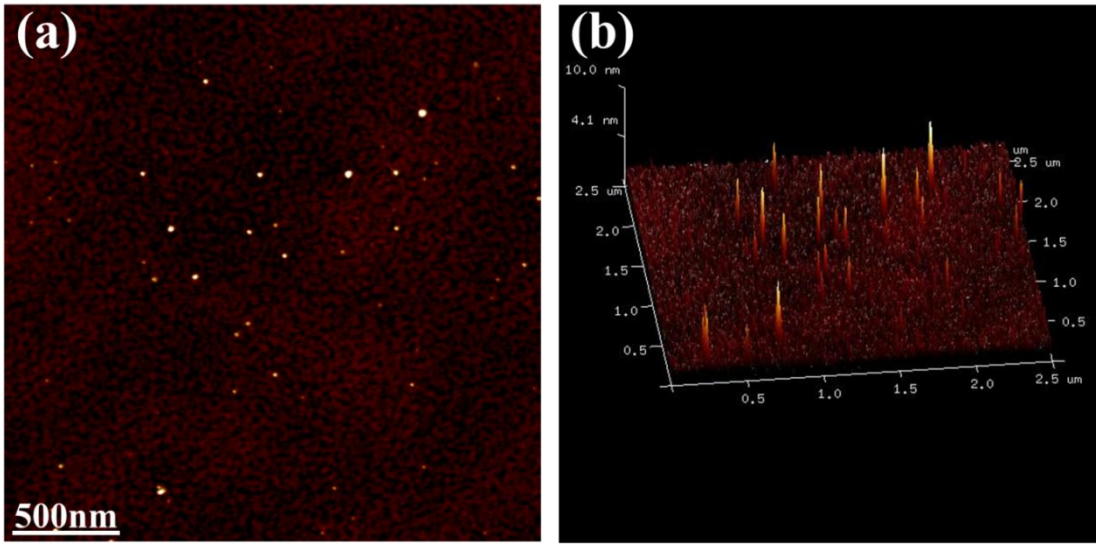

Figure 4.9. AFM height images of star-like PCL-*b*-P(S-N_3) diblock copolymer template. (a) Top view, and (b) the corresponding 3D profile.

TEM imaging further substantiated that the crafted polymer nanoparticles were spherical and monodisperse (**Figure 4.10**). By selectively staining the crosslinked PS shell, core-shell structure of nanoparticles can be clearly revealed by TEM. RuO_4 was employed in the study due to its differential staining capability on PS over PCL. It is crucial to carefully control the staining time to be able to visualize the core-shell structure. The light staining enabled outer PS domains of nanoparticles to be selectively and lightly stained (i.e., appeared dark), so the shell of nanoparticles can be observed under TEM, while the inner PCL blocks appeared transparent (**Figures 4.10a & 4.10d**). Increasing staining time resulted in intermediate staining. This allowed hollow nanoparticles to be distinctively visualized due to an improved contrast of heavily stained PS shell (**Figure 4.10b & 4.10e**). Clearly, hollow interiors originating from the unstained PCL core can be seen in almost every nanocapsule (**Figures 4.10a & 4.10b**). The interface between PCL core and PS shell was rather distinct (**Figure 4.10b & 4.10e**). Further increase in staining time led to the staining of PCL core as well. Consequently, entire nanoparticles composed of stained PCL core and PS shell were observed (**Figure 4.10c & 4.10f**). The average core diameter ($D_{core,\ TEM}$) and overall size ($D_{overall,\ TEM}$) were 25.1 ± 7.9 nm and 58.4 ± 15.1 nm, respectively, based on the TEM image analysis at intermediate staining (**Figure 4.11a**). The comparatively large standard deviation can be attributed to non-uniform staining effect at this staining stage. The image analysis on heavily stained nanoparticles revealed a monodispersed size distribution with $D_{overall,\ TEM}$ of 50.2 ± 7.1 nm (**Figure 4.11c**). It is worth noting that the core diameter was close to the hydrodynamic diameter D_h of star-like PCL homopolymer, while the overall size was consistent with D_h of star-like PCL-*b*-P(S-N_3) template obtained by DLS (**Table 4.2**), signifying that the core size and the shell thickness of nanoparticles were dictated by

molecular weights of inner PCL block and outer PS block, respectively. Intriguingly, the diameter determined by TEM correlated well with the height of nanoparticles measured by AFM, suggesting that the fully crosslinked nanoparticles had a rigid shell to maintain the spherical shape without flattening upon the deposition on substrate. The narrow size distribution observed by TEM was also corroborated by AFM measurement. Moreover, the DLS measurement on polymeric nanoparticles in chloroform afforded the intensity-average D_h of 180.4±1.8 nm and a very low polydispersity of 0.11 (**Figure 4.12**). Compared to $D_{overall,\ TEM}$ determined by TEM, the large D_h was due possibly to significant swelling of nanoparticles in solution and their surface property.[255] On the basis of DLS, AFM and TEM measurements, star-like PCL-*b*-P(S-N_3) templates prior to crosslinking exhibited a narrow size distribution.

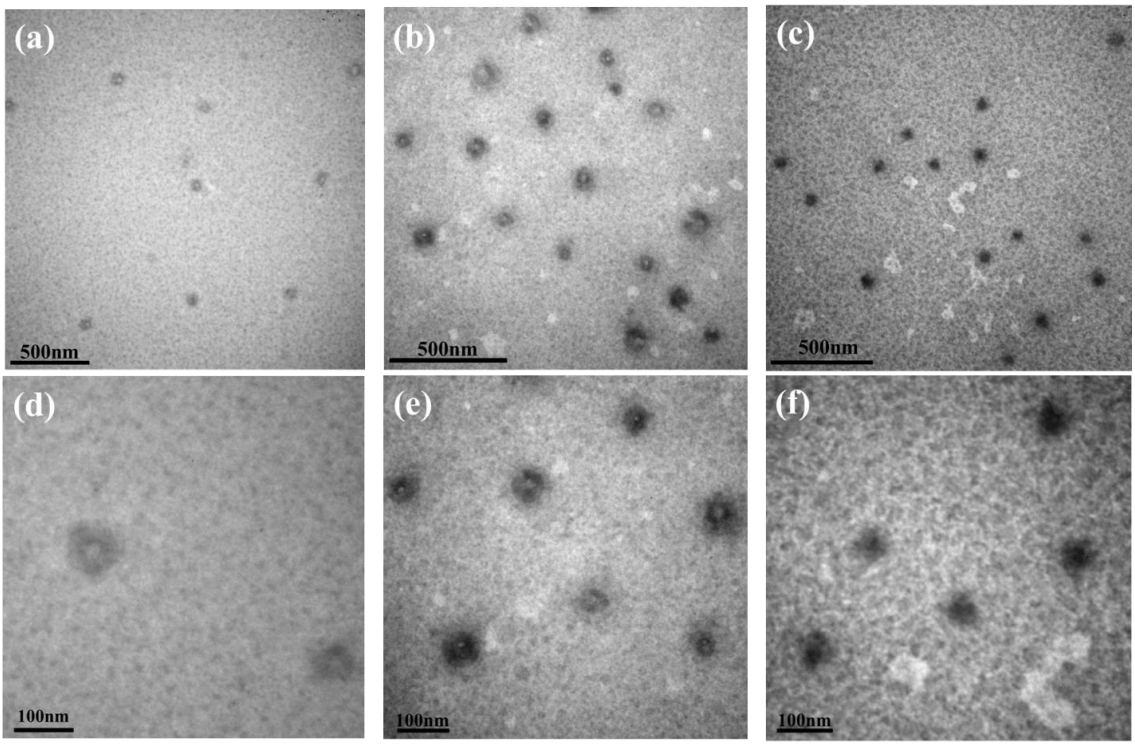

Figure 4.10. TEM images of core-shell polymeric nanoparticles. (a & d) light staining where PS shell of nanoparticles was selectively and lightly stained, (b & e) intermediate staining where PS shell was preferentially and heavily stained, and (c & f) heavy staining where both PCL core and PS shell of nanoparticles were stained.

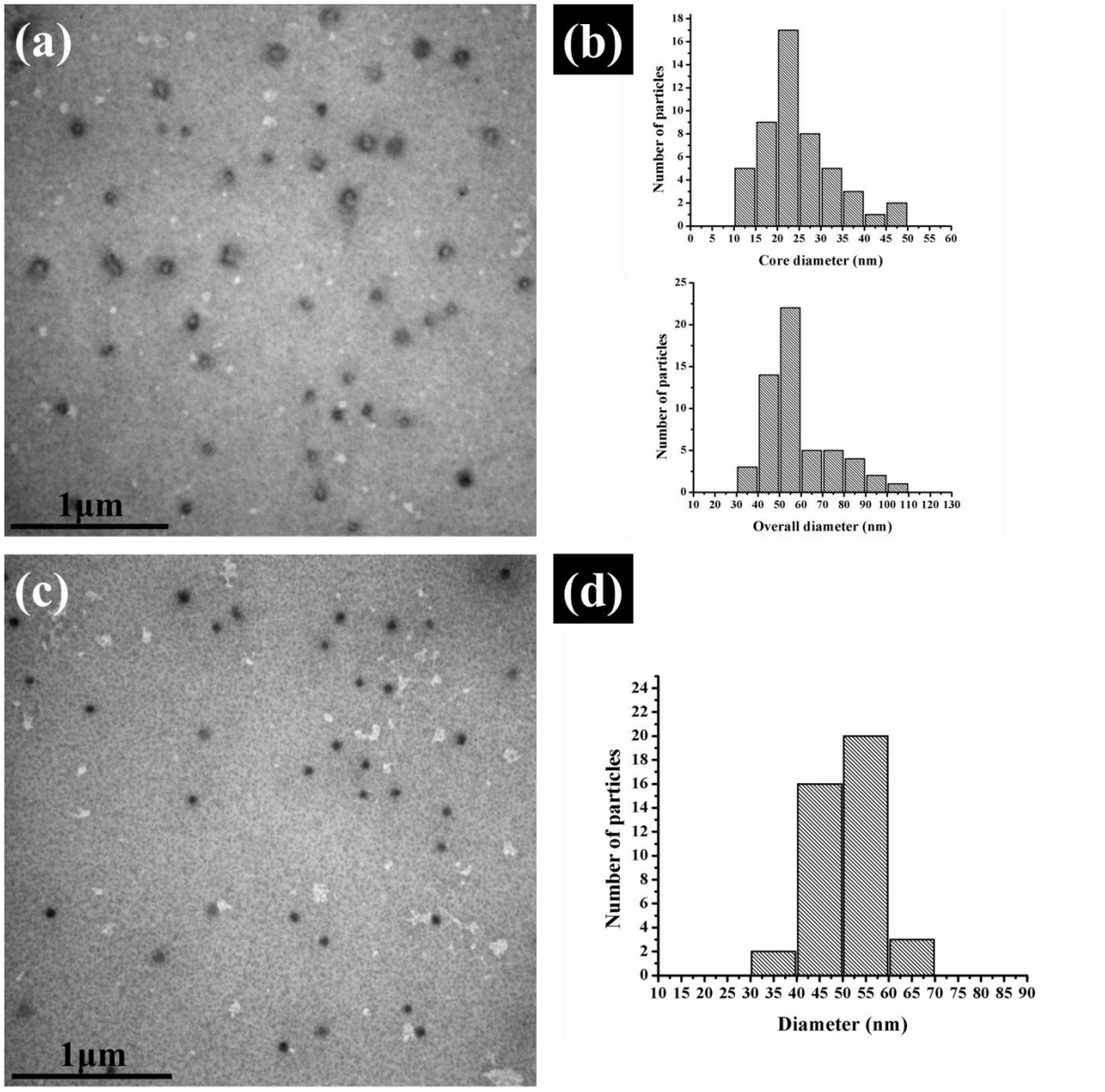

Figure 4.11. (a) TEM image of intermediately stained core-shell nanoparticles, and (b) the core and overall size distributions of nanoparticles for TEM image in (a). (c) TEM image of heavily stained core-shell nanoparticles, and (d) size distribution of nanoparticles for TEM image in (c).

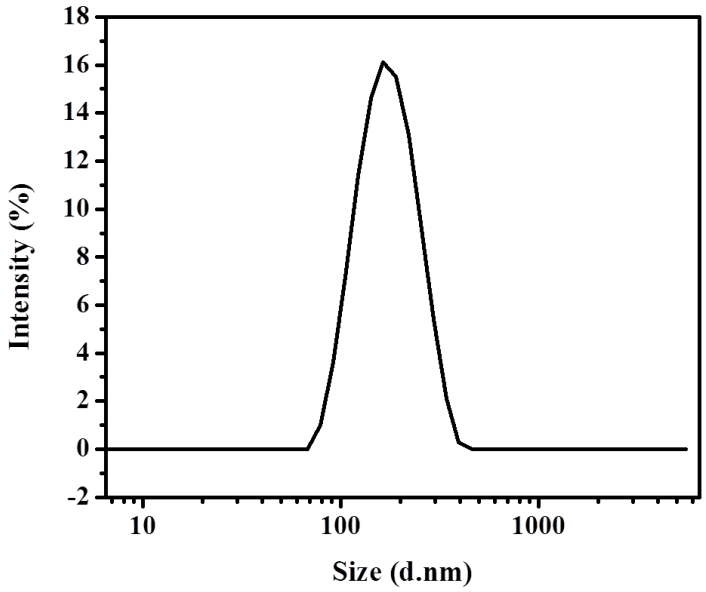

Figure 4.12. Dynamic light scattering (DLS) characterizations on core-shell nanoparticles.

For comparison, partially crosslinked nanoparticles (i.e., crosslinked for 20 min, **Figure S6**) was also examined by AFM, showing an average height of 38.6 ± 2.9 nm and an average diameter of 90.7 ± 9.5 nm (**Figure 4.8d**). Cross-sectional analysis of nanoparticles (**Figure 4.8e**) revealed a clear decrease in height (approximately 29%) of partially crosslinked nanoparticles (i.e., 38.6 ± 2.9 nm, **Figure 4.8d**) compared to fully crosslinked nanoparticles (i.e., 54.1 ± 2.3 nm, **Figure 4.8b**), which can be attributed to the fact that nanoparticles with lower crosslinking density are relatively more flexible due to a less rigid shell. As a result, flattening on the substrate would occur for partially crosslinked nanoparticles, and thus a decreased height was observed.[254] The diameter of partially crosslinked nanoparticles (i.e., 90.7 ± 9.5 nm, **Figure 4.8d**) was comparable with fully crosslinked one (i.e., 95 ± 5.6 nm, **Figure 4.8b**) due to the combination of the flattening effect noted above and the lower extent of AFM tip convolution from the reduced height.[256-258] It is worth noting that higher degree of crosslinking led to lower

dispersability and reduced stability of nanoparticles. Fully-crosslinked nanoparticles were found to exhibit a good short-term stability, but started to aggregate after long-term storage driven by the minimization of their surface energy as shown in **Figure 4.13**. Interestingly, partially crosslinked nanoparticles have a good long-term stability and can be easily re-dispersed in common organic solvents after drying. Nanoparticles with lower crosslinking density (i.e., partially crosslinked) allowed the penetration of solvent molecules and the swelling of shell, thereby resulting in a good dispersability. Conversely, a higher degree of crosslinking led to a more rigid structure yet decreased dispersability of the resulting core-shell nanoparticles.

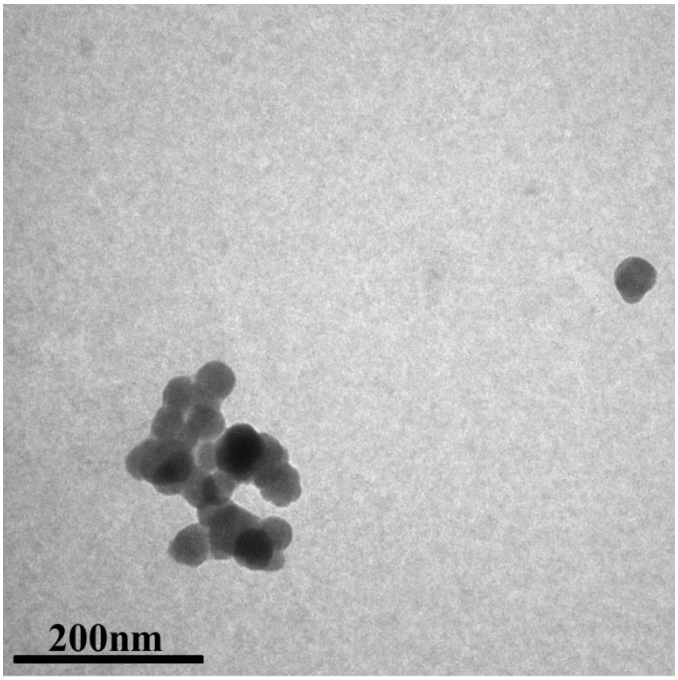

Figure 4.13. TEM image of nanocapsules after a long-term storage (heavily stained sample), showing aggregations of nanocapsules.

4.3.3. Monodisperse Hollow Polymer Nanoparticles

In order to demonstrate in vitro degradability of inner PCL blocks and the stability of crosslinked nanoparticles, core-shell nanoparticles were hydrolytically degraded under acidic condition, yielding hollow polymer nanoparticles. The success in degradation and formation of hollow nanoparticles was confirmed by a suite of characterization techniques. Complete disappearance of characteristic carbonyl stretching peak at 1732 cm^{-1} from PCL block in FTIR spectra was indicative of the successful degradation of PCL core (**Figure 4.7**). A small new peak appeared at 1716 cm^{-1} after the degradation can be attributed to carbonyl stretching vibration from pendant carboxylic acid groups of the last hydrolyzed PCL unit which remained attached to the inner surface of PS shell.[70] AFM imaging further supported hollow structures of etched nanoparticles (**Figure 4.14**). The average height ($h_{hollow,\ AFM}$) and diameter ($D_{hollow,\ AFM}$) of hollow nanoparticles deposited on Si substrate were approximately 23.3 ± 2.5 nm and 66.7 ± 2.4 nm, respectively (**Figure 4.14a**). The height of nanoparticles decreased about 57% after etching of the PCL core (**Figure 4.14b**) from 54.1 ± 2.3 nm ($h_{core\text{-}shell,\ AFM}$, **Figure 4.14c**) to 23.3 ± 2.5 nm ($h_{hollow,\ AFM}$, **Figure 4.14a)**, suggesting the collapse and flattening of hollow nanoparticles on substrate as illustrated in **Figure 4.14e** due to the absence of PCL inside to provide the support for degraded hollow structure and the soft nature of polymer shell. Notably, in comparison to core-shell nanoparticles, the diameter of hollow nanoparticles measured by AFM was closer to the size evaluated by TEM, which can be ascribed to the lower extent of tip convolution effect as the height of nanoparticles decreased, and thus a higher accuracy in diameter determined by AFM.[256-258] TEM observation showed the formation of remarkably uniform hollow nanoparticles (**Figure 4.14d**). The average size obtained from TEM analysis ($D_{overall,\ TEM}$ = 53.6 ± 2.6 nm) was in substantial agreement with the diameter of core-shell nanoparticles prior to core etching ($D_{overall,\ TEM}$ = 50.2 ± 7.1 nm in **Figure 4.11c**), implying that the structural integrity of nanoparticles was well retained after degradation. No hollow structure can be observed throughout the whole stage of staining; this is not surprising and consistent with

AFM characterization, suggesting that hollow nanoparticles collapsed on the substrate in dry-state (**Figure 4.14e**). Taken together, the abovementioned results substantiated the formation of hollow polymer nanoparticles and the maintenance of structural integrity of nanoparticles upon removal of the PCL, which are indicative of the good stability of polymeric nanoparticles.

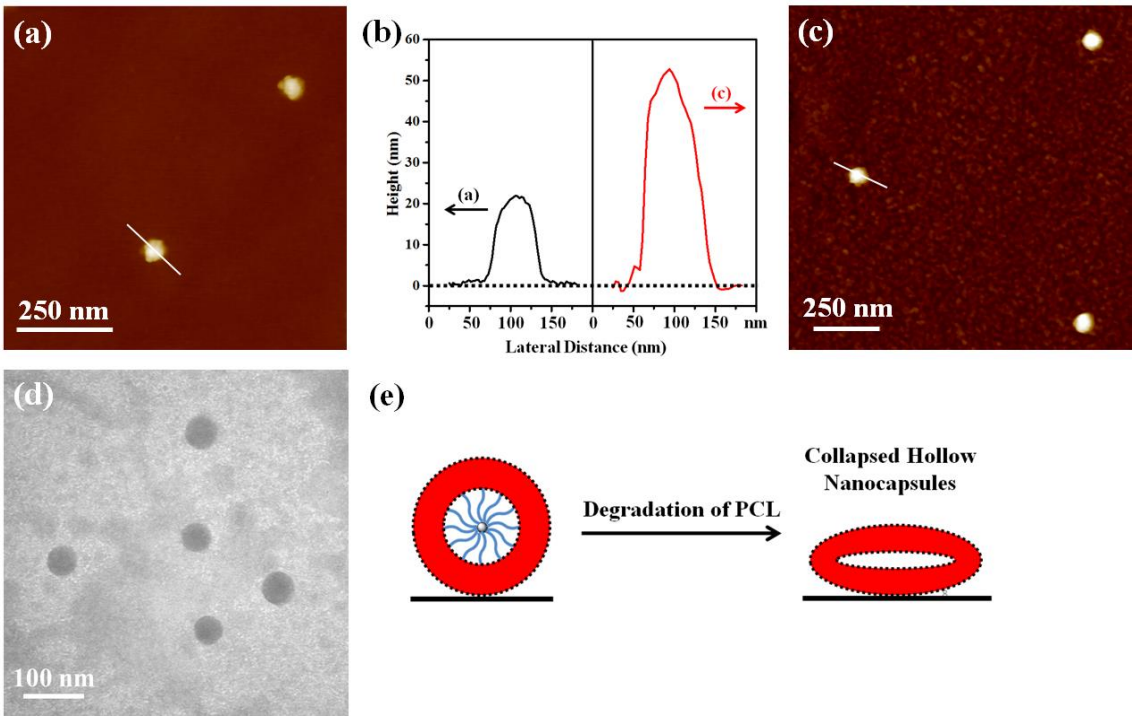

Figure 4.14. Morphologies of hollow polymer nanoparticles. (a) and (c) AFM height images of hollow nanoparticles and core-shell nanoparticles (i.e., prior to degradation of PCL core; fully crosslinked), respectively. (b) Cross-sectional profiles of hollow and core-shell nanoparticles obtained from the corresponding AFM height images in (a) and (c), respectively (i.e., straight lines across nanoparticles in (a) and (c)). (d) TEM image of hollow nanoparticles after staining. (e) Schematic illustration of the transition from core-shell nanocapsule (left) to collapsed hollow nanoparticles (right) on substrate after degradation of PCL blocks.

4.3.4. Encapsulation and Controlled Release of Fluorescent Probes

The architecture of nanoparticles plays an important role in encapsulation of a variety of species, and can thus be employed for controlled release of drugs. In this

context, core-shell nanoparticles were exploited as effective nanocarriers by performing encapsulation and release study with dye as a model guest compound. Due to intrinsically spherical architecture of star-like PCL-*b*-P(S-N_3) templates and the ease of UV-induced crosslinking, we developed a simple and viable route to encapsulating dyes in nanoparticles. Star-like diblock copolymer templates and dyes were first dissolved in solvent. The resulting solution was then exposed to UV irradiation to photo-crosslink the azido-containing PS shell. The extensive purification was subsequently carried out to remove excess dyes outside nanoparticles, thereby yielding dye-loaded core-shell nanoparticles (denoted nanocarriers; **Scheme 4.1b**). Compared to the commonly used nanoprecipitation method,[259] the implemented encapsulation methodology is much simpler. It afforded guest-encapsulated nanocarriers with well-controlled size and narrow size distribution due to monodispersity of star-like PCL-*b*-P(S-N_3) diblock copolymer template. Two kinds of dyes were selected in the study to demonstrate the versatility of the encapsulation technique. A dye containing Os atom (osmapentalyne[250], **Figure 4.15**) was chosen because its inherent metal-containing molecular structure provided dye-loaded nanocarriers the ability for direct TEM imaging.[260]

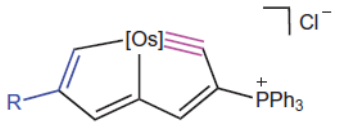

Figure 4.15. Structure of Os-atom containing dye: osmapentalyne.[1]

After encapsulation and purification, dye-loaded nanocarriers displayed a characteristic absorption maximum at 424 nm from osmapentalyne,[250] signifying its successful encapsulation (**Figure 4.16a**). More importantly, nanocapsule encapsulated with osmapentalyne was directly observed by TEM (**Figure 4.16b**). The diameter of

nanocarriers was in accordance with that of nanoparticles, reflecting the presence of dyes in both PCL core and PS shell of nanoparticles. On the other hand, when a fluorescent dye is trapped within nanoparticles, the fluorescence self-quenching due to π-π interaction would occur due to high local concentration of fluorophore inside.[261] After being released to the surrounding medium, free dyes would manifest a stronger fluorescence upon dilution (i.e., no or much reduced self-quenching). By tracking the increase of fluorescence, the release behavior of guest molecules from nanocarriers can thus be scrutinized.[136] To this end, Rhodamine B (RhB) was selected as the second fluorescent dye for this study. Star-like PCL-*b*-P(S-N_3) template was crosslinked for 20 min (i.e., partially crosslinked) together with RhB, and the purification was conducted to remove excess RhB. The characteristic absorption peak of RhB at 559 nm from RhB-loaded nanocarriers was clearly evident (**Figure 4.16a**), and the emission peak at 572 nm in fluorescence spectra (excitation at 559 nm, **Figure 4.16c**) further confirmed the successful encapsulation. A gradual increase in fluorescence intensity was seen when nanocarriers were dissolved in chloroform ($CHCl_3$) (**Figure 4.16c**), which was due to the release of RhB triggered by the swelling of nanoparticles in chloroform solution. The release kinetics can be obtained by monitoring the fluorescence increase. As shown in **Figure 4.16d**, an initial release of RhB was fast and then reached a plateau within 2 h (black squares). The initial burst release was caused by an initial high dilution of RhB outside nanoparticles (i.e., a large concentration gradient of RhB from inside to outside nanocapsule). The release rate was then slowed down due to the decrease in the concentration gradient of RhB across the PS shell of nanoparticles. Quite interestingly, when nanocarriers were dissolved in THF, the RhB release did not obviously occur in light of relatively poor solubility of RhB in THF (blue triangles, **Figure 4.16d**), and thus a smaller driving force for dye molecule release. In addition, the effect of shell crosslinking density on release rate was investigated by preparing fully crosslinked nanoparticles loaded with RhB. No obvious dye release in $CHCl_3$ was found over the

same time period using partially crosslinked nanoparticles (red circles, **Figure 4.16d**), suggesting a substantially slower release rate. This is due likely to smaller pore sizes in the PS shell because of higher crosslinking density.[253] It is worth noting that we provided a proof-of-principle demonstration that core-shell nanoparticles can act as effective nanocarriers.

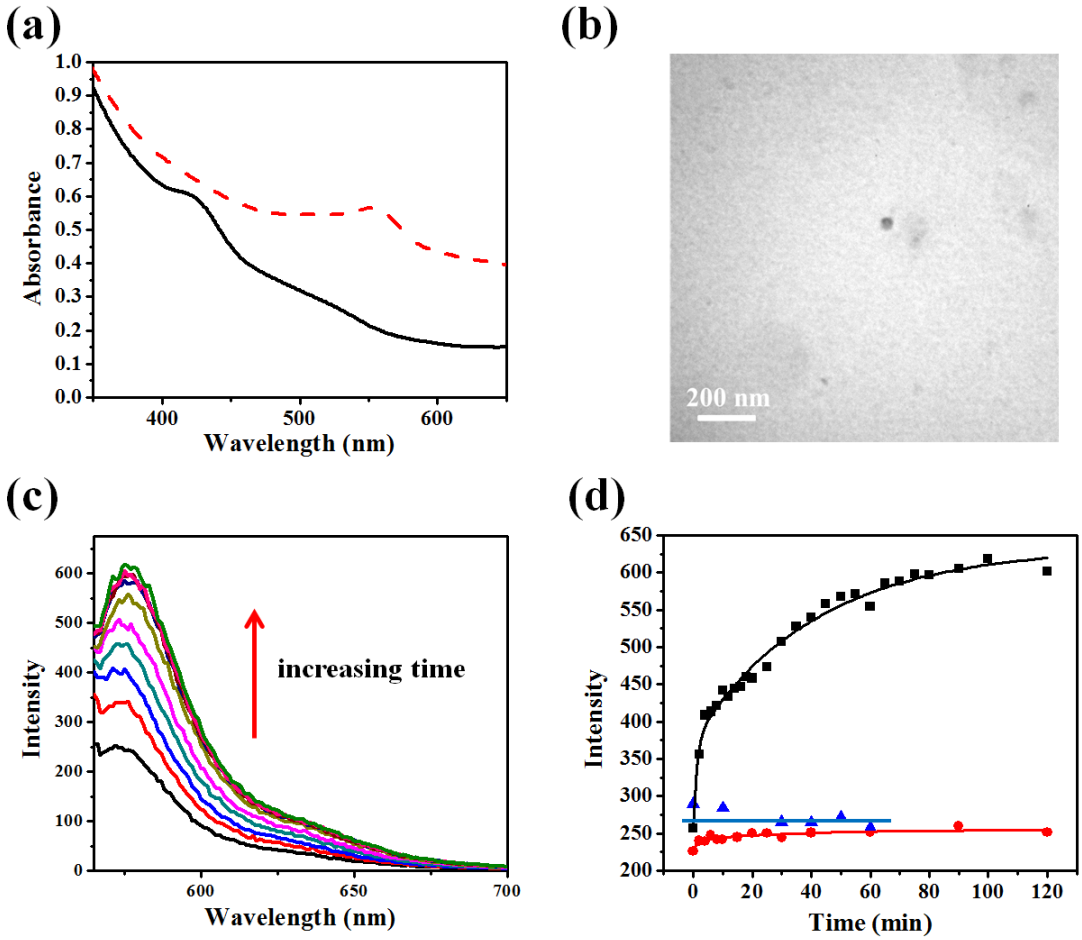

Figure 4.16. Encapsulation and release of dyes. (a) UV-Vis spectra of core-shell nanoparticles loaded with two different dyes (i.e., RhB with an absorption maximum of 559 nm (red dash curve) and osmapentalyne with an absorption maximum of 424 nm (black curve)). (b) TEM image of nanoparticles loaded with osmapentalyne. (c) Fluorescence spectra of partially crosslinked nanoparticles loaded with RhB in chloroform, and (d) florescence intensity at the emission of 572 nm as a function of time, showing different release rates of RhB from nanoparticles of different crosslinking density in THF and $CHCl_3$ (i.e., partially crosslinked nanoparticles in $CHCl_3$ (black squares), fully crosslinked nanoparticles in $CHCl_3$ (red circles), and partially crosslinked nanoparticles in THF (blue triangles)). The curves are used for guidance.

The new nanocarriers offer several important and advantageous features, including precise size control via tailoring molecular weights of constituent blocks in star-like diblock copolymers, uniformity, and good stability. Looking ahead, the shell block can be easily replaced with biocompatible crosslinkable polymers to develop new prospective drug nanovehicles. Moreover, PCL blocks situated inside nanoparticles facilitate the loading of drug via hydrophobic interaction,[262-264] and can be readily degraded in vivo with drug release. This will be the subject of future studies.

4.4 Summary

We developed a robust strategy to craft tailorable core-shell and hollow polymer nanoparticles with well-defined architecture, and exploited them as a new type of nanocarrier via the dye encapsulation and release study. The key to our preparative route was the use of photo-crosslinkable core-shell star-like diblock copolymers as templates. Star-like core-shell diblock copolymers were first synthesized by a combination of ring opening polymerization and reversible addition-fragmentation chain transfer polymerization, followed by introducing photo-crosslinking azide moieties on the shell blocks. Interestingly, upon UV irradiation these unimolecular micelles were subsequently transformed into uniform spherical nanoparticles composed of biodegradable inner core blocks and a stable crosslinked shell. The degree of crosslinking can be tailored by varying UV exposure time. The size of nanoparticles is governed by molecular weights of constituent blocks in the core-shell star-like diblock copolymer template, and the uniformity of nanoparticles was translated from narrow molecular weight distribution of star-like diblock copolymer template. Through the selective removal of the biodegradable inner core, nanoparticles with hollow interiors were produced which retained the

structural integrity and stability of as-prepared core-shell nanoparticles. The encapsulation and release of dyes by capitalizing on unimolecular core-shell nanoparticles were also explored as a means to demonstrate the intriguing and effective nanocarrier functionality. We envision that a wide range of well-tailored unimolecular polymer nanoparticles with different compositions and functionalities can be crafted based on this viable templating strategy, dispensing with the need for amphiphilicity as in micelles self-assembled using amphiphilic linear block copolymers. More importantly, drug release may be viably controlled by simply tailoring the crosslinking density of the nanocapsule shell. In addition to spherical star-like diblock copolymers, this strategy can, in principle, be further expanded to utilize more complex polymer compositions and architectures (e.g., bottlebrush-like block copolymer) to create a diversity of truly tailored nanostructures (e.g., polymer nanorods). As such, the development of this new class of polymer nanoparticles with good uniformity and stability, adjustable size, and surface chemistry may present a platform in which to address the size and stability issues widely encountered in current drug nanocarriers.

CHAPTER 5

ORGANO-SILICA HYBRID NANOPARTICLES AND NANOCAPSULES FROM STAR POLYMERS WITH DIFFERENT ARCHITECTURES AS UNIMOLECULAR NANOREACTORS

5.1 Introduction

Organic/inorganic hybrid nanoparticles represent an important class of multifunctional nanomaterials that exhibit fascinating optical, electronic, magnetic, and biological properties in single nano-objects.[181-183] The chemical properties (e.g., solubility and photo-crosslinking) of such hybrid nanoparticles are mainly imparted by organic constituent, while the physical properties are often dictated by the synergy of inorganic nanoparticle and organic component.[184-186] Among various organic/inorganic hybrid nanoparticles developed, silica/polymer hybrid nanoparticles, including polymer-functionalized silica nanoparticles and organo-silica hybrid nanoparticles, have garner much attention due largely to their ease of preparation and a wide range of applications for polymer matrix nanocomposites,[187,188] biomedical engineering,[189-191] and fluorescent thermometers.[192] Moreover, they have also been utilized as model colloids for evaluating the steric stabilization theory.[193,194] The commonly used approaches to produce silica/polymer hybrid nanoparticles include physical adsorption,[195,196] grafting from,[197-202] grafting onto,[203] self-assembly,[204-207] etc.

On the other hand, organo-silica hybrid nanocapsules with a well-controlled cavity are of particular interest as the hollow interior offers peculiar advantages, such as the ability to load guest molecules for delivery or act as nanoscale reactor by encapsulating reactive compounds.[208] However, the effective methods to form organo-silica hybrid nanocapsules are comparatively few and limited in scope. The preparation of hybrid nanocapsules primarily involves the use of self-assembled polymer micelles or

vesicles.[208-211] It is worth noting that the self-assembly approach provides access to organo-silica hybrid nanoparticles and nanocapsules, depending on the morphology of self-assembled nanostructures.[207,208,211] However, there are several challenges associated with this approach. First, it is difficult to precisely control the size and shape of self-assembled nanostructures as they depend sensitively on solvent property, solution concentration, temperature, etc.[204,211] Second, the amphiphilicity requirement of linear block copolymers in order to enable self-assembly greatly limits the compositions and functionalities of polymers that can be selected.[211] Finally, the self-assembly process of polymers to form micelles or vesicles may be tedious.

Herein, we report on a versatile and effective strategy to craft uniform organo-silica hybrid nanostructures by judiciously capitalizing on star-like polymers as nanoreactors, followed by intramolecular gelation. Star-like polymers are spherical macromolecules with multiple arms covalently linked to a multifunctional core.[22,130,265,266] They readily form thermodynamically stable unimolecular micelle in solution with the size governed by the molecular weight of polymer.[20,267] Specifically, organo-silica hybrid nanoparticles and nanocapsules were created by employing star-like Si-containing homopolymer and star-like diblock copolymer with Si-containing moities incorporated in the outer block as nanoreactors, respectively. It is noteworthy that as star-like homopolymer and diblock copolymer were synthesized by atom transfer radical polymerization (ATRP), a living polymerization technique, each arm in star-like polymers possessed well-defined chain length, thereby templating the formation of uniform, precisely size-controllable organo-silica hybrid nanoparticles and nanocapsules, respectively. In stark contrast to polymer micelles yielded from self-assembly of linear block copolymer micelles as noted above, the use of star-like polymers dispenses with the need for the self-assembly process and the requirement of amphiphilic component as in linear block copolymers. As such, it renders the wide selection of polymer composition and functionality for yielding functional, size tunable, spherical nanostructures. These

hybrid nanoparticles and nanocapsules may have a broad range of applications in water purification, controlled delivery systems, lithium ion batteries, and as lightweight fillers in polymer composites.

5.2 Experimental Details

Materials

3-(trimethoxysilyl)-propyl methacrylate (TMSPMA monomer, 98%), *N,N,N′,N′,N″*-pentamethyldiethylene triamine (PMDETA, 99%), ammonium hydroxide solution (28%), β-cyclodextrin (β-CD), 2-Bromoisobutyryl bromide (98%) and anhydrous benzene (99.8%) were purchased from Sigma-Aldrich and used as received. CuBr (98%, Sigma-Aldrich) was stirred in acetic acid overnight, filtrated, then washed with ethanol and diethyl ether successively, and finally dried in vacuum. Styrene (St., Sigma-Aldrich, ⩾ 99%) was washed with 10% NaOH aqueous solution and water successively, then dried over anhydrous $MgSO_4$ and CaH_2 sequentially, and finally distilled under reduced pressure. Petroleum ether was distilled over CaH_2 prior to use. Anhydrous toluene and dichloromethane (DCM) were obtained from a commercial solvent purification system (MB-SPS, MBraun Inc.). All other reagents were purified by common purification procedures.

Synthesis of heptakis[2,3,6-tri-O-(2-bromo-2-methylpropionyl]-β-cyclodextrin) (i.e., 21 Br-β-CD)

21 Br-β-CD is prepared according to the previous reports in literature.[1,2] β-CD (6.82 g, 6 mmol, dried in vacuum oven at 80 °C overnight) was dissolved in anhydrous 1-methyl-2-pyrrolidione (NMP, 60 mL). Subsequently, 2-Bromoisobutyryl bromide (58.0 mL, 252 mmol) was added to the β-CD solution dropwise at 0 °C under stirring. The reaction was allowed to proceed for 24h at ambient temperature. After that, the solution was

concentrated by the reduced pressure distillation and then diluted with dichloromethane. The product solution was washed with saturated $NaHCO_3$ aqueous solution and DI water sequentially for three times. The organic layer was concentrated and then crystallized in cold n-hexane to obtain pure product. The chemical compositions of 21 Br-β-CD were confirmed by ^{1}H-NMR in $CDCl_3$: δ=1.8 (broad s, 126H, CH_3), 3.5–5.4 (49H, sugar protons); FTIR: 2931 cm^{-1} (ν_{C-H}), 1737 cm^{-1} ($\nu_{C=O}$), 1158 cm^{-1} (ν_{C-O-C}), 1039 and 1105 cm^{-1} (coupled ν_{C-C} and ν_{C-O}).

Synthesis of star-like PTMSPMA homopolymer by ATRP using 21-Br β-CD as initiator

Atom transfer radical polymerization (ATRP) of 3-(trimethoxysilyl)-propyl methacrylate (TMSPMA) monomer was performed using 21-Br β-CD possessing 21 initiation sites as the initiator to yield star-like PTMSPMA homopolymer. In a typical process, an ampule was quickly charged with 21-Br β-CD (0.02g), CuBr (0.0142g), PMDETA (0.0171g), TMSPMA (11.7ml), anhydrous toluene (15ml) and then degassed by three freeze−evacuate−thaw cycles in liquid N_2. The ampule was immersed in an oil bath at 50 °C. After proceeding to a desirable time (30 min for sample-1, and 2 h for sample-2), the polymerization was quenched by dipping the ampule in liquid N_2. The crude product was diluted with anhydrous dichloromethane, passed through a neutral alumina column, and then precipitated in anhydrous petroleum ether for three times to obtain pure product. The polymers were dried under reduced pressure.

Crafting organo-silica hybrid nanoparticles via intramolecular gelation

Organo-silica hybrid nanoparticles were crafted by hydrolysis and subsequent condensation of trimethoxysilyl moieties on star-like PTMSPMA with ammonia as catalyst. The reaction was conducted under high dilution to facilitate intramolecular gelation. Typically, star-like PTMSPMA (sample-1 and sample-2, 5mg) was dissolved in 1,4-dioxane (10ml). The solution was filtered using a 0.45-μm PTFE filter. 28%

ammonium hydroxide (0.1ml) was then added to the solution dropwise under vigorous magnetic stirring. The reaction proceeded at ambient temperature for 5 days. The product was purified by dialysis against dioxane.

Synthesis of star-like polystyrene

21-arm star-like PS was synthesized by ATRP of styrene using 21-Br β-CD as the initiator. The reaction mixture (styrene : -Br (in 21-Br β-CD) : CuBr : PMDETA = 400 : 1 : 1 : 1 (molar ratio) in toluene (1 g St in 1 mL solvent)) in an ampule was degassed by three freeze−evacuate−thaw cycles in liquid N_2, and then immersed in an oil bath at 80 °C. The polymerization was allowed to proceed to the desirable time, and then quenched by dipping into liquid N_2. The mixture was diluted with chloroform and passed through a neutral alumina column to remove copper catalyst. After concentration, the polymers were recovered by precipitating in methanol and filtration for three times. The product was finally dried to constant weight in a vacuum oven.

Synthesis of star-like PS-b-PTMSPMA diblock copolymers via sequential ATRP

Star-like PS-*b*-PTMSPMA composed of inner PS blocks and outer PTMSPMA blocks was prepared by sequential ATRP of TMSPMA with star-like PS as the macroinitiator as noted above. In a typical ATRP procedure, an ampule was quickly charged with 21-arm star PS (0.1g), CuBr (0.0044g), PMDETA (0.0053g), TMSPMA (3.6ml), and anhydrous benzene (4ml). The reaction mixture was degassed by three freeze−evacuate−thaw cycles in liquid N_2 and then placed in an oil bath at 70 °C. After the polymerization proceeded to a desirable conversion, the ampule was dipped in liquid N_2 to quench the reaction. The solution was diluted with anhydrous dichloromethane and passed through a column of neutral alumina to remove the catalyst. The mixture was then concentrated and precipitated in anhydrous petroleum ether for three times to recover the pure polymer. Final product was dried under reduced pressure.

Creating organo-silica hybrid nanocapsules by intramolecular crosslinking

Organo-silica hybrid nanocapsules were created by gelation of outer PTMSPMA blocks in star-like PS-*b*-PTMSPMA diblock copolymer under dilute condition. The reaction mixture (star-like PS-*b*-PTMSPMA (sample-a and sample-d, 5 mg) in 10 ml 1,4-dioxane mixed with 28% ammonium hydroxide (0.5 ml)) was allowed to proceed at ambient temperature for 5 days under constant stirring. Pure product was finally obtained by dialysis against dioxane.

Characterizations

All ^{1}H NMR spectra were obtained with a Bruker 400MHz spectrometer with solvent resonances as the internal standard. $CDCl_3$ was used as the solvent in all measurements. The molecular weights of polymers were obtained using a Shimadzu GPC equipped with a LC-20AD HPLC pump and a refractive index detector (RID-10A, 120V). Tetrahydrofuran (THF) was used as the mobile phase at 35 °C at 1.0 mL/min. One Phenogel 5u Linear (2) column and one Phenogel 5u 10E4A mixed bed column were calibrated with 10 polystyrene standard samples from 1.2×10^{6} to 500 g/mol. The morphologies of organo-silica hybrid nanoparticles and nanocapsules were examined by transmission electron microscopy (TEM) (JEOL TEM 100CX; operated at 100kv). TEM samples were prepared by drop-coating a dilute hybrid nanoparticles (or nanocapsules) solution onto a 400 mesh carbon-coated copper TEM grid. Dynamic light scattering (DLS) data was acquired using laser light scattering spectrometer (Malvern Zetasizer Nano ZS) at 25°C.

5.3 Results and Discussion

5.3.1. Synthesis of Star Homopolymer, Poly [3-(trimethoxysilyl)-propyl methacrylate] (PTMSPMA)

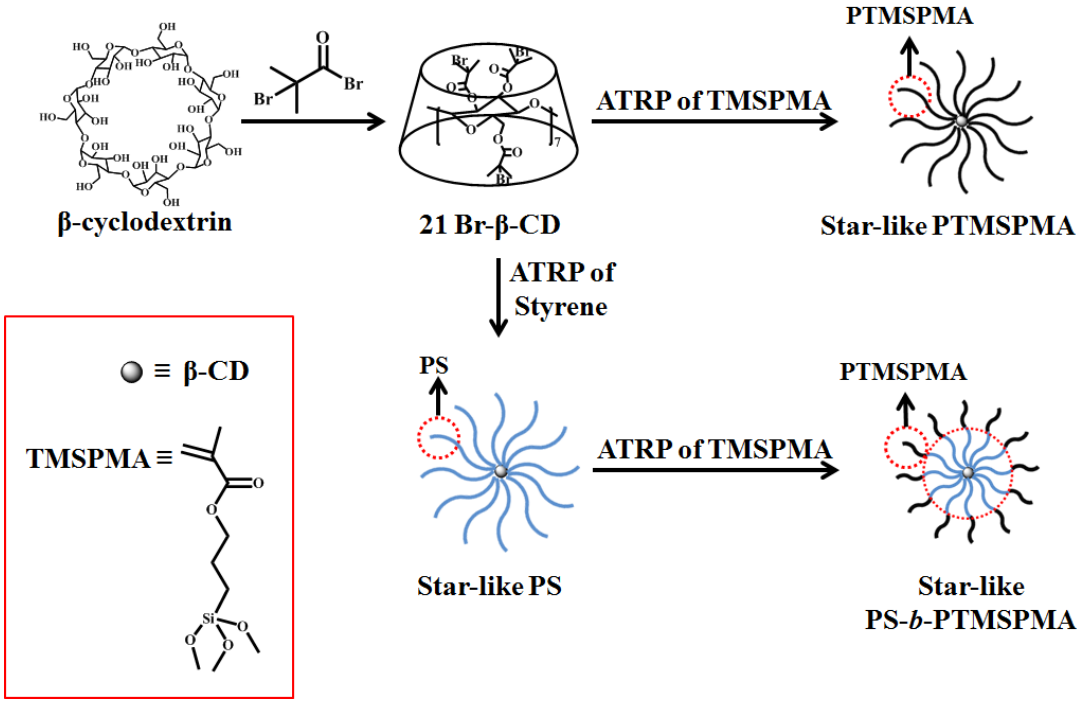

Scheme 5.1. Synthetic route to star-like PTMSPMA homopolymer (upper right panel) and star-like PS-*b*-PTMSPMA diblock copolymer (lower right panel).

Star-like homopolymer poly[3-(trimethoxysilyl)-propyl methacrylate] (PTMSPMA) and diblock copolymer polystyrene-*block*-poly[3-(trimethoxysilyl)-propyl methacrylate] (PS-*b*-PTMSPMA) containing trimethoxysilyl units were first rationally designed and synthesized (**Scheme 5.1**). For the synthesis of star-like PTMSPMA homopolymer (upper right panel in **Scheme 5.1**), Heptakis[2,3,6-tri-O-(2-bromo-2-methylpropionyl]-β-cyclodextrin) (denoted 21 Br-β-CD) was first prepared by reacting β-cyclodextrin (β-CD) with 2-bromoisobutyric bromide.[20] It has been demonstrated that all bromines on 21 Br-β-CD are capable of initiating ATRP to form 21-arm star-like polymers.[20,48] Star-like PTMSPMA was synthesized by ATRP of 3-(trimethoxysilyl)-propyl methacrylate (TMSPMA) using 21 Br-β-CD as an initiator (see *Experimental*

Section in *Supporting Information*). Due to the high reactivity of TMSPMA,[204] the reaction was conducted at dilute condition and a low conversion was maintained in order to minimize the coupling termination between star-like PTMSPMA radicals. The successful polymerization was confirmed by ^{1}H NMR analysis in which all characteristic peaks can be assigned to the corresponding protons on the polymer backbone (**Figure 5.1**). The gel permeation chromatography (GPC) traces exhibited monomodal peaks (**Figure 5.2**), indicating the formation of structurally well-defined products with low polydispersity. Two samples with different molecular weights were prepared by varying the ATRP time. Their structural parameters were summarized in **Table 5.1**. The star-like PTMSPMA can form spherical unimolecular micelle in solution,[265,267] and their intensity-average hydrodynamic diameter, D_h obtained by dynamic light scattering (DLS; **Figure 5.3**) was 10.7 ± 0.8 nm and 38.8 ± 5.7 nm for sample-1 and sample-2, respectively (Table 1). It is interesting to note that about 4 times increase in monomer conversion (13% in sample 2 compared to 3% in sample 1) resulted in approximately 4 times increase in molecular weight of star-like polymers due to the living characteristic of ATRP (**Table 5.1**).[268] Clearly, the size of star-like PTMSPMA can be tailored during the ATRP process, which is essential for control over the dimension of hybrid nanoparticles produced by this approach.

Table 5.1. Structural parameters of star-like PTMSPMA homopolymer and the corresponding organo-silica hybrid nanoparticles (NPs).

	Star-like PTMSPMA					**Organo-silica hybrid NPs**
	$M_{n,th}$[a] (kg/mol)	$M_{n,GPC}$[b] (kg/mol)	*PDI*[b]	*C*[d]	D_h[c] (nm)	*D*[e] (nm)
Sample-1	78	26	1.04	3%	11 ± 1	13 ± 2
Sample-2	340	110	1.10	13%	39 ± 6	38 ± 4

[a]Theoretical molecular weights calculated based on monomer conversion. [b]Obtained from GPC measurement using PS as the calibration standard. [c]Intensity-average hydrodynamic diameter, D_h of polymers obtained by dynamic light scattering (DLS). [d]Determined by

gravimetric method. [e]Average diameter of nanoparticles estimated from the TEM size analysis.

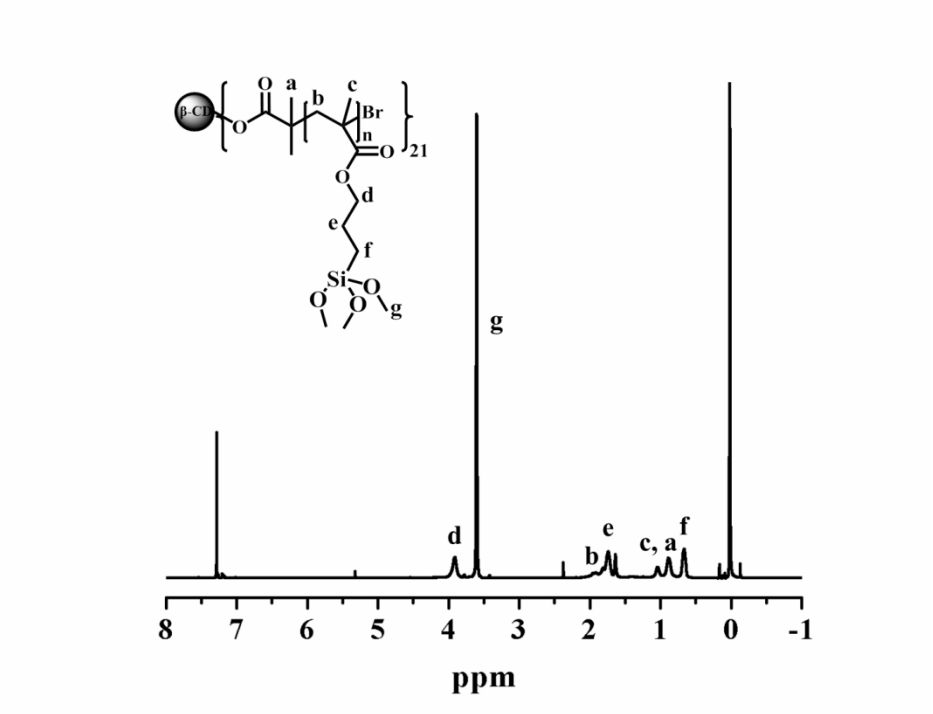

Figure 5.1. [1]H-NMR spectrum of star-like PTMSPMA homopolymer in $CDCl_3$ (i.e., sample-2 in Table 5.1).

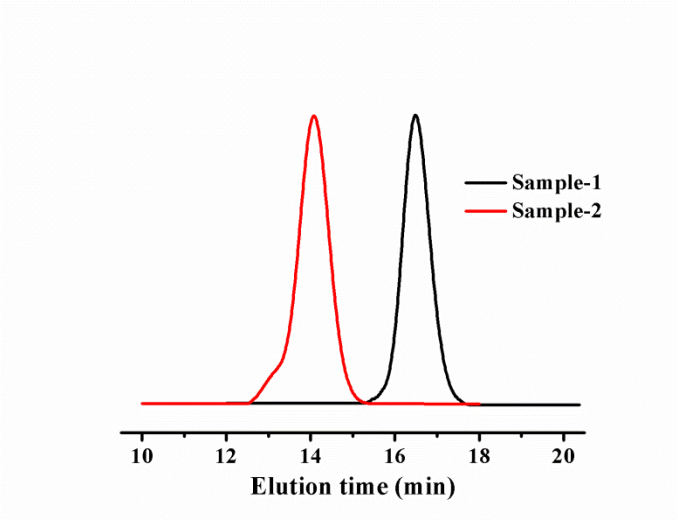

Figure 5.2. GPC traces of star-like PTMSPMA with different molecular weights as summarized in Table 5.1.

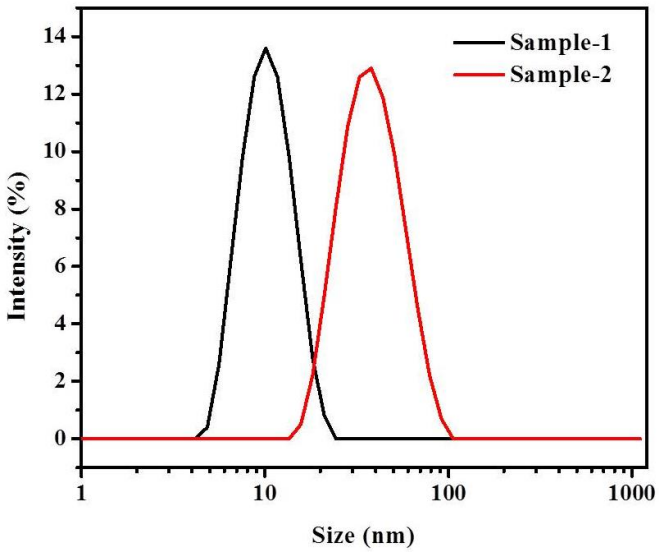

Figure 5.3. Dynamic light scattering (DLS) characterizations on star-like PTMSPMA homopolymers.

5.3.2. Preparation of Organo-silica Hybrid Nanoparticles

Subsequently, intramolecular crosslinking (i.e. gelation) of star-like PTMSPMA led to the formation of uniform organo-silica hybrid nanoparticles (**Scheme 5.2a**). Trimethoxysilyl moities ($Si(OCH_3)_3$) in star-like PTMSPMA were hydrolyzed into trihydroxylsilyl ($Si(OH)_3$). The hydrolyzed star-like polymer was then transformed into a crosslinked silsesquioxane network via polycondensation.[269,270] The reaction was catalyzed by small amount of ammonia and performed under highly dilute condition to avoid intermolecular crosslinking (see *Experimental Section*). The sample-1 (i.e., star-like PTMSPMA) with lower molecular weight was first used as nanoreactor itself to produce smaller organo-silica hybrid nanoparticles. The nanoparticles were formed after reaction at ambient temperature for 5 days as evidenced by the TEM measurement

(**Figure 5.4a**). The low contrast of nanoparticles was due possibly to its very small size. The average size of nanoparticles was 13 ± 2 nm (**Figure 5.5a**), which is close to the hydrodynamic diameter of original star-like PTMSPMA (10.7 ± 0.8 nm; sample-1 in **Table 5.1**). This suggested that hybrid nanoparticles were created from individual star-like polymers, and such spherically shaped polymers served as unimolecular nanoreactors.

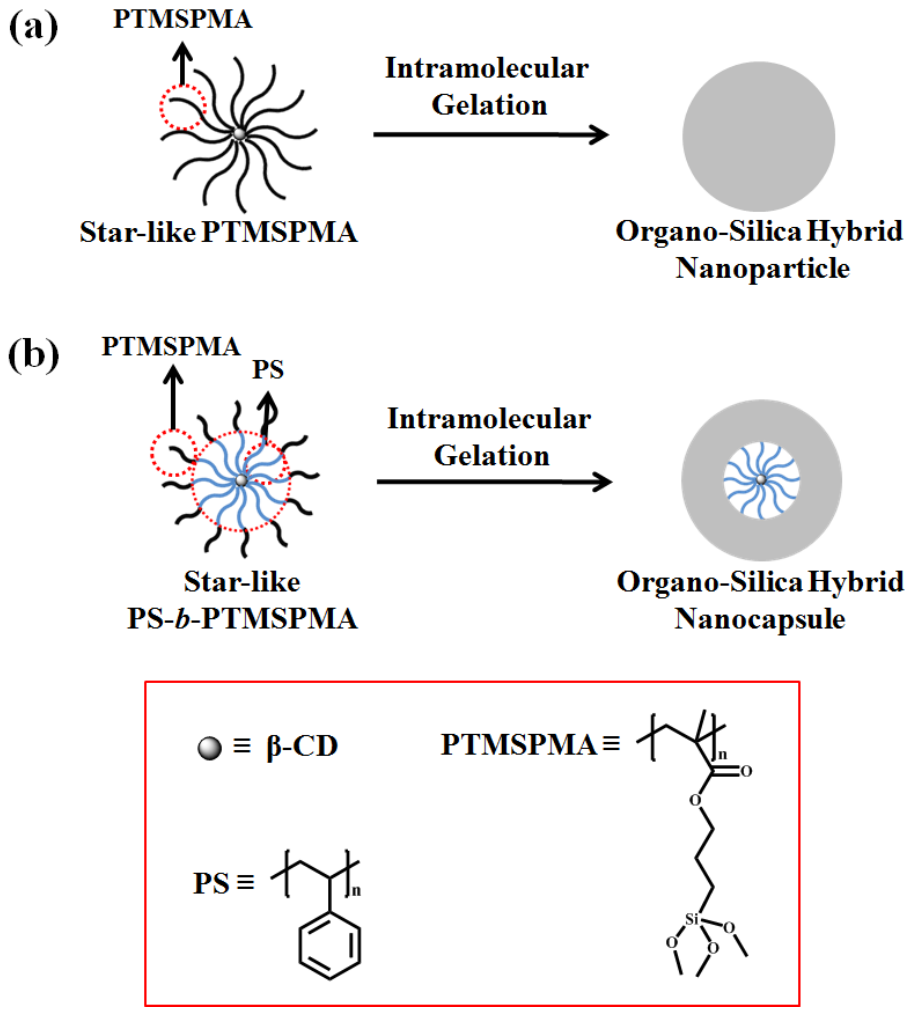

Scheme 5.2. Star-like polymer nanoreactor strategy for organo-silica hybrid nanoparticles and nanocapsules. (a) Synthesis of organo-silica hybrid nanoparticles by capitalizing on star-like PTMSPMA homopolymer containing trimethoxysilyl moieties as unimolecular nanoreactor. (b) Preparation of organo-silica hybrid nanocapsules by exploiting star-like PS-*b*-PTMSPMA diblock copolymer as unimolecular nanoreactor in which trimethoxysilyl moieties are incorporated in the outer PTMSPMA blocks.

In order to demonstrate the exquisite control over the size of hybrid nanoparticles using the star-like polymer nanoreactor approach, star-like PTMSPMA with larger molecular weight (i.e., sample-2; approximately 4 times larger than sample-1) was synthesized and utilized as nanoreactor. The hybrid nanoparticles with larger size and higher contrast were clearly observed (**Figure 5.4b**). The average diameter of nanoparticles was 38 ± 4 nm based on the TEM image analysis (**Figure 5.5b**), which is also consistent with the hydrodynamic diameter of original star-like PTMSPMA (38.8 ± 5.7 nm; sample-2 in **Table 5.1**), and was almost 4 times larger than that of nanoparticles produced from sample-1. Obviously, the increase in the nanoparticle size can be attributed to the increase in molecular weight of star-like PTMSPMA. Consequently, the size of nanoparticles can be easily tuned by varying the molecular weight of star-like polymer during ATRP of TMSPMA.

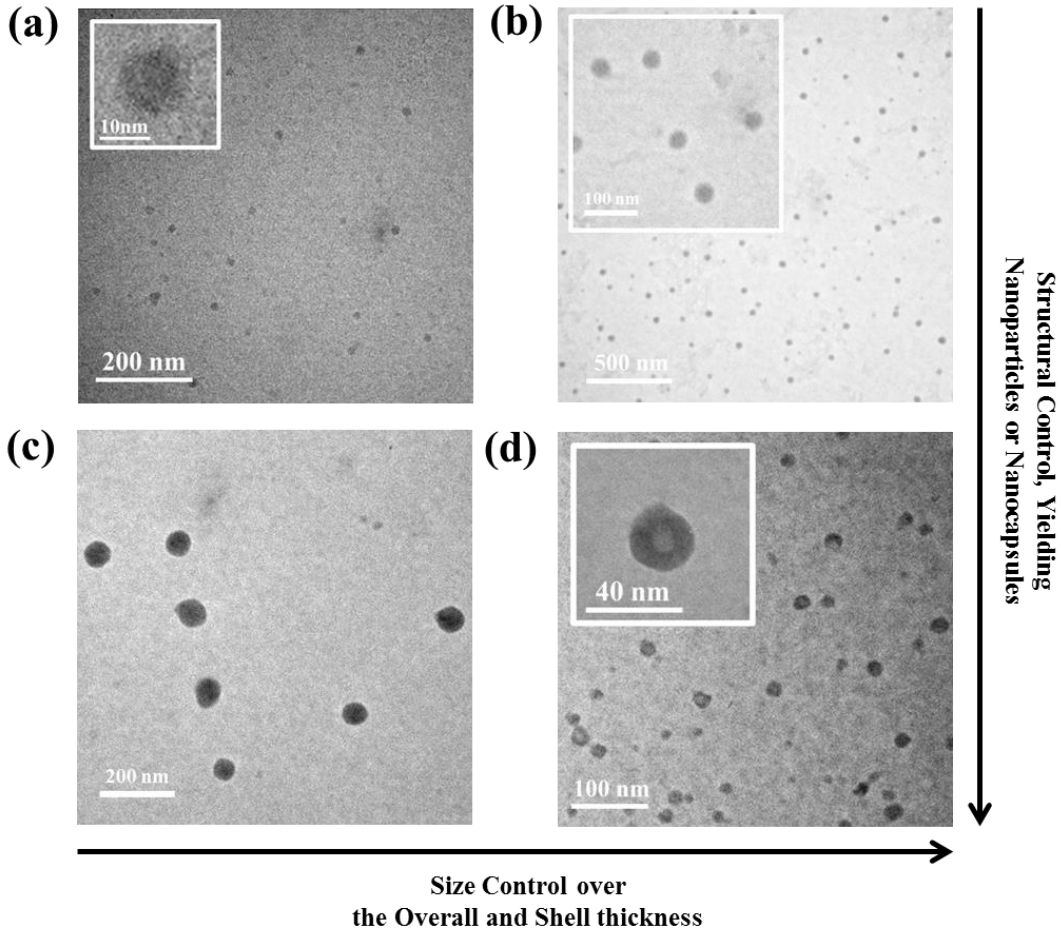

Figure 5.4. TEM characterizations of organo-silica hybrid nanoparticles and nanocapsules. (a) Hybrid nanoparticles crafted from sample-1 (i.e., star-like PTMSPMA) with smaller molecular weight; the average diameter of nanoparticle, D_{ave} = 13 ± 2 nm. (b) Hybrid nanoparticles created from sample-2 (i.e., star-like PTMSPMA) with larger molecular weight; the average diameter of nanoparticle, D_{ave} = 38 ± 4 nm. (c) Hybrid nanocapsules produced from sample-a (i.e. star-like PS-*b*-PTMSPMA) with larger molecular weight of the outer PTMSPMA block; the average diameter of nanocapsule, D_{ave} = 71 ± 5 nm. (d) Hybrid nanocapsules yielded from sample-d, with smaller molecular weight of the outer PTMSPMA block; the average diameter of nanocapsule, D_{ave} = 28 ± 5 nm.

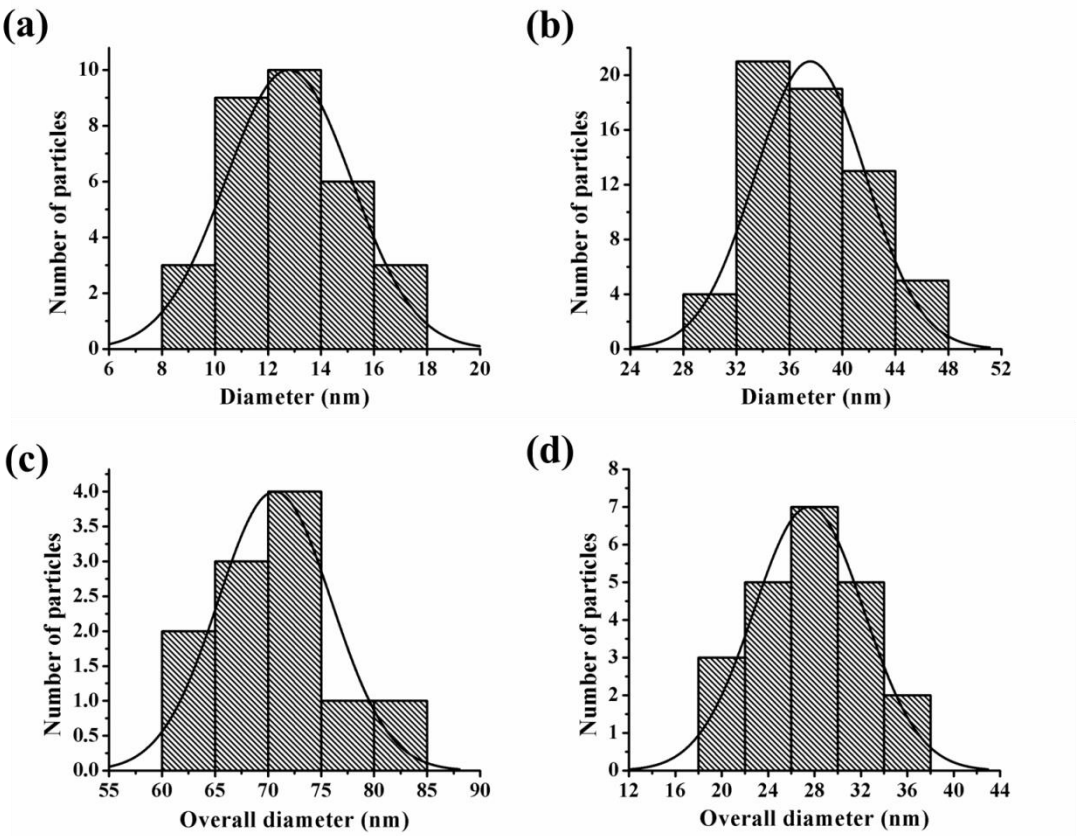

Figure 5.5. Size distributions of hybrid nanoparticles and nanocapsules obtained from the TEM image analysis. The average diameters of nanoparticles or nanocapsules are summarized in Table 5.1 and Table 5.3, respectively. (a) Organo-silica hybrid nanoparticles crafted from sample-1 (i.e. star-like PTMSPMA with smaller molecular weight). (b) Organo-silica hybrid nanoparticles crafted from sample-2 (i.e. star-like PTMSPMA with larger molecular weight). (c) Organo-silica hybrid nanocapsules created from sample-a (i.e. star-like PS-*b*-PTMSPMA with larger molecular weight of outer PTMSPMA block). (d) Organo-silica hybrid nanocapsules created from sample-d (i.e. star-like PS-*b*-PTMSPMA with smaller molecular weight of outer PTMSPMA block).

5.3.3. Synthesis of Core-shell Star PS-*b*-PTMSPMA Block Copolymers

Quite intriguingly, the star-like nanoreactor strategy is versatile in crafting uniform nanostructures. In addition to organo-silica hybrid nanoparticles, the application of judiciously designed star-like PS-*b*-PTMSPMA diblock copolymer composed of inner PS block and outer PTMSPMA block as nanoreactor rendered the creation of organo-silica hybrid nanocapsules after subsequent intramolecular crosslinking (i.e., gelation) of

outer PTMSPMA blocks (**Scheme 5.2b**). In star-like PS-*b*-PTMSPMA diblock copolymer, PS was chosen as the inner block due to its ease of polymerization and chemical inertia for the subsequent gelation process. Specifically, star-like PS was synthesized by ATRP of styrene using 21-Br β-CD as the initiator. Successful polymerization was verified by ^{1}H NMR measurement (**Figure 5.6**). Notably, the resonance at 4.4 - 4.6 ppm (g) can be ascribed to the methine protons near terminal bromines at the chain end.[271] The GPC measurements showed the narrow molecular weight distribution of product (**Figure 5.7**). The small shoulder observed at low elution time was originated from the coupling termination between star-like PS radicals which dominated the termination process in radical polymerization of PS and is difficult to avoid.[272] Two star-like PS samples with different molecular weights were prepared (**Table 5.2**). The number-average molecular weights estimated from NMR end group analysis, which was based on the integration ratio of H^c to H^d (I^c/I^d) assuming that each bromine on 21-Br β-CD initiated the polymerization, agreed well with the theoretical molecular weights calculated based on the monomer conversion. This implied that the initiation efficiency of bromoisobutyryl was nearly quantitative, yielding 21-arm star-like PS. The molecular weights obtained from GPC measurements deviated from the theoretical values, which due to the smaller hydrodynamic volume star-like PS compared to linear PS standards.[20]

Table 5.2. Structural parameters of star-like PS synthesized under varied reaction conditions

Star-like PS	$M_{n,GPC}$[a] ***(kg/mol)***	$M_{n,th}$[b] ***(kg/mol)***	$M_{n,NMR}$[c] ***(kg/mol)***	N_{PS}[c] **per arm**	***PDI***[a]	***C***[d]
Sample-1	52	96	94	43	1.04	11%
Sample-2	69	120	130	59	1.09	14%

[a]Obtained from GPC measurement using PS as the calibration standard. [b]Theoretical molecular weights calculated based on the monomer conversion. [c]Number-average molecular weights, $M_{n,NMR}$ and the number of repeating units, N estimated from the NMR analysis. [d]Determined by gravimetric method.

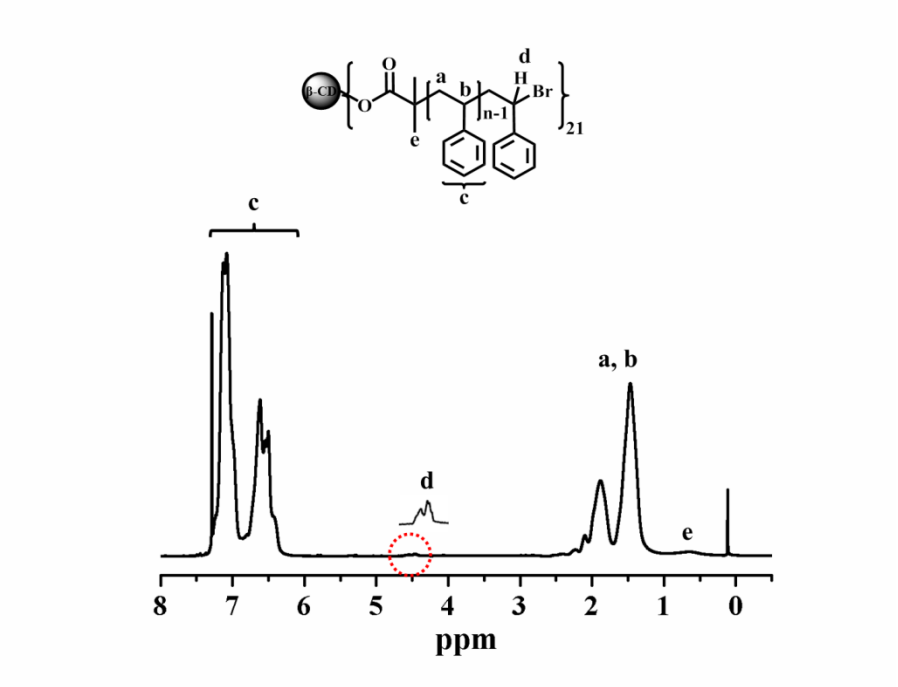

Figure 5.6. [1]H-NMR spectrum of 21-arm star-like PS in $CDCl_3$ (i.e., sample-1 in Table 5.2).

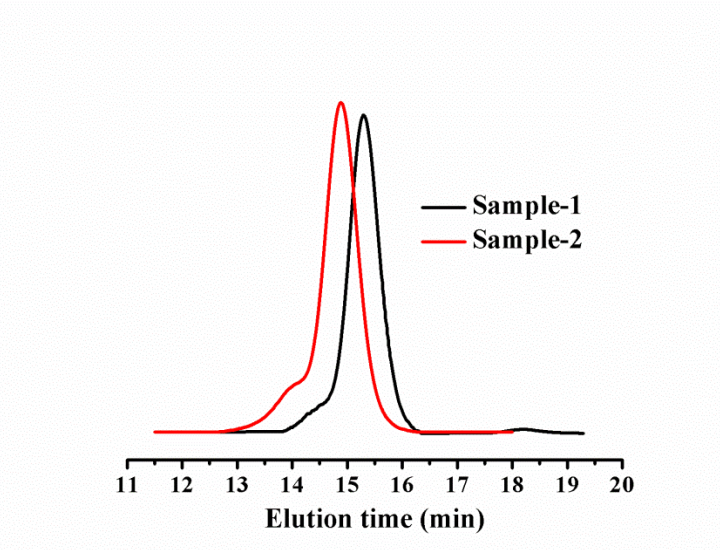

Figure 5.7. GPC traces of 21-arm star-like PS with different molecular weights as summarized in Table 5.2.

Star-like PS-*b*-PTMSPMA diblock copolymers were then synthesized via the chain extension from 21-arm star-like PS by the ATRP of TMSPMA (lower right panel in **Scheme 5.1**). The proton resonances from outer PTMSPMA blocks emerged in ^{1}H NMR spectrum of the resulting star-like PS-*b*-PTMSPMA (**Figure 5.8**), signifying the success in the growth of outer PTMSPMA blocks. The molecular weights of star-like diblock copolymers can be estimated from the ^{1}H NMR analysis based on the integration ratio between PTMSPMA and PS blocks (I^{c}/I^{h}) as summarized in **Table 5.3**. The GPC characterization also corroborated the successful chain extension with the elution peak of star-like PS shifted to the higher molecular weight region after reaction (**Figure 5.9**). Five samples with various molecular weights of outer PTMSPMA blocks were synthesized by changing the reaction conditions (**Table 5.3**). As the molecular weights of inner PS and outer PTMSPMA blocks were independently controlled, the polydispersity of star-like diblock copolymers remained low. These star-like diblock copolymers also formed unimolecular micelles in solution with the sizes determined by DLS (**Figure 5.10**).

Table 5.3. Structural parameters of star-like PS-*b*-PTMSPMA diblock copolymers and the corresponding organo-silica hybrid nanocapsules (NCs).

	Star-like PS-*b*-PTMSPMA							**Organo-silica hybrid NCs**
	Inner PS block	$M_{n,NMR}$[a] (kg/mol)	$M_{n,,GPC}$[b] (kg/mol)	PDI[b]	N_{PS}[a] per arm	$N_{PTMSPMA}$[a] per arm	D_h[c](nm)	D[d] (nm)
Sample-a	(Sample-1)	530	350	1.27	43	84	83 ± 18	71 ± 5
Sample-b	(Sample-2)	140	73	1.10	59	3	-	-
Sample-c	(Sample-2)	160	78	1.12	59	6	-	-
Sample-d	(Sample-2)	210	96	1.14	59	15	30 ± 1	28 ± 5
Sample-e	(Sample-2)	550	270	1.36	59	80	-	-

[a]Number-average molecular weights, $M_{n,NMR}$ and the number of repeating units, N estimated from the NMR analysis. [b]Obtained from GPC measurement using PS as the calibration standard. [c]Intensity-average hydrodynamic diameter, D_h of polymers obtained by DLS. [d]Average diameter of nanocapsules estimated from the TEM size analysis.

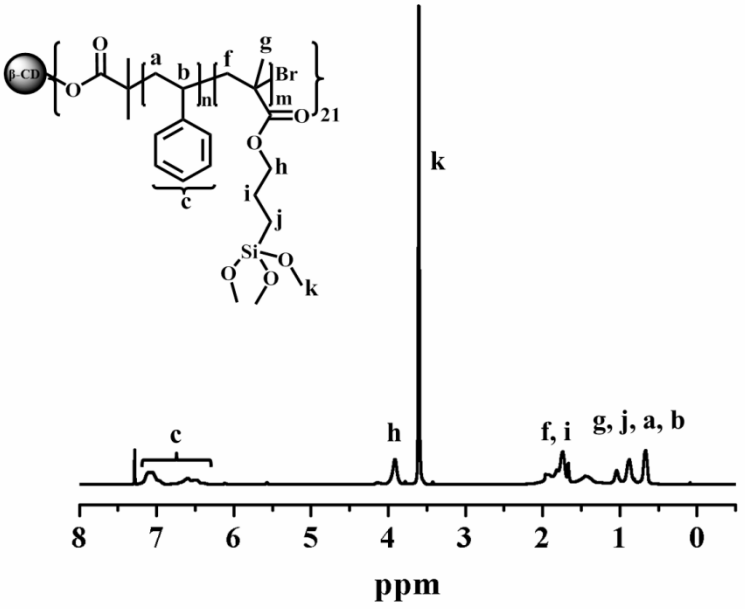

Figure 5.8. ^{1}H-NMR spectrum of star-like PS-*b*-PTMSPMA diblock copolymer in $CDCl_3$ (i.e., sample-e in Table 5.3).

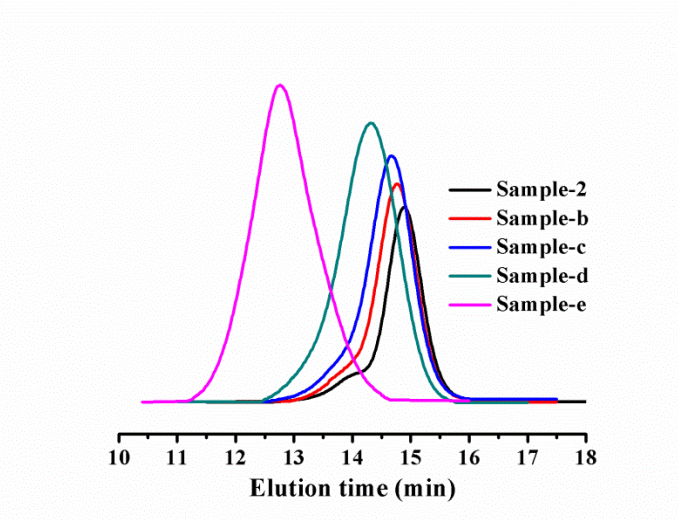

Figure 5.9. GPC traces of star-like PS-*b*-PTMSPMA diblock copolymers with varied molecular weights of outer PTMSPMA block (Table 5.3) prepared by the chain extension from 21-arm star-like PS macroinitiator (i.e. sample-2 in Table 5.2) via the ATRP of TMSPMA.

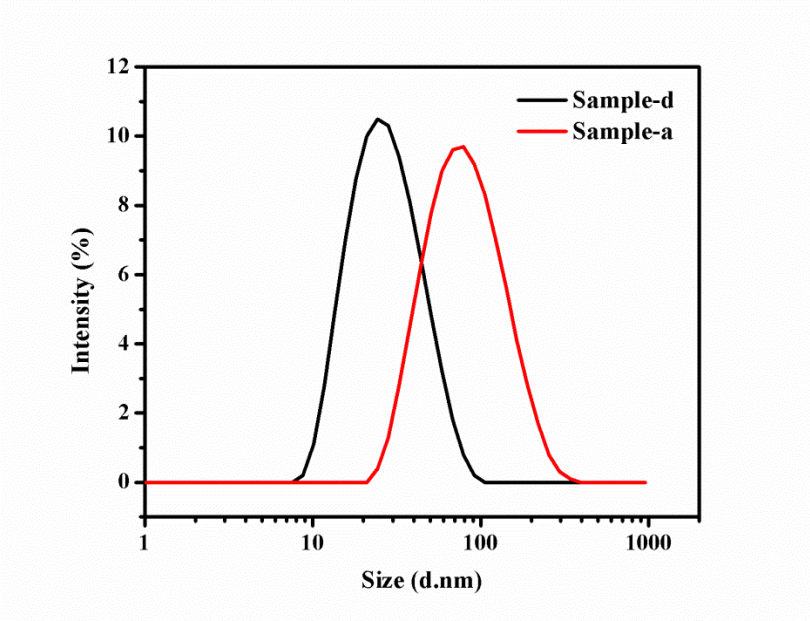

Figure 5.10. DLS measurements on star-like PS-*b*-PTMSPMA diblock copolymers (samples in Table 5.3).

5.3.4. Creation of Organo-silica Hybrid Nanocapsules

Similar to the crafting of organo-silica hybrid nanoparticles, by employing star-like PS-*b*-PTMSPMA as unimolecular nanoreactor, organo-silica hybrid nanocapsules with an interior cavity were created via the selective intramolecular gelation of the outer PTMSPMA blocks. Likewise, the reaction was catalyzed by ammonia and performed under high dilution. The sample-a (i.e. star-like PS-*b*-PTMSPMA) with a large molecular weight of outer PTMSPMA block was first studied. The TEM characterization revealed the formation of nanoparticles with an average size of 71 ± 5 nm (**Figure 5.4c** and **Figure 5.5c**), which is close to the hydrodynamic diameter of star-like diblock copolymer nanoreactor (83.2 ± 17.5 nm; sample-a in **Table 5.3**), suggesting the nanoparticle was templated by individual star-like PS-*b*-PTMSPMA. We note that as the outer PTMSPMA block had much higher molecular weight than that of inner PS block (84 repeat units of TMSPMA compared to 43 repeat units of styrene), the interior cavity occupied by PS chains cannot be visualized by TEM. To this end, star-like PS-*b*-PTMSPMA with a relatively low molecular weight of PTMSPMA and higher molecular weight of PS (sample-d) was then selected to prepare the hybrid nanostructure. Clearly, a hollow interior was seen in hybrid nanocapsules (**Figure 5.4d**) as a result of the formation of a thinner outer PTMSPMA block with a much decreased molecular weight (i.e., decreased approximately 5.6 times in comparison to sample-a), substantiating that hybrid nanocapsules with a cavity possessing PS arms were successfully produced by crosslinking the outer PTMSPMA blocks of star-like diblock copolymer. On the basis of the TEM image analysis, the average overall diameter of nanocapsules was 28 ± 5 nm (**Figure 5.5d**), which is in good agreement with the size of the star-like diblock copolymer nanoreactor (sample-d) and smaller than the size of nanocapsules obtained from sample-a (**Table 5.3**). The decreased size was due to the reduction in the overall molecular weight of the copolymer nanoreactor. Although it may be difficult to obtain accurate shell thickness of nanocapsules because of the non-uniform shell observed in

TEM (**Figure 5.4d**), an important piece of information can be gained from this study: the overall size and the shell thickness of nanocapsules are dictated by the chain lengths of star-like diblock copolymer and outer PTMSPMA block, respectively, and can be readily regulated during the ATRP of star-like PS-*b*-PTMSPMA.

5.4 Summary

In summary, we developed a versatile preparative route to uniform organo-silica hybrid nanoparticles and nanocapsules by capitalizing on star-like polymers as nanoreactors. The star-like PTMSPMA homopolymer and PS-*b*-PTPMSPMA diblock copolymer containing trimethoxysilyl functionalities in PTPMSPMA blocks were synthesized by ATRP. The hydrolysis and subsequent condensation of trimethoxysilyl moieties introduced a crosslinked silsesquioxane network in star-like PTMSPMA homopolymer and in the outer PTMSPMA blocks of star-like PS-*b*-PTMSPMA to yield hybrid nanoparticles and nanocapsules, respectively. The dimensions of hybrid nanoparticles and nanocapsules are dictated by the chain lengths (i.e., molecular weights) of star-like PTMSPMA and PS-*b*-PTMSPMA nanoreactors, respectively, which can be precisely engineered by living polymerizations (i.e., ATRP of TMSPMA for star-like PTMSPMA, and sequential ATRPs of styrene and TMSPMA for star-like PS-*b*-PTMSPMA).

It is worth noting that other polymer composition can also be employed as the inner block in star-like diblock copolymer (e.g., polycaprolactone (PCL), a biocompatible and biodegradable polymer), and thus the inner block in nanocapsule can be facilely tuned (e.g., the degradation of PCL would result in purely hollow nanocapsule). We envision that silica nanoparticles and nanocapsules can be obtained after pyrolysis and further reduced to silicon nanoparticles and nanocapsules for use as anode materials in lithium ion batteries and as controlled-release vehicles in biomedical applications. This

will be the subject of our future work. Moreover, the nanoreactor strategy is general and robust, and may provide enormous opportunities for the development of materials with new structures and functionalities. For example, by rationally designing and synthesizing nonlinear yet structurally regular polymers including star-like polymers that possess metal-containing moieties in the constituent blocks of nonlinear polymers, other exotic metal- and metal oxide-containing nanostructures can be readily accessed for a large variety of applications.

CHAPTER 6

DESIGN AND SYNTHESIS OF CYCLIC BRUSH COPOLYMER FOR MORPHOLOGICAL AND ASSEMBLY STUDY AT NANAOSCALE

6.1 Introduction

Conjugated polymers (e.g. poly(3-alkylthiophenes) (P3AT)) has attracted considerable interest as promising semiconductor materials for electronic applications in light-emitting diodes (LEDs), field-effect transistors, thin film transistors, and organic photovoltaics. Regioregular poly(3-hexylthiophene) (*rr*-P3HT) is among the most heavily studied conjugated polymers owing to its ease of preparation, good solution processability, and excellent hole mobility. P3HT is composed of a rigid conjugated backbone which allows for efficient π-π stacking, as well as pendant hexyl side chains for improving the solubility. While research efforts on P3HT mainly involve linear or block copolymers, other complex macromolecular architectures have been recently prepared and discovered to exhibit unique properties. For example, a macrocyclic regioregular P3HT was prepared by intramolecular imperfect aldol reaction. Interestingly, the P3HT macrocycles self-assembled into a tubular nanostructure via effective π-π stacking interaction. Moreover, a P3HT molecular bottlebrush was also synthesized by ring opening metathesis polymerization (ROMP) of a conjugated macromonomer. The molecular bottlebrush grafted with P3HT side chains exhibits strong aggregation property attributed to the enhanced π-π interaction of P3HTs in bottlebrush architecture. As macromolecular architectures profoundly influence the physical properties and morphology of polymer materials, synthesis of complex P3HT-based structures and investigation of their properties has received growing interest and become a recent research focus in the field.

Brush copolymers consisted of polymer side chains which are densely grafted along a polymeric backbone represents an important class of comb-shaped macromolecular architecture. The steric repulsion originating from the high density of grafted side chains forces the macromolecule to adopt an extended cylindrical conformation. As a result, the brush copolymers exhibit worm-like nanostructures during molecular imaging. The extended molecular architecture and reduced chain entanglement render brush copolymers with distinct chemical and physical properties compared to traditional coiled polymers, which make them excellent research subject for understanding structure-property relationship and other technological applications. Most of the brush copolymers that were synthesized and studied over the past decade feature a linear backbone or star shape. However, the report on cyclic brush copolymers which features a toroidal nanostructure remains rare, due partly to the challenging in synthesizing high molecular weight cyclic backbone and achieving high grafting density of side chains.

Since the inspiring work on synthesis of high molecular weight cyclic brush copolymers and their assembly into huge supramolecular tubes reported by Deffieux and co-workers, cyclic brush polymers have garnered much attention with the emphasis on simplifying the experimental conditions, reducing linear brush polymer impurities, and incorporating functionalities. Synthetic approaches to construct the cyclic backbone include end-to-end ring closure method, ring-chain equilibrium, and ring-expansion polymerization techniques. Among them, ring-expansion polymerization (REP) allows the synthesis of cyclic polymers without high dilution requirement and the polymer product to possess high structural purity. On the other hand, the grafting of polymeric side chains can generally be realized by three strategies: grafting onto, grafting from, and grafting through. It is worth mentioning that click chemistry has been widely utilized to graft side chains onto a polymeric backbone bearing clickable functionalities for the preparation of graft polymers, due to its excellent selectivity, high efficiency and high

yields. The cyclic brush copolymers reported to date mainly contain insulated polymer side chains. However, to the best of our knowledge, those composed of conjugated polymer side chains which may display interesting morphology and unique properties have not yet been prepared.

Herein, we report, for the first time, the synthesis of cyclic brush copolymer densely grafted with conjugated side chains via a judicious combination of anionic ring opening polymerization (ROP) and click chemistry, as shown in **Scheme 6.1**. The cyclic brush polymer, cyclic poly(ethylene glycol)-*g*-poly(3-hexylthiophene) (*c*-PEG-*g*-P3HT), is composed of hydrophilic PEG as the cyclic backbone and conjugated P3HT as side chains. The product has well-defined architecture and controlled molecular weight. The cyclic backbone which bears hydroxyl groups in each repeating unit was synthesized by ring closure of a telechelic a,ω-dihydroxyl linear polymer precursor prepared through anionic ROP under high dilution condition. Azide functionalities were then introduced to the cyclic backbone via several transformational steps for click reaction. Ethynyl-terminated P3HT was synthesized by a quasi-living Grignard Metathesis method (GRIM), and subsequently grafted onto the functional cyclic backbone via the facile click chemistry to obtain the final cyclic brush polymers grafted with conjugated side chains (**Scheme 6.1**). Interestingly, this new P3HT-based molecular architecture showed distinctive property and morphology. The conjugated cyclic brush polymers self-assembled into a macrocyclic nanostructure in a selective solvent for P3HT branches, as revealed by AFM imaging.

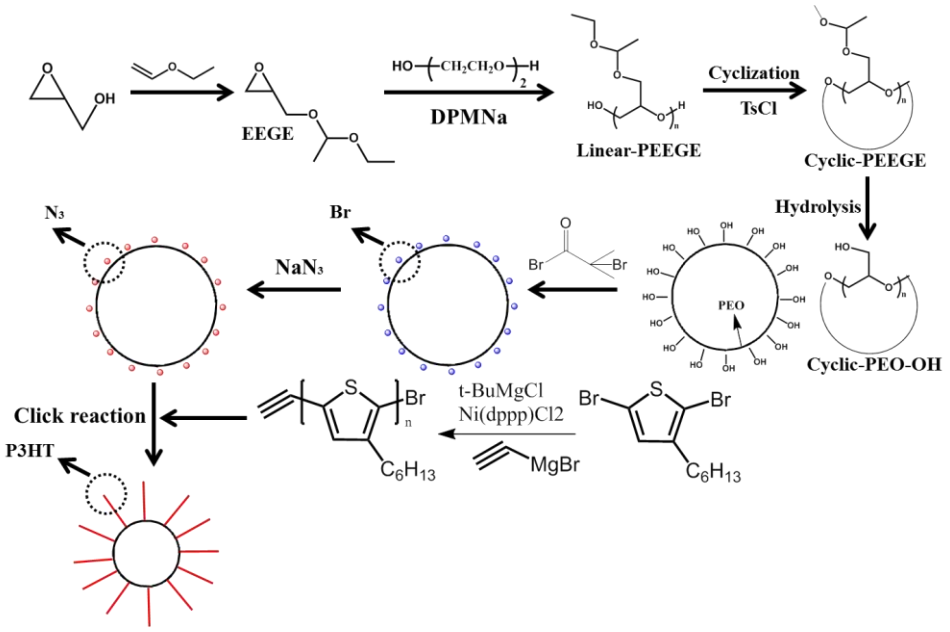

Scheme 6.1. Synthetic scheme of cyclic brush copolymer, *c*-PEG-*g*-P3HT, composed of PEG as the cyclic backbone and conjugated P3HT as side chains.

6.2 Experimental Details

Materials

Anhydrous 1-Methyl-2-pyrrolidone (NMP; 99.5%), 2-Bromoisobutyryl bromide (98%), ethyl vinyl ether (98%), *p*-toluene sulfonic acid (TsOH; >98%), sodium (stored under mineral oil; ≥99%), sodium azide (NaN_3; ≥99%), tert-butylmagnesium chloride (2.0 M solution in diethyl ether), [1,3-bis(diphenylphosphino)propane]dichloronickel-(II), ethynylmagnesium bromide (0.5 M solution in tetrahydrofuran), *N,N,N′,N″,N″*-pentamethyldiethylene triamine (PMDETA, 99%), and 2,5-dibromo-3-hexylthiophene (97%) were purchased from Sigma-Aldrich and used as received. Glycidol (96%) was purchased from Sigma-Aldrich, dried over CaH_2, and then distilled under reduced pressure prior to use. Triethylene glycol and 1,1-diphenylethylene (99%) purchased from Sigma-Aldrich were also distilled over calcium hydride under reduced pressure before use. Dry THF was prepared by refluxing THF (99%) over sodium wire and distilling

from the sodium naphthalenide solution. Potassium hydroxide (KOH; 96%) and *p*-toluenesulfonyl chloride (TsCl; 98%) purchased from Sigma-Aldrich were dried in vacuum oven before use. CuBr (98%, Sigma-Aldrich) was stirred in acetic acid overnight, filtrated, then washed with ethanol and diethyl ether successively, and finally dried in vacuum.

Synthesis of 2,3-epoxypropyl-1-ethoxyethyl ether (EEGE) monomer

Ethyl vinyl ether was used to protect the hydroxyl group of glycidol according to a literature described procedure.[273] In a typical procedure, 50 g (0.675 mol) glycidol and 200 mL ethyl vinyl ether solution were loaded in a 250 ml round-bottom flask with a magnetic stirrer, to which 1.25 g TsOH was then added. The reaction was allowed to proceed at room temperature (RT) for 3h. The resulting mixture was then purified by washing with 100 ml saturated aqueous solution of $NaHCO_3$ for 3 times. The organic layer obtained was dried with $MgSO_4$. After filtration of $MgSO_4$, the excess ethyl vinyl ether was removed by rotary evaporation. The fraction at 51 ° C /80 Pa from the remaining solution was collected under reduced pressure distillation. The final product EEGE monomer is a colorless liquid (bp: 152 – 154° C, Yield: 84%). FTIR (film, ν): 1350, 1254 cm^{-1}.

Synthesis of linear poly(2,3-epoxypropyl-1-ethoxyethyl ether) (*l*-PEEGE) via anionic ring opening polymerization

The catalyst for polymerization, diphenylmethyl sodium (DPMNa) was prepared as follows: 7.7 mL (0.06 mol) 1,1-diphenylethylene and 100 mL dry THF were loaded in a 150 ml round-bottom flask, to which 1.38 g (0.06 mol) sodium with fresh surface was then added under nitrogen atmosphere. After reaction at room temperature for 4 h, 11.1 g (0.066 mol) diphenylmethane was added to the system via syringe and the solution was

refluxed at 80° C for 1d. The concentration of DPMNa was determined to be 0.57 M by titration with 0.1 M HCl.

The typical polymerization procedure was as follows: an ampule was vacuumed for 2 h under 80° C to remove trace amount of water, and then gradually cooled to 0° C. The ampule was charged with the initiator solution [triethylene glycol (2.19 mmol) together with DPMNa (2.0 mL, 1.14 mmol) in a THF/DMSO mixed solvent (1/4 v/v, 50 mL)] and EEGE monomer (11.1 g, 75.8 mmol) successively under stirring. The system was allowed to react at 60° C for 2d, after which the polymerization was quenched by a few drops of acidified methanol. The solvents were removed by reduced pressure distillation. The crude product was diluted with dichloromethane, and then dried over anhydrous $MgSO_4$. After filtration of $MgSO_4$, concentration, and precipitation in cold heptane, a yellow viscous product was finally obtained.

Preparation of cyclic PEEGE (*c*-PEEGE) by ring closure of *l*-PEEGE under high dilution condition

Typically, KOH (1.0 g) which was finely ground was dispersed in THF/heptane mixed solvent (7/3 v/v, 100 mL) in a round-bottom flask. The system was kept under vigorous stirring and nitrogen atmosphere at 40° C. The poor solvent heptane was added in order to facilitate the ring closure process over intermolecular condensation by reducing the end-to-end chain distance. Liner PEEGE (*l*-PEEGE, 7.0 g) and TsCl (161 mg) solution dissolved in 100 mL THF was prepared in a separate flask, and then added to the KOH dispersion system using a syringe pump dropwise over 2d. The mixture was allowed to react for another 3d under reflux (40 ° C). After filtration and concentration, the cyclized product was obtained after precipitation in cold heptane.

Deprotection of hydroxyl groups by hydrolysis to obtain cyclic polyglycidol (*c*-PEO-OH)

In a typical procedure, cyclic PEEGE (*c*-PEEGE, 0.6g) was dissolved in 15 ml THF. pH of the solution was adjusted to around 1 by adding hydrochloric acid. The system was refluxed at 80 ° C for 2h. After reaction is complete, hydrolyzed product cyclic polyglycidol (*c*-PEO-OH) was obtained by removing the solvent under reduced pressure.

Bromination of the hydroxyl groups on *c*-PEO-OH to obtain *c*-PEO-Br

Bromine (Br) was incorporated into the cyclic polymer as substrate for later introduction of azide functionalities by reacting *c*-PEO-OH with 2-bromoisobutyryl bromide. In a typical example, 1 g *c*-PEO-OH was dissolved in 30 mL anhydrous N-Methyl-2-pyrrolidone (NMP) solvent under dry nitrogen atmosphere, to which 10 mL 2-bromoisobutyryl bromide was added at 0 ° C dropwise for 30 min under vigorous stirring. The reaction mixture was then allowed to proceed at room temperature for 1d. After that, the solution was concentrated by reduced pressure distillation to remove NMP solvent and excess 2-bromoisobutyryl bromide. The crude product was then washed with saturated aqueous solution of $NaHCO_3$ and water sequentially for 3 times, dried over $MgSO_4$, and precipitated in cold *n*-hexane to obtain a final brown product.

Preparation of *c*-PEO-N_3 by substituting the Br on *c*-PEO-Br with azide functionalities

Typically, *c*-PEO-Br (0.55g) and NaN_3 (0.73g) were dissolved in 20 ml DMF in a flask. The mixture was reacted at room temperature for 24h. After the reaction is complete, the mixture was filtered through a column of neutral alumina with dichloromethane as eluent. The solution was then concentrated under reduced pressure to remove the solvents, and finally precipitated in cold *n*-hexane for three times to obtain the product *c*-PEO-N_3.

Synthesis of ethynyl-terminated poly(3-hexylthiophene) (P3HT) by Grignard Metathesis method (GRIM)

Ethynyl-terminated P3HT was prepared according to the literature.[274] 2,5-dibromo-3-hexylthiophene monomer (0.815 g, 2.5 mmol) dissolved in 5 ml THF was added to an ampule with a syringe under Ar atmosphere, to which *tert*-Butylmagnesium chloride (1.25 mL, 2.5 mmol) was subsequently added using a syringe. The solution was stirred at room temperature for 2 h to produce the active monomer. After the mixture was diluted with 25 ml THF, Ni(dppp)Cl_2 (22.5 mg, 0.041 mmol) was then added to initiation the polymerization. After reacting at room temperature for 10 min to produce intermediate P3HT, the living polymer was then quenched with ethynylmagnesium bromide (2 ml, 1 mmol). The functionalization process took 30 min. After precipitation in methanol and filtration, the crude product was then washed sequentially with methanol, hexanes, and chloroform by Soxhlet extraction. The final pure ethynyl-terminated P3HT (i.e., P3HT−≡) was recovered by evaporation of chloroform.

Grafting of ethynyl-terminated P3HT onto *c*-PEO-N_3 backbone via click reaction

Briefly, *c*-PEO-N_3, P3HT−≡, CuBr and PMDETA (-N_3 : P3HT−≡ : CuBr : PMDETA = 1 : 1 : 10 : 10) were dissolved in 10 ml toluene, and the solution was loaded in an ampule. The mixture was degassed for three freeze-pump-thaw cycles by liquid nitrogen. The click reaction then proceeded at 80 ° C for 1d. After that, the mixture was passed through a neutral alumina column with chloroform as eluent to remove the copper salt. The solution was then concentrated, precipitated in methanol, and finally dried in vacuum oven to yield the product cyclic poly(ethylene glycol)-*g*-poly(3-hexylthiophene) (*c*-PEG-*g*-P3HT).

Characterizations

All ^{1}H NMR spectra were obtained with a Bruker 400MHz spectrometer with solvent resonances as the internal standard. Dimethyl sulfoxide-d6 (DMSO-d6) was used as the solvent for NMR measuement of cyclic polyglycidol (*c*-PEO-OH), and $CDCl_3$ was used as the solvent for other polymer measurements. The molecular weights of polymers were obtained using a Shimadzu GPC equipped with a LC-20AD HPLC pump and a refractive index detector (RID-10A, 120V). Tetrahydrofuran (THF) was used as the mobile phase at 35 °C at 1.0 mL/min. One Phenogel 5u Linear (2) column and one Phenogel 5u 10E4A mixed bed column were calibrated with 10 polystyrene standard samples from 1.2×10^6 to 500 g/mol. FTIR spectra were collected on the Shimadzu IRAffinity1 spectrometer equipped with a Miracle Single Reflection Horizontal ATR Accessory (Pike Technologies). Matrix Assisted Laser Desorption Ionization Time-of-Flight (MALDI-TOF) mas spectra were recorded with an Autoflex III mass spectrometer (Bruker Daltonics), using α-cyano-4-hydroxy cinnamic acid (CHCA) as the matrix. The morphology of cyclic poly(ethylene glycol)-*g*-poly(3-hexylthiophene) (*c*-PEG-*g*-P3HT) was studied by atomic force microscope (AFM; Bruker Dimension Icon; operated in the tapping mode at 0.5Hz scanning rate). The thin film deposits for AFM measurements were prepared by spin-coating the dilute toluene solution (1 mg/ml) of cyclic brush polymer onto silicon substrate at 2000 rpm for 1 min (Headway PWM32 spin coater).

6.3 Results and Discussion

6.3.1. Synthesis of Cyclic Backbone Bearing Azide Functionalities

In anionic ring opening polymerization, hydroxyl groups on monomer should be protected to avoid their exchange reaction with reactive oxanion intermediate to produce hyperbranched structure. Thus, hydroxyl functionalities on glycidol were protected by

ethyl vinyl ether to yield a new monomer 2,3-epoxypropyl-1-ethoxyethyl ether (EEGE) for subsequent polymerization (**Scheme 6.1**).

The successful protection was verified by ^{1}H NMR as shown in **Figure 6.1**: ($CDCl_3$, δ, ppm) 4.76 [m, -O-CH(CH_3)-O-], 3.35-3.90 (m, -O-CH_2CH_3 an-O-CH_2-C_2H_4O), 3.15 (m, methane CH of the epoxy ring), 2.61-2.91 (m, methylene CH_2 of the epoxy ring), 1.33[d,-OCH(CH_3)-O-], 1.19 (t,-O-CH_2-CH_3).

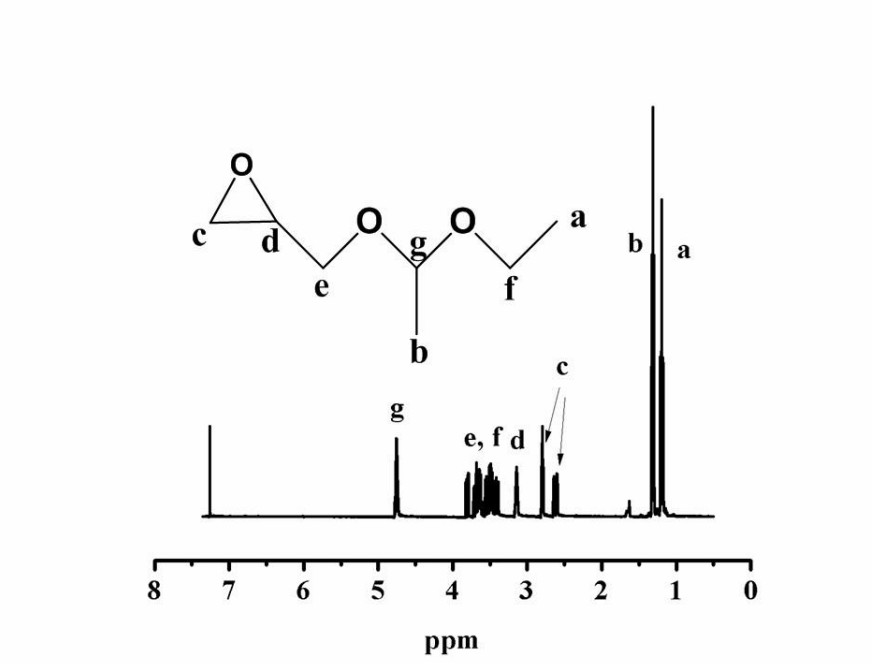

Figure 6.1. NMR of EEGE monomer.

Ring opening polymerization of EEGE was then conducted with triethylene glycol as initiator and DPMNa as the catalyst to prepare linear a,ω-dihydroxyl PEEGE (**Scheme 6.1**). Only 20-40% hydroxyl groups on triethylene glycol were activated by DPMNa to avoid the aggregation of the propagating alkoxides. In addition, a mixed solvent of THF and DMSO (v/v: 1/4) was used as a co-solvent for the polymerization. It is crucial to add DMSO since the alkoxide propagating centers would aggregate and

precipitate in pure THF. All hydroxyl functionalities on triethylene glycol efficiently initiated the polymerization of EEGE under such condition. The concurrent chain growth from each hydroxyl group was achieved due to the rapid dynamic exchange between dormant hydroxyl groups and the propagating alkoxides active species. The product with narrow molecular weight distribution was obtained and summarized in **Table 6.1**. In addition, the molecular weight was controlled by the feeding ratio of monomer to initiator.

Table 6.1. Summary of parameters of linear PEEGE and cyclic PEEGE

	N_{EEGE}	$M_{n,th}$[a]	M_p[b]	$M_{n,GPC}$[b]	PDI[b]
***l*-PEEGE**	34	5000	6676	5700	1.23
***c*-PEEGE**	34	5000	5251	4300	1.16

[a]Calculated from feeding ratio between monomer and initiator $M_{n,th} = \frac{[M]_0}{[I]_0} * 146$.

[b]Obtained from GPC measurement.

Figure 6.2 is a typical ^{1}H NMR spectrum of linear PEEGE. The quadruplets at δ=4.70-4.73 are assigned to the methine protons (H_d) of PEEGE, the doublets at δ=1.30, 1.29 (H_e) and the triplet at δ=1.21, 1.19, 1.18 (H_g) are assigned to methyl protons of PEEGE, the chemical shift at δ=3.53-3.80 are assigned to protons of main chain (H_a, H_b) and protons of lateral chains (H_c, H_f). Moreover, GPC (**Figure 6.3**) indicated that number average molecular weight of linear PEEGE relative to linear PS standards was 5654 g/mol.

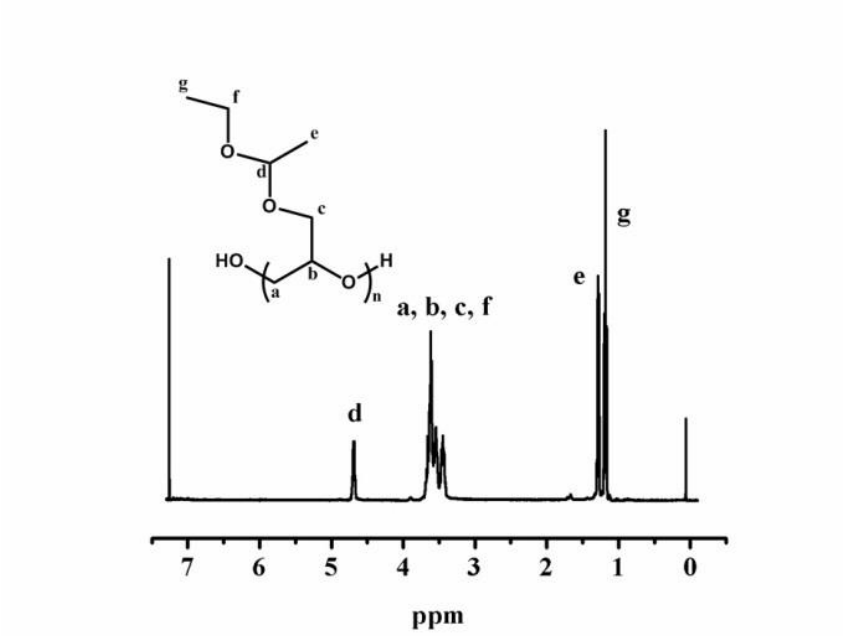

Figure 6.2. NMR of *l*-PEEGE.

Ring closure of a,ω-dihydroxyl PEEGE was achieved via KOH-catalyzed reaction between chain end hydroxyl functionalities with tosyl chloride (TsCl), forming a ether linkage (**Scheme 6.1**). Cyclization was conducted at high dilution [C* < 10^{-5} mol/L] to facilitate the end-to-end intramolecular coupling over intermolecular chain extension. Furthermore, a small fraction of poor solvent n-heptane was added in addition to THF to decrease end-to-end distance of polymer chain, thus promoting intramolecular cyclization.

Crude product obtained after cyclization was a mixture of cyclic polymer and chain-extended product as illustrated in GPC chromatogram (**Figure 6.3**). GPC curve of the linear precursor (**Figure 6.3**) consisting of a single narrow peak. After cyclization, the elution peak of linear PEEGE shifted to longer elution time region. The peak molecular weight changed from 6676 for linear PEEGE (M_{pl}) to 5251 for cyclic PEEGE (M_{pc}) due to the decrease in hydrodynamic volume for cyclic polymer (M_{pc}/M_{pl} = 0.78), indicating

successful cyclization of the linear precursor. Moreover, a shoulder located at higher molecular weight region was assigned to small fraction of chain extended polymer.

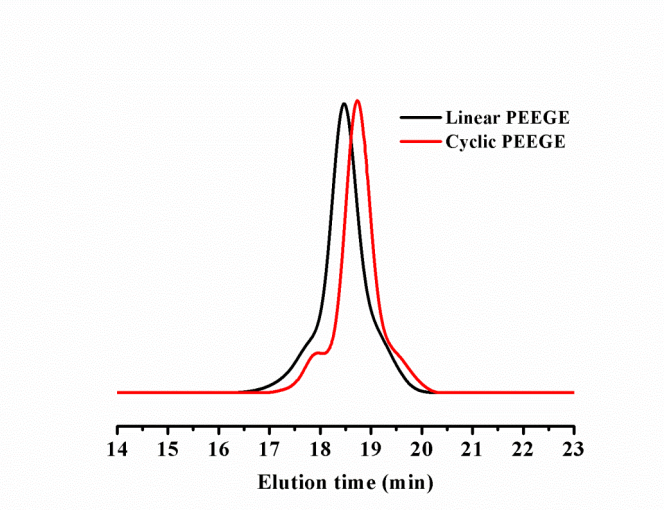

Figure 6.3. GPC traces of *l*-PEEGE and *c*-PEEGE.

To obtain direct evidence for successful cyclization, matrix-assisted laser desorption/ionization time-of-flight (MALDI-TOF) was employed and the spectra of linear PEEGE precursor and cyclized product *c*-PEEGE is shown in **Figure 6.4**. The 146 amu spacing between two major peaks of either *l*-PEEGE or *c*-PEEGE can be ascribed to the molar mass of each EEGE unit. Moreover, molecular weight of the product decreased approximately 18 amu upon cyclization, which is consistent with the loss of one water molecule with the formation of ether linkage.

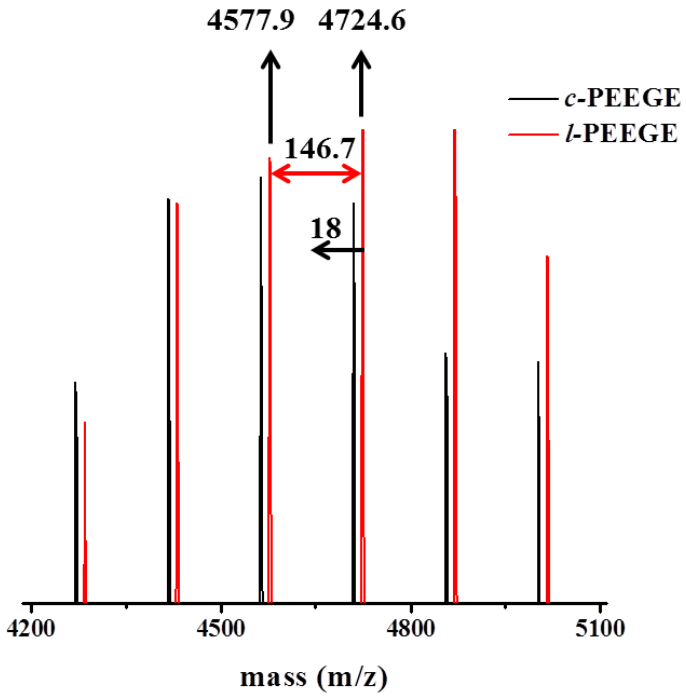

Figure 6.4. MALDI-TOF of *l*-PEEGE and *c*-PEEGE.

Hydrolysis of both *l*-PEEGE and *c*-PEEGE was performed by mixing the polymers with 0.1N HCl in THF. The solution was refluxed for 3h. Hydrolyzed products were characterized by ^{1}H NMR and MALDI-TOF. ^{1}H NMR of hydrolyzed products *l*-polyglycidol (*l*-PEO-OH) and *c*-polyglycidol (*c*-PEO-OH) was shown in **Figure 6.5**. Disappearance of protons from acetal group confirmed successful hydrolysis.

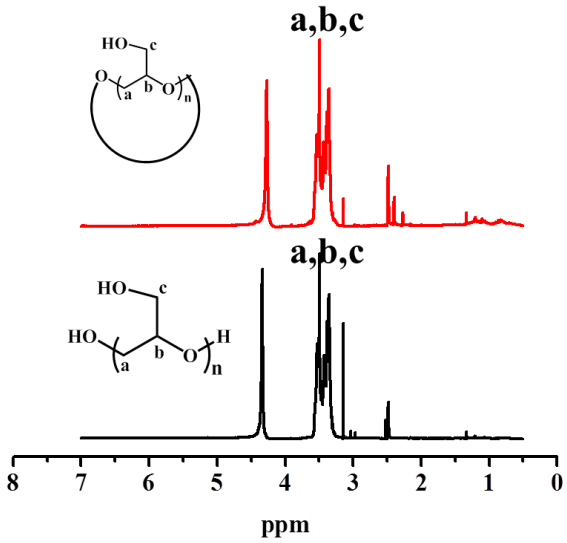

Figure 6.5. ^{1}H NMR of *l*-polyglycidol and *c*-polyglycidol.

In addition, MALDI-TOF of *l*-polyglycidol was shown in **Figure 6.6**. The spacing between two major peaks was 74, corresponding to the molar mass of each repeating unit of glycidol. Thus, MALDI-TOF provided the direct evidence for successful hydrolysis of *l*-PEEGE. However, *c*-polyglycidol was also characterized by MALDI-TOF, but no signal can be obtained. This may be due to the different structure of *c*-polyglycidol compared to *l*-polyglycidol. The product can be utilized as a universal cyclic template to produce a variety of cyclic brush copolymers by grafting onto different functionalities such as RAFT agent.

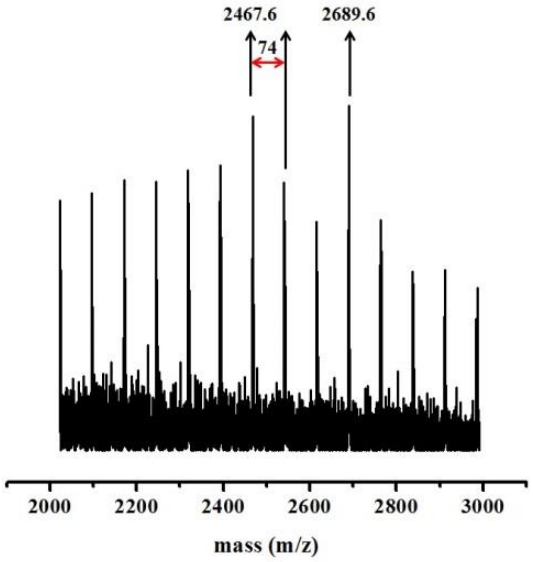

Figure 6.6. MALDI-TOF of *l*-polyglycidol.

2-bromoisobutyryl bromide was subsequently utilized to modify hydroxyl groups on *c*-PEO-OH by esterification, and a cyclic macroinitiator for ATRP was obtained (**Scheme 6.1**). Complete transformation of all the hydroxyl functionalities of *c*-PEO-OH was confirmed by ^{1}H-NMR.

The resulting product can serve as a universal cyclic macroinitiator to synthesize a variety of cyclic block copolymers by ATRP polymerization. However, bromine in this study was used as substrate to introduce azide functionalities for subsequent click reaction with alkyne terminated P3HT (**Scheme 6.1**). Successful and quantitative substitution was confirmed by ^{1}H-NMR and FTIR.

Figure 6.7 (I) displays typical ^{1}H NMR spectra of *c*-PEO-Br after esterification. The new resonance at δ = 1.93 ppm assigned to protons of methyl groups from 2-bromoisobutyryl bromide indicates the successful esterification. The esterification efficiency can be calculated according to the following equation:

$$E_T = \frac{A_d/6}{A_c/2} * 100\%$$

where E_T is the conversion efficiency of hydroxyl groups on *c*-PEO-OH; and A_d and A_c represent the integral area of methyl protons adjacent to bromine (H^d) and integral area of methylene protons linked to the ester group (H^c), respectively. The estimated E_T value is nearly 100%, suggesting that almost all the hydroxyl functionalities were converted to the bromoisobutyryl units. Moreover, as shown in **Figure 6.7 (II)**, complete disappearance of the peak at 1.93 ppm and appearance of a new signal with the same relative intensity at 1.47 ppm that were attributed to methyl protons after substitution by $–N_3$ confirmed the quantitative transformation of bromine atoms to azide groups.

FT-IR measurement was performed to identify the presence of azide functionalities in *c*-PEO-N_3 after substitution. As evidenced in **Figure 6.8**, the strong absorbance peak at 2117 cm^{-1} was attributed to -N_3 group. In addition, GPC trace of *c*-PEO-N_3 indicated that a functional cyclic backbone with low polydispersity (PDI = 1.22) was obtained, and number-average molecular weight of the product was 6132 g/mol (**Figure 6.10**).

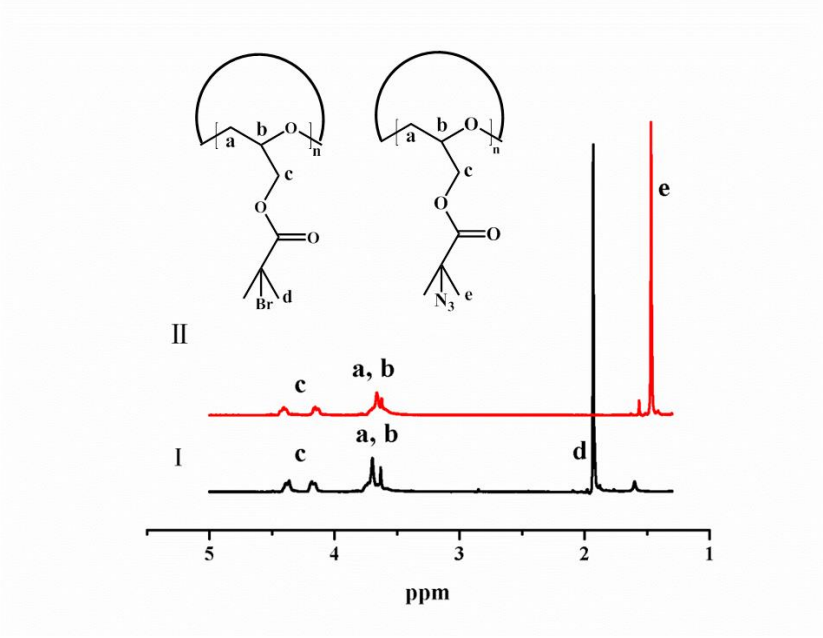

Figure 6.7. NMR of *c*-PEO-Br and *c*-PEO-N_3.

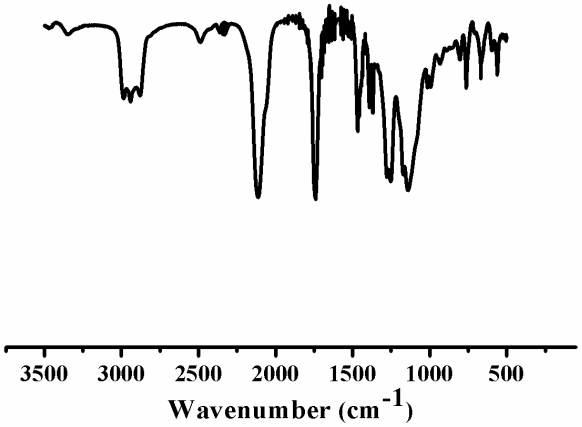

Figure 6.8. FT-IR of *c*-PEO-N_3.

6.3.2. Synthesis of Conjugated Side Chains Capped with Ethynyl Group

Ethynyl group functionalized poly(3-hexylthiophene) (P3HT−≡) was prepared by a quasi-living Grignard metathesis (GRIM) method with ethynylmagnesium bromide as termination agent (**Scheme 6.1**). GRIM method is a living polycondensation technique as described in Chapter 3. Product was analyzed by ^{1}H-NMR and GPC.

Figure 6.9 shows a representative ^{1}H-NMR of ethynyl-terminated P3HT: (CDCl3, δ(ppm)) 6.98 (s, 1H), 3.53 (s,1H), 2.8 (t, J =3 Hz, 2H), 1.7 (m, 2H), 1.44 (m, 2H), 1.36 (m, 4H) and 0.91 (t, 3H). The number average molecular weight and PDI of alkyne-terminated P3HT were 11000 g/mo1 (based on ^{1}H-NMR), 11500g/mol (based on GPC) and 1.15(GPC), respectively.

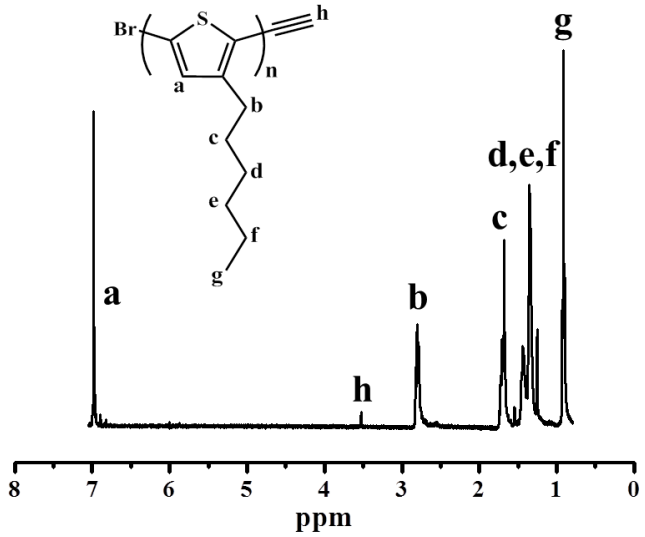

Figure 6.9. NMR of ethynyl-terminated P3HT.

6.3.3. Preparation of Cyclic Brush Copolymer Grafted with Conjugated Side Chains

The ethynyl-terminiated P3HT was subsequently grafted onto the cyclic backbone via click reaction between the terminal alkyne group on P3HT−≡ and azide functional groups on the *c*-PEO-N_3 (**Scheme 6.1**). The reaction was performed in toluene at 80 °C with CuBr/PMDETA as the catalytic system. GPC trace of *c*-PEO-N_3 shifted to the higher molecular weight region after reaction with P3HT−≡, indicating the successful grafting of P3HT−≡ onto the cyclic backbone and formation of cyclic poly(ethylene glycol)-*g*-poly(3-hexylthiophene) (*c*-PEG-*g*-P3HT) brush copolymer (**Figure 6.10**). The number average molecular weight and PDI of *c*-PEG-*g*-P3HT obtained were 220.1 kg/mol and 1.18, respectively, and single peak was observed in GPC measurement.

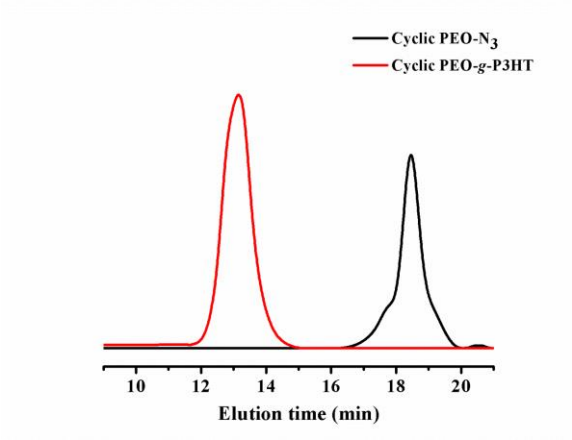

Figure 6.10. GPC traces of *c*-PEO-N_3 and *c*-PEG-*g*-P3HT.

In ^{1}H NMR spectrum (**Figure 6.11**) of *c*-PEG-*g*-P3HT, characteristic peaks of thiophene at δ = 6.98ppm and hexyl group at δ = 0.92 – 2.80 ppm from P3HT are clearly eviddent, while proton resonances from PEG were not observed. This is due possibly to much lower content of PEG backbone compared to P3HT side chains in the *c*-PEG-*g*-P3HT macromolecule. In addition, protons on PEG are buried inside the P3HT side chains, and possibly shielded by the side chains during NMR measurement. However, the characteristic peak of ethynyl end group on P3HT−≡ at δ = 3.53 ppm disappeared in the *c*-PEG-*g*-P3HT brush copolymer, indicating the successful click reaction.

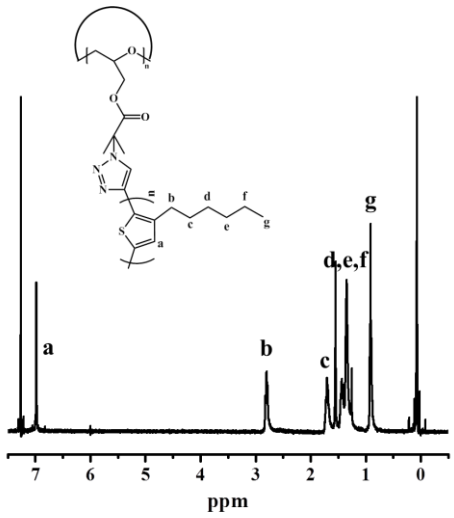

Figure 6.11. NMR of *c*-PEG-*g*-P3HT.

6.3.4 Morphological and Self-Assembly Study at Nanoscale

To explore the property and self-assembly behavior of the new P3HT-based cyclic brush architecture, the morphology of thin film of *c*-PEG-*g*-P3HT deposited on the silicon substrate was examined by atomic force microscopy (AFM). Interestingly, the thin deposit of *c*-PEG-*g*-P3HT revealed a macro-ring-like morphology with the outer diameter of the rings around 169 nm (**Figure 6.12**). Cross-section analysis (**Figure 6.12b**) indicated that the width and the height of ring were approximately 32 nm and 2 nm, respectively. The distinctive macrocyclic morphology possibly originated from the interaction between chemically distinct constituent blocks with a selective solvent in conjunction with the unique macromolecular architecture (i.e., cyclic brush as the building blocks). The self-assembly of *c*-PEG-*g*-P3HT into macrocyclic nanostructure may be rationalized as follows as illustrated in **Figure 6.13**. Toluene is a selective solvent for P3HT block, while a poor solvent for PEG block on *c*-PEG-*g*-P3HT. When the "amphiphilic" cyclic brush copolymer was dissolved in toluene, the PEG cyclic backbone

may preferentially organize and pack into an internal ring which was surrounded by the solvophilic P3HT side chains to minimize the unfavorable interfacial contact between solvophobic PEG blocks and toluene. Thus, a "fragile" macro-ring formed in the solution. During the spin coating of the solution on the substrate, the macro-ring collapsed[70,269] along with the crystallization of P3HT grafts via the interchain π-π stacking, leading to the ultimate formation of a "flattened" macro-ring on the substrate. The width of macro-ring determined by AFM (about 32 nm) is consistent with the hydrodynamic diameter of individual cyclic brush polymer (D_h = 38.5 nm, obtained from DLS in chloroform). It is worth mentioning that the height (about 2 nm) was much smaller than the lateral width of the ring, which was due possibly to the collapse and flattening of the macromolecule on the substrate.[70,269]

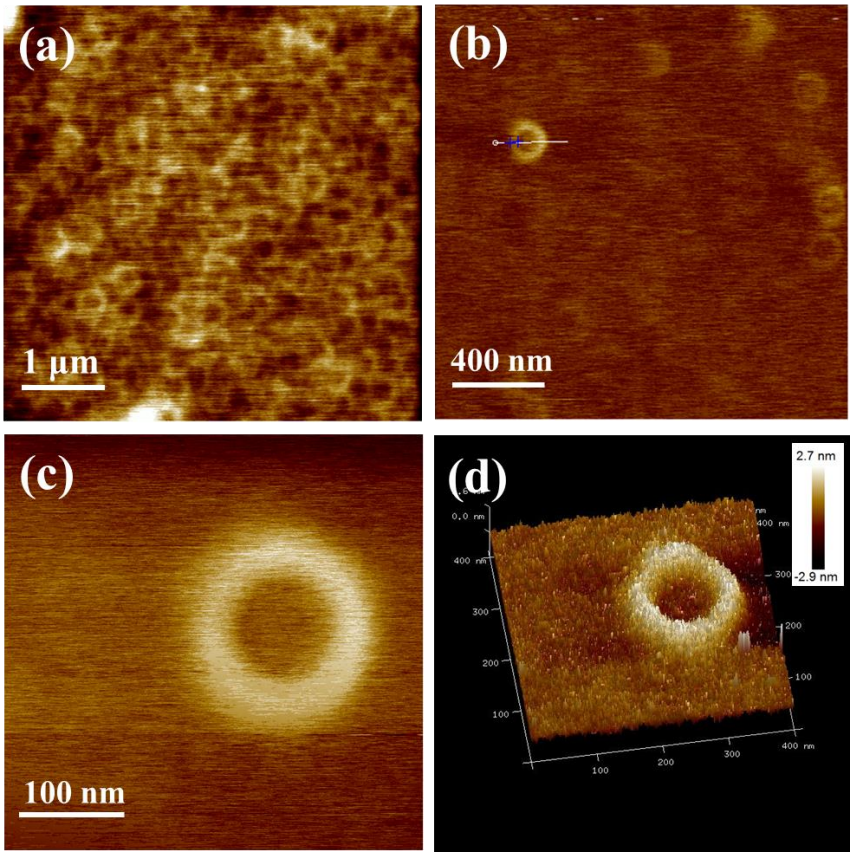

Figure 6.12. AFM images of thin film of *c*-PEG-*g*-P3HT spin-coated from toluene solution on silicon substrate. (a), (b), and (c) Height images showing macro-rings self-assembled from *c*-PEG-*g*-P3HT with different scan areas. (d) Representative 3D height image of macro-ring.

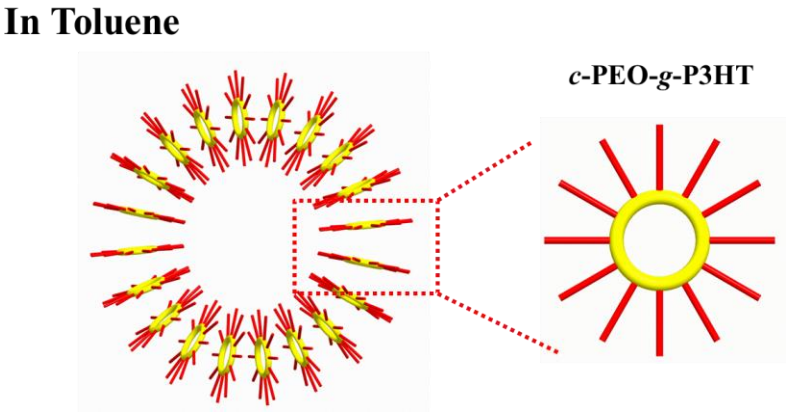

Figure 6.13. Illustration of possible self-assembly mechanism of *c*-PEG-*g*-P3HT in toluene.

6.4 Summary

In summary, a novel cyclic brush copolymer, *c*-PEG-*g*-P3HT, comprising a cyclic PEG backbone and P3HT conjugated side chains, was rationally designed and successfully synthesized via a combination of GRIM, anionic ROP, and click reaction. The functional cyclic backbone was prepared via end-to-end ring closure approach, while the P3HT branches were attached by "grafting onto" strategy. The intermediate cyclic PEG backbone, conjugated side chains, and the final cyclic brush copolymer (*c*-PEG-*g*-P3HT) possessed well-defined molecular topologies and low polydispersities, owing to the benign characteristics of living/controlled polymerizations employed in each synthetic steps. The complex macromolecular architecture together with ingenious combination of chemically distinct constituent blocks which show different affinities to a selective solvent affords the resulting conjugated cyclic brush polymer unique property

and interesting macro-ring morphology. Remarkably, the *c*-PEG-*g*-P3HT self-assembled into a macrocyclic nanostructure in toluene, a selective solvent for P3HT blocks. The synthetic approach in the study presents a general strategy to create a large diversity of conjugated branches-based cyclic brush polymers with different compositions (i.e., varying either the backbone or the brush composition) and various functionalities for fundamental study on the structure-property relationship as well as for potential applications in solar cells, OFETs, LEDs etc.

CHAPTER 7

GENERAL CONCLUSIONS AND BROADER IMPACT

7.1 General Conclusions

Significant progress has been made in the field of living/controlled polymerizations in the past decades, including ATRP, RAFT, NMP, living ROP etc. The living/controlled polymerization technique has enabled the preparation of structurally well-defined polymers with controlled molecular weights, and rendered the design of macromolecules with complex architectures such as star-like polymers, brush-like copolymers, and cyclic polymers. Polymers with complex molecular architectures often exhibit properties that are distinct from their linear counterparts. For example, star-like polymers are a class of branched macromolecules with multiple linear chains stably and covalently connected to a multifunctional core, which display intrinsically spherical shape. In this dissertation, we exploited the unique properties of non-linear polymers that simple linear polymers do not possess to ***practically address the challenges*** related to the preparation of polymeric and hybrid nanostructured materials, and ***explored*** the properties and morphology of new macromolecular architecture (i.e., cyclic brush copolymers grafted with conjugated side chains).

In the first part of this dissertation, we addressed the practical challenges in preparation of polymeric and hybrid nanostructured materials conventionally based on self-assembled linear block copolymer micelle approach by rationally design and utilize polymers with complex star-like architecture. By incorporating crosslinking functionalities into the self-assembled polymer micelles, core-shell polymeric nanoparticles can be synthesized via crosslinking in either core or shell domain of the micelle. Hollow polymer nanoparticles can be further crafted if inner core of a shell cross-linked micelle is made of a degradable polymer. Moreover, if metal elements (e.g.,

Si) are integrated during the crosslinking of micelles, hybrid nanostructured materials can be produced. Clearly, crosslinked micelle system is a versatile method for preparing organic and hybrid nanostructures, and has been widely studied in the literature. However, there are several challenges associated with this traditional polymer micelle approach. First, the size of nanostructures formed from this method is difficult to control due to the relatively poor size-control of self-assembled micelles. Second, the crosslinked frameworks are usually non-uniform as a result of the comparatively high polydispersity of micelles. Finally, chemical compositions or functionalities of components in nanostructures that can be accessed are limited due to the common amphiphilic requirement of copolymer composition in order to impart the self-assembly. In stark contrast, in our study, we developed a novel and robust star-like macromolecular templating strategy in which the self-assembled polymer micelles were replaced with intrinsically spherical star-like polymers containing crosslinking moieties. The star-like polymers spontaneously formed unimolecular micelles in solution with multiple branches covalently and stably connected to a multi-functional core, and subsequent crosslinking led to the formation of stable polymeric or hybrid nanostructures. As a result, self-assembly process as often encountered in linear block copolymer is no longer required and this new approach is much simpler. The key advantage is that polymer composition and functionality can be freely selected without the need for amphiphilic composition as in the polymer micelle system. In addition, the star-like macromolecules which served as unimolecular templates in this approach were rationally designed and prepared by living/controlled polymerization techniques. This allows for good control over their molecular weight and low polydispersity of the polymers. Consequently, uniform nanostructures were produced and their dimensions were well-tailored by tuning the molecular weights of constituent blocks in star-like polymer templates. In particular, two different systems were studied to demonstrate the viability and impacts of this new approach, including 1) polymeric nanostructures, and 2) polymer/silica hybrid

nanostructures. The detailed summaries on the work concerning important technical developments and findings in this study are presented below.

For polymeric nanostructures, a robust strategy for crafting tailorable core-shell and hollow polymer nanoparticles with well-defined architecture was developed. In addition, they were exploited as a new type of nanocarrier via the dye encapsulation and release study. The key to our preparative route was the use of photo-crosslinkable core-shell star-like diblock copolymers as templates. Star-like core-shell diblock copolymers were first synthesized by a combination of ring opening polymerization and reversible addition-fragmentation chain transfer polymerization, followed by introducing photo-crosslinking azide moieties on the shell blocks. Interestingly, upon UV irradiation these unimolecular micelles were subsequently transformed into uniform spherical nanoparticles composed of biodegradable inner core blocks and a stable cross-linked shell. The degree of crosslinking can be tailored by varying UV exposure time. The size of nanoparticles is governed by molecular weights of constituent blocks in the core-shell star-like diblock copolymer template, and the uniformity of nanoparticles was translated from narrow molecular weight distribution of star-like diblock copolymer template. Through the selective removal of the biodegradable inner core, nanoparticles with hollow interiors were produced, which retained the structural integrity and stability of as-prepared core-shell nanoparticles. The encapsulation and release of dyes by capitalizing on unimolecular core-shell nanoparticles were also explored as a means to demonstrate the intriguing and effective nanocarrier functionality. More importantly, drug release may be viably controlled by simply tailoring the crosslinking density of the nanocapsule shell.

For hybrid nanostructures, a versatile preparative route to uniform organo-silica hybrid nanoparticles and nanocapsules was pioneered by us by capitalizing on star-like polymers as nanoreactors. The star-like PTMSPMA homopolymer and PS-*b*-PTPMSPMA diblock copolymer containing trimethoxysilyl functionalities in PTPMSPMA blocks were synthesized by ATRP. The hydrolysis and subsequent

condensation of trimethoxysilyl moieties introduced a crosslinked silsesquioxane network in star-like PTMSPMA homopolymer and in the outer PTMSPMA blocks of star-like PS-*b*-PTMSPMA to yield hybrid nanoparticles and nanocapsules, respectively. The dimensions of hybrid nanoparticles and nanocapsules are dictated by the chain lengths (i.e., molecular weights) of star-like PTMSPMA and PS-*b*-PTMSPMA nanoreactors, respectively, which can be precisely engineered by living polymerizations (i.e., ATRP of TMSPMA for star-like PTMSPMA, and sequential ATRP of styrene and TMSPMA for star-like PS-*b*-PTMSPMA).

In the second part of this dissertation, we investigated and understood the morphology and property of a new cyclic brush copolymergrafted with P3HT as conjugated side chains, which is rationally designed and prepared in this study. As macromolecular architectures profoundly affect the properties of the polymeric products, macromolecules with complex structures including star shape, graft polymer, molecular bottlebrush, and cyclic polymer have been widely prepared over the past decades, and their properties were systematically studied in order to understand the fundamental structure-property relationship and to facilitate their applications. Regioregular poly(3-hexylthiophene) (*rr*-P3HT) has attracted considerable attention as one of the most important conjugated polymers owing to its ease of preparation, good solution processability, and excellent hole mobility. Other than linear or block copolymers, P3HT-based copolymers with complex architectures such as macrocyclic structure or molecular bottlebrush were recently prepared as well and studied in the context of their morphologies and properties. However, P3HT-based copolymers with cyclic brush architecture have not yet been reported.

To this end, in our study, we rationally designed the synthetic route to a novel cyclic brush copolymer, *c*-PEG-*g*-P3HT, composed of cyclic PEG as the backbone and P3HT as the side chains via a combination of living/controlled polymerizations with click chemistry. The morphology of this new P3HT-based macromolecular architecture was

then carefully examined. The functional cyclic backbone was prepared via end-to-end ring closure approach, while the P3HT branches were attached by the "grafting onto" strategy. The intermediate cyclic PEG backbone, conjugated side chains, and the final cyclic brush copolymer (*c*-PEG-*g*-P3HT) possessed well-defined molecular topologies and low polydispersity, owing to the benign characteristics of living/controlled polymerizations employed in each synthetic step. The significant finding from this study is that *c*-PEG-*g*-P3HT self-assembled into an intriguing macrocyclic nanostructure in toluene, which is a selective solvent for P3HT blocks. Such remarkable self-assembly behavior and the resulting macro-ring morphology can be understood as a result of the complex macromolecular architecture together with the distinct chemical compositions of the cyclic backbone and the P3HT side chains.

7.2 Outlook

The findings presented in this dissertation may provide fundamental insights or practical strategies for rational design of polymers with complex macromolecular architectures via living/controlled polymerizations.

The core-shell or hollow polymeric nanoparticles have a wide range of potential applications, including hydraulic fluids, recording materials, solvation, drug/gene delivery, biomedical applications, catalysis, coatings, phase transfer reactions, chromatography, fillers for plastics, nanoreactors, and host for removing hydrophobic contaminants from aqueous solutions. While the silica/polymer hybrid nanoparticles/nanocapsules can be used for a board spectrum of applications such as polymer matrix nanocomposites,[187,188] biomedical engineering,[189-191] fluorescent thermometers,[192] controlled release, and model colloids for evaluating the steric

stabilization theory.[193,194] Crosslinking the self-assembled polymeric nanostructures via different mechanism provide a versatile approach for preparing the polymeric and hybrid nanostructured materials, which has been the subject of many studies. However, certain disadvantages of nanomaterials prepared through this approach, including size non-uniformity and limited access to the constituent compositions, may restrict their properties and performance for the practical applications. In this dissertation, through rational design of spherical star-like polymers with different architectures (i.e., homopolymer and block copolymer) and various compositions, we developed a robust and versatile unimolecular strategy for creating various dimensionally and functionally well-defined nanostructured materials. We envision that a large set of uniform polymeric and polymer/silica hybrid nanoparticles, including core-shell and hollow structures, with a diversity of compositions and functionalities can be crafted based on this viable templating strategy, dispensing with the need for amphiphilicity as in self-assembled micelles. For example, reversibly crosslinked unimolecular nanoparticles with well-defined structural characteristics can be created if cleavable functionalities are integrated into the crosslinked framework. Responsive unimolecular nanoparticles can be developed if responsive polymer is employed as constituent block to construct the nanoparticles. In addition, other polymer composition can be employed as the inner core of the organo-silica nanocapsule such as PAA. After the coordination of PAA with metal ions, an inorganic core can form inside the nanocapsule, yielding an inorganic core-shell nanoparticle. Another important advantage of the new approach is that dimensions of different components in the nanostructures can be tailored by tuning the corresponding constituent blocks in the star-like polymer templates. As a result, the properties of the polymeric and hybrid nanostructures prepared through this new approach can be improved and their accessible scope of compositions can be expanded, which will ultimately facilitate and benefit their wide range of applications.

Future directions in this area that we have pioneered can be divided into two categories: 1) fundamental study; and 2) practical applications of the newly developed unimolecular nanomaterials. As a next step, the polymer chemists or materials scientists need to address the fundamental questions regarding the feasibility and the versatility of this new approach, such as the size limitation of nanostructures that it can create, the morphology of other materials compositions, the efficiency of other initiation systems and polymerization techniques, the development of other possible structures (e.g. core-shell-corona, nanorods, and nanotubes), and the integration of responsive functionalities into materials. On the other hand, from the practical viewpoint, scientists across a broad discipline of fields such as biotechnology can specifically engineer the unimolecular nanostructures (e.g., dimension, composition and structure) according to their need for the targeted applications via macromolecular engineering of the star-like polymer templates.

Especially, the unimolecular polymeric nanoparticles developed in this study can be further engineered to create a promising drug delivery device, which may pronouncedly impact the field of drug/gene delivery and controlled release. Shell cross-linked polymer micelles have received much attention as drug vehicles for prolonging the *in vivo* drug circulation and controlling the release times. However, it can be problematic to create uniform self-assembled micelles with predictable dimension, composition, and morphology. It is worth noting that a well-controlled size is particularly important for tumor-targeted drug delivery as the effective size of nanocarriers falls in the range of 20-100 nm.[228,229] In this context, the development of crosslinked polymer nanoparticles with well-defined structures and precise size controllability is needed. In this study, we have demosntrated a proof-of-principle that core-shell nanoparticles can act as effective nanocarriers by the dye loading and release study. The new nanocarriers offer several important and advantageous features, including precise size control via tailoring molecular weights of constituent blocks in star-like diblock copolymers, uniformity, and

good stability. Looking ahead, the shell domain can be facilely replaced with biocompatible cross-linkable polymers to develop new prospective drug vehicles. Moreover, the surface of nanoparticles can be engineered with PEG ligand to impart stealth characteristics. As such, the development of this new class of polymer nanoparticles with good uniformity and stability, adjustable size, and surface chemistry may present a platform with which the size and stability issues widely encountered in current drug nanocarriers can be addressed.

Furthermore, the macromolecular templating strategy is general and robust, and may provide enormous opportunities for the development of materials with new structures and functionalities. In addition to spherical star-like diblock copolymers, this approach can, in principle, be further expanded to utilize other structurally regular complex polymer compositions and architectures (e.g., bottlebrush-like block copolymer) to create a diversity of truly tailored nanostructures (e.g., 1-dimensional polymer nanorods and nanotubes). Moreover, particularly for the polymer/silica hybrid nanostructures, silica nanoparticles and nanocapsules can be obtained after pyrolysis and further reduced to silicon nanoparticles and nanocapsules for potential applications as anode materials in lithium ion batteries and as controlled-release vehicles in biomedical applications.

On the other hand, we designed a robust synthetic route to P3HT-based cyclic brush architecture. The synthetic approach in the study afford a unique platform for creating a series of cyclic brush polymers grafted with conjugated branches with different compositions (i.e., varied backbone and brush compositions) and various functionalities for fundamental study to explore their structure-property relationship and their potential applications in diverse fields, such as solar cells, OFETs, and semiconductors. In addition, it was discovered that this new class of cyclic brush copolymer comprising a solvophobic backbone and conjugated side chains exhibited a very interesting self-assembly behavior and macro-ring morphology. These findings may inspire polymer

chemists and materials scientists to design and explore other conjugated polymer-based macromolecular architectures and compositions, which may display other intriguing morphologies and properties.

DISSEMINATION OF WORK

The work presented in this dissertation has been conveyed to the scientific community by the following publications and presentations.

Publications

1. **Feng, C.**, Pang, X., He, Y., Li, B. & Lin, Z. Robust Route to Unimolecular Core−Shell and Hollow Polymer Nanoparticles. Chem. Mater., 26, 6058 (**2014**) (Highlighted by American Chemical Society (ACS) as **Noteworthy Chemistry**; Reported by VerticalNews).

2. **Feng, C.**, Pang, X., He, Y., Wan, C. & Lin, Z. A Versatile Strategy for Uniform Hybrid Nanoparticles and Nanocapsules (under review).

3. Pang, X., **Feng, C.**, Xu, H., Han, W., Xin, X., Xia, H., Qiu, F. & Lin, Z. Unimolecular micelles composed of inner coil-like blocks and outer rod-like blocks crafted by combination of living polymerization with click chemistry. Polym. Chem., 5, 2747 (**2014**).

4. Pang, X., Zhao, L., **Feng, C.** & Lin, Z. Novel Amphiphilic Multiarm, Starlike Coil-Rod Diblock Copolymers via a Combination of Click Chemistry with Living Polymerization. Macromolecules, 44, 3746–3752 (**2011**).

5. Pang, X., Zhao, L., **Feng, C.**, Wu, R., Ma, H. & Lin, Z. Functional copolymer brushes composed of a hydrophobic backbone and densely grafted conjugated side chains via a

combination of living polymerization with click chemistry. Polym. Chem., 4, 2025 (**2013**).

6. **Feng, C.**, Pang, X. & Lin, Z. Amphiphilic Cyclic Copolymer Brush Grafted with Conjugated Side Chains via a Combination of Living Polymerization with Click Chemistry (in preparation).

7. Jung, J., Pang, X., **Feng, C.** & Lin, Z. Semiconducting Conjugated Polymer-Inorganic Tetrapods Nanocomposites. Langmuir, 29, 8086 (**2013**).

8. Zhao, L., **Feng, C.**, Pang, X., Jung, J., Stefan, M. C., Sista, P., Han, R., Fang, N. & Lin, Z. Self-Assembly of Hydrophobic Conjugated Triblock Copolymer with High Photoluminescence via Dewetting at the Air/Water Interface. Soft Matter, 33, 8050 (**2013**).

9. Ma, H., Pang, X., Jung, J., Zhao. L., **Feng, C.**, Han, W., Xin, X. & Lin, Z. Synthesis and Characterization of Semiconducting Conjugated Polymer-Nanowire Nanocomposites. Sci. Adv. Mater., 7, 727 (**2013**).

Conference presentations

1. **Feng, C.**, Pang, X., Lin, Z. Novel unimolecular polymeric nanocapsules from photocrosslinkable core-shell star-like block copolymer template as nanocarriers. 247th ACS National Meeting & Exposition, Dallas, TX, March **2014**.

2. **Feng, C.**, Pang, X., Lin, Z. Functional amphiphilic cyclic brush copolymers grafted with conjugated side chains via a combination of living polymerization with click chemistry. 247th ACS National Meeting & Exposition, Dallas, TX, March **2014** (Poster).

3. Pang, X., Zhao, L., **Feng, C.**, Lin, Z. Novel Amphiphilic Multi-arm, Star-like Coil-rod Diblock Copolymers via a Combination of Click Chemistry with Living Polymerization and Their Use as Nanoreactor for Crafting CdSe Nanoparticle-capped Poly(3-hexylthiophene). 2012 MRS Spring Meeting & Exhibit, San Francisco, CA, April **2012**.

4. Lin, Z., Pang, X., Zhao, L., **Feng, C.** Responsive nanoparticle brushes crafted from functional star-like diblock copolymers. 243rd ACS National Meeting & Exposition, San Diego, CA, March **2012**.

5. Zhao, L., Pang, X., **Feng, C.**, Lin, Z. Patterning of Conjugated Polymer with Enhanced Photoluminescence via Self-assembly at the Air/Water Interface. 2012 MRS Spring Meeting & Exhibit, San Francisco, CA, April **2012**.

6. Jung, J., **Feng, C.**, Pang, X., Lin, Z. Semiconducting organic-inorganic nanocomposites crafted based on cadmium-conjugated complexes. 247th ACS National Meeting & Exposition, Dallas, TX, March **2014**.

7. Lin, Z., Pang, X., Zhao, L., **Feng, C.** Amphiphilic multi-arm, star-like coil-coil and coil-rod core-shell diblock copolymer: From synthesis, self-assembly to functional nanoparticles. 242nd ACS National Meeting & Exposition, Denver, Colorado, USA, August - September **2011**.

8. Zhao, L., Pang, X., **Feng, C.**, Lin, Z. Self-assembly of PtBA-P3HT multi-arms star-like block copolymer at the air/water interface. APS March Meeting, Dallas, Texas, USA, March **2011**.

9. Lin, Z., Pang, X., **Feng, C.** Multi-arm, star-like core-shell polymer-vitamin C biomaterials as drug carriers. 244th ACS National Meeting and Exposition, Philadelphia, Pennsylvania, USA, August 19-23, **2012**.

10. Lin, Z., Zhao, L. Pang, X. and **Feng, C**. Self-Assembly of Novel Amphiphilic 21-Arm, Star-Like Coil-Rod Diblock Copolymers at Interfaces. APS March Meeting, Boston, Massachusetts, USA, March **2012**.

REFERENCES

(1) Szwarc, M. *Nature* **1956**, *178*, 1168.

(2) Kim, J.; Kim, S. S.; Kim, K. H.; Jin, Y. H.; Hong, S. M.; Hwang, S. S.; Cho, B.-G.; Shin, D. Y.; Im, S. S. *Polymer* **2004**, *45*, 3527.

(3) Ji, H.; Sato, N.; Nonidez, W. K.; Mays, J. W. *Polymer* **2002**, *43*, 7119.

(4) Quirk, R. P.; Lizárraga, G. M. *Macromolecules* **1998**, *31*, 3424.

(5) Welch, F. J. *J Am Chem Soc* **1959**, *81*, 1345.

(6) Li, Z.; Chau, Y. *Polym Chem* **2011**, *2*, 873.

(7) Wang, J.-S.; Matyjaszewski, K. *J Am Chem Soc* **1995**, *117*, 5614.

(8) Braunecker, W. A.; Matyjaszewski, K. *Prog. Polym. Sci.* **2007**, *32*, 93.

(9) Yuan, W.; Yuan, J.; Zhang, F.; Xie, X.; Pan, C. *Macromolecules* **2007**, *40*, 9094.

(10) Storey, R. F.; Sherman, J. W. *Macromolecules* **2002**, *35*, 1504.

(11) Chagneux, N.; Trimaille, T.; Rollet, M.; Beaudoin, E.; Gérard, P.; Bertin, D.; Gigmes, D. *Macromolecules* **2009**, *42*, 9435.

(12) Zhou, J.; Wang, L.; Ma, J.; Wang, J.; Yu, H.; Xiao, A. *Eur. Polym. J.* **2010**, *46*, 1288.

(13) Yokozawa, T.; Yokoyama, A. *Prog. Polym. Sci.* **2007**, *32*, 147.

(14) Bielawski, C. W.; Grubbs, R. H. *Prog. Polym. Sci.* **2007**, *32*, 1.

(15) Wang, J.-S.; Matyjaszewski, K. *Macromolecules* **1995**, *28*, 7901.

(16) Matyjaszewski, K. *Macromolecules* **1998**, *31*, 4710.

(17) Isse, A. A.; Gennaro, A.; Lin, C. Y.; Hodgson, J. L.; Coote, M. L.; Guliashvili, T. *J Am Chem Soc* **2011**, *133*, 6254.

(18) Gao, H.; Matyjaszewski, K. *J Am Chem Soc* **2007**, *129*, 6633.

(19) Cheng, G.; Böker, A.; Zhang, M.; Krausch, G.; Müller, A. H. E. *Macromolecules* **2001**, *34*, 6883.

(20) Pang, X.; Zhao, L.; Akinc, M.; Kim, J. K.; Lin, Z. *Macromolecules* **2011**, *44*, 3746.

(21) Du, J.; Chen, Y. *Macromolecules* **2004**, *37*, 3588.

(22) Gao, H.; Matyjaszewski, K. *Macromolecules* **2006**, *39*, 4960.

(23) Jakubowski, W.; Matyjaszewski, K. *Angew. Chem. Int. Ed.* **2006**, *118*, 4594.

(24) Matyjaszewski, K.; Dong, H.; Jakubowski, W.; Pietrasik, J.; Kusumo, A. *Langmuir* **2007**, *23*, 4528.

(25) Jakubowski, W.; Min, K.; Matyjaszewski, K. *Macromolecules* **2005**, *39*, 39.

(26) Tsarevsky, N. V.; Matyjaszewski, K. *Chem. Rev.* **2007**, *107*, 2270.

(27) Treat, N. J.; Sprafke, H.; Kramer, J. W.; Clark, P. G.; Barton, B. E.; Read de Alaniz, J.; Fors, B. P.; Hawker, C. J. *J Am Chem Soc* **2014**, *136*, 16096.

(28) Miyake, G. M.; Theriot, J. C. *Macromolecules* **2014**, *47*, 8255.

(29) Ogawa, K. A.; Goetz, A. E.; Boydston, A. J. *J Am Chem Soc* **2015**.

(30) Moad, G.; Rizzardo, E.; Thang, S. H. *Aust J Chem* **2006**, *59*, 669.

(31) Moad, G.; Rizzardo, E.; Thang, S. H. *Aust J Chem* **2009**, *62*, 1402.

(32) Lowe, A. B.; McCormick, C. L. *Prog. Polym. Sci.* **2007**, *32*, 283.

(33) Nakabayashi, K.; Oya, H.; Mori, H. *Macromolecules* **2012**, *45*, 3197.

(34) Semsarilar, M.; Perrier, S. *Nat Chem* **2010**, *2*, 811.

(35) Goto, A.; Sato, K.; Tsujii, Y.; Fukuda, T.; Moad, G.; Rizzardo, E.; Thang, S. H. *Macromolecules* **2001**, *34*, 402.

(36) Chiefari, J.; Chong, Y. K.; Ercole, F.; Krstina, J.; Jeffery, J.; Le, T. P. T.; Mayadunne, R. T. A.; Meijs, G. F.; Moad, C. L.; Moad, G.; Rizzardo, E.; Thang, S. H. *Macromolecules* **1998**, *31*, 5559.

(37) Mayadunne, R. T. A.; Rizzardo, E.; Chiefari, J.; Chong, Y. K.; Moad, G.; Thang, S. H. *Macromolecules* **1999**, *32*, 6977.

(38) Hawker, C. J.; Bosman, A. W.; Harth, E. *Chem. Rev.* **2001**, *101*, 3661.

(39) Moad, G.; Rizzardo, E.; Thang, S. H. *Acc. Chem. Res.* **2008**, *41*, 1133.

(40) Gao, H.; Matyjaszewski, K. *Prog. Polym. Sci.* **2009**, *34*, 317.

(41) Gregory, A.; Stenzel, M. H. *Prog Polym Sci* **2012**, *37*, 38.

(42) Hadjichristidis, N.; Iatrou, H.; Pitsikalis, M.; Mays, J. *Prog. Polym. Sci.* **2006**, *31*, 1068.

(43) Gao, H.; Matyjaszewski, K. *Macromolecules* **2008**, *41*, 1118.

(44) Gao, H.; Min, K.; Matyjaszewski, K. *Macromol. Chem. Phys.* **2007**, *208*, 1370.

(45) Fournier, D.; Hoogenboom, R.; Schubert, U. S. *Chem. Soc. Rev.* **2007**, *36*, 1369.

(46) Altintas, O.; Vogt, A. P.; Barner-Kowollik, C.; Tunca, U. *Polym Chem* **2012**, *3*, 34.

(47) Gao, H.; Matyjaszewski, K. *Macromolecules* **2006**, *39*, 3154.

(48) Pang, X.; Zhao, L.; Feng, C.; Lin, Z. *Macromolecules* **2011**, *44*, 7176.

(49) París, R.; de la Fuente, J. L. *React Funct Polym* **2008**, *68*, 1004.

(50) Sheiko, S. S.; Sumerlin, B. S.; Matyjaszewski, K. *Prog. Polym. Sci.* **2008**, *33*, 759.

(51) Zhang, M.; Müller, A. H. E. *J Polym Sci Part A: Polym Chem* **2005**, *43*, 3461.

(52) Pang, X.; Zhao, L.; Feng, C.; Wu, R.; Ma, H.; Lin, Z. *Polym Chem* **2013**, *4*, 2025.

(53) Rzayev, J. *Macromolecules* **2009**, *42*, 2135.

(54) Jha, S.; Dutta, S.; Bowden, N. B. *Macromolecules* **2004**, *37*, 4365.

(55) Börner, H. G.; Beers, K.; Matyjaszewski, K.; Sheiko, S. S.; Möller, M. *Macromolecules* **2001**, *34*, 4375.

(56) Beers, K. L.; Gaynor, S. G.; Matyjaszewski, K.; Sheiko, S. S.; Moller, M. *Macromolecules* **1998**, *31*, 9413.

(57) Neugebauer, D.; Zhang, Y.; Pakula, T.; Sheiko, S. S.; Matyjaszewski, K. *Macromolecules* **2003**, *36*, 6746.

(58) Zhang, M.; Breiner, T.; Mori, H.; Müller, A. H. E. *Polymer* **2003**, *44*, 1449.

(59) Xia, Y.; Kornfield, J. A.; Grubbs, R. H. *Macromolecules* **2009**, *42*, 3761.

(60) Adachi, K.; Honda, S.; Hayashi, S.; Tezuka, Y. *Macromolecules* **2008**, *41*, 7898.

(61) Zhang, K.; Lackey, M. A.; Wu, Y.; Tew, G. N. *J Am Chem Soc* **2011**, *133*, 6906.

(62) Schappacher, M.; Deffieux, A. *Science* **2008**, *319*, 1512.

(63) Van Krevelen, D. W.; Te Nijenhuis, K. *Properties of polymers: their correlation with chemical structure; their numerical estimation and prediction from additive group contributions*; Elsevier, 2009.

(64) Mathieu, L. M.; Mueller, T. L.; Bourban, P.-E.; Pioletti, D. P.; Müller, R.; Månson, J.-A. E. *Biomaterials* **2006**, *27*, 905.

(65) Hadjichristidis, N.; Pitsikalis, M.; Iatrou, H.; Pispas, S. *M Macromol. Rapid Commun.* **2003**, *24*, 979.

(66) Anderson, D. G.; Akinc, A.; Hossain, N.; Langer, R. *Molecular Therapy* **2005**, *11*, 426.

(67) Yuan, J.; Drechsler, M.; Xu, Y.; Zhang, M.; Müller, A. H. E. *Polymer* **2008**, *49*, 1547.

(68) Müllner, M.; Yuan, J.; Weiss, S.; Walther, A.; Förtsch, M.; Drechsler, M.; Müller, A. H. E. *J Am Chem Soc* **2010**, *132*, 16587.

(69) Yuan, J.; Xu, Y.; Walther, A.; Bolisetty, S.; Schumacher, M.; Schmalz, H.; Ballauff, M.; Muller, A. H. E. *Nat Mater* **2008**, *7*, 718.

(70) Huang, K.; Rzayev, J. *J Am Chem Soc* **2009**, *131*, 6880.

(71) Huang, K.; Canterbury, D. P.; Rzayev, J. *Macromolecules* **2010**, *43*, 6632.

(72) Huang, K.; Canterbury, D. P.; Rzayev, J. *Chem Commun* **2010**, *46*, 6326.

(73) Bates, F. S.; Fredrickson, G. H. *Annu. Rev. Phys. Chem.* **1990**, *41*, 525.

(74) Park, M.; Harrison, C.; Chaikin, P. M.; Register, R. A.; Adamson, D. H. *Science* **1997**, *276*, 1401.

(75) Wang, X.-S.; Jackson, R.; Armes, S. *Macromolecules* **2000**, *33*, 255.

(76) Li, W.; Yoon, J. A.; Matyjaszewski, K. *J Am Chem Soc* **2010**, *132*, 7823.

(77) Rowan, S. J. *Nat Mater* **2009**, *8*, 89.

(78) Alexandridis, P.; Lindman, B. *Amphiphilic block copolymers: self-assembly and applications*; Elsevier, 2000.

(79) Rösler, A.; Vandermeulen, G. W.; Klok, H.-A. *Adv. Drug Deliv. Rev.* **2012**, *64*, 270.

(80) Ikkala, O.; ten Brinke, G. *Science* **2002**, *295*, 2407.

(81) Yan, Q.; Zhao, Y. *Angew. Chem. Int. Ed.* **2013**, *125*, 10132.

(82) Yan, Q.; Zhao, Y. *J Am Chem Soc* **2013**, *135*, 16300.

(83) Wang, X.; Guerin, G.; Wang, H.; Wang, Y.; Manners, I.; Winnik, M. A. *Science* **2007**, *317*, 644.

(84) Massey, J. A.; Winnik, M. A.; Manners, I.; Chan, V. Z.; Ostermann, J. M.; Enchelmaier, R.; Spatz, J. P.; Möller, M. *J Am Chem Soc* **2001**, *123*, 3147.

(85) Williams, D.; Fredrickson, G. *Macromolecules* **1992**, *25*, 3561.

(86) Zhong, S.; Cui, H.; Chen, Z.; Wooley, K. L.; Pochan, D. J. *Soft Matter* **2007**, *4*, 90.

(87) Li, Z.; Zhang, Y.; Fullhart, P.; Mirkin, C. A. *Nano Lett.* **2004**, *4*, 1055.

(88) Cornelissen, J. J.; Fischer, M.; Sommerdijk, N. A.; Nolte, R. J. *Science* **1998**, *280*, 1427.

(89) Liu, X.; Kim, J.-S.; Wu, J.; Eisenberg, A. *Macromolecules* **2005**, *38*, 6749.

(90) Riegel, I. C.; Eisenberg, A.; Petzhold, C. L.; Samios, D. *Langmuir* **2002**, *18*, 3358.

(91) Noguchi, H.; Takasu, M. *Phys Rev E* **2001**, *64*, 041913.

(92) Smith, A. E.; Xu, X.; McCormick, C. L. *Prog. Polym. Sci.* **2010**, *35*, 45.

(93) Kakizawa, Y.; Harada, A.; Kataoka, K. *J Am Chem Soc* **1999**, *121*, 11247.

(94) Chung, J.; Yokoyama, M.; Aoyagi, T.; Sakurai, Y.; Okano, T. *J Control Release* **1998**, *53*, 119.

(95) Selvan, T.; Spatz, J. P.; Klok, H.-A.; Möller, M. *Adv Mater* **1998**, *10*, 132.

(96) Chung, J.; Yokoyama, M.; Suzuki, K.; Aoyagi, T.; Sakurai, Y.; Okano, T. *Colloids Surf., B* **1997**, *9*, 37.

(97) Gohy, J. F.; Willet, N.; Varshney, S.; Zhang, J. X.; Jérôme, R. *Angew. Chem. Int. Ed.* **2001**, *113*, 3314.

(98) Gou, M.; Zheng, X.; Men, K.; Zhang, J.; Wang, B.; Lv, L.; Wang, X.; Zhao, Y.; Luo, F.; Chen, L. *Pharm Res* **2009**, *26*, 2164.

(99) Cuong, N.-V.; Li, Y.-L.; Hsieh, M.-F. *J Mater Chem* **2012**, *22*, 1006.

(100) Jette, K. K.; Law, D.; Schmitt, E. A.; Kwon, G. S. *Pharm Res* **2004**, *21*, 1184.

(101) Knop, K.; Hoogenboom, R.; Fischer, D.; Schubert, U. S. *Angew. Chem. Int. Ed.* **2010**, *49*, 6288.

(102) Masayuki, Y.; Mizue, M.; Noriko, Y.; Teruo, O.; Yasuhisa, S.; Kazunori, K.; Shohei, I. *J Control Release* **1990**, *11*, 269.

(103) Kataoka, K.; Matsumoto, T.; Yokoyama, M.; Okano, T.; Sakurai, Y.; Fukushima, S.; Okamoto, K.; Kwon, G. S. *J Control Release* **2000**, *64*, 143.

(104) Shuai, X.; Ai, H.; Nasongkla, N.; Kim, S.; Gao, J. *J Control Release* **2004**, *98*, 415.

(105) Schumers, J. M.; Fustin, C. A.; Gohy, J. F. *Macromol. Rapid Commun.* **2010**, *31*, 1588.

(106) Hu, J.; Liu, S. *Macromolecules* **2010**, *43*, 8315.

(107) McCormick, C. L.; Kirkland, S. E.; York, A. W. *J Macromol Sci Polymer Rev* **2006**, *46*, 421.

(108) Zhang, Q.; Ko, N. R.; Oh, J. K. *Chem Comm* **2012**, *48*, 7542.

(109) Dong, J.; Wang, Y.; Zhang, J.; Zhan, X.; Zhu, S.; Yang, H.; Wang, G. *Soft Matter* **2013**, *9*, 370.

(110) Dan, M.; Huo, F.; Xiao, X.; Su, Y.; Zhang, W. *Macromolecules* **2014**, *47*, 1360.

(111) Nakayama, M.; Okano, T.; Miyazaki, T.; Kohori, F.; Sakai, K.; Yokoyama, M. *J Control Release* **2006**, *115*, 46.

(112) Lee, E. S.; Oh, K. T.; Kim, D.; Youn, Y. S.; Bae, Y. H. *J Control Release* **2007**, *123*, 19.

(113) Ko, J.; Park, K.; Kim, Y.-S.; Kim, M. S.; Han, J. K.; Kim, K.; Park, R.-W.; Kim, I.-S.; Song, H. K.; Lee, D. S. *J Control Release* **2007**, *123*, 109.

(114) Convertine, A.; Diab, C.; Prieve, M.; Paschal, A.; Hoffman, A.; Johnson, P.; Stayton, P. *Biomacromolecules* **2010**, *11*, 2904.

(115) Wang, G.; Tong, X.; Zhao, Y. *Macromolecules* **2004**, *37*, 8911.

(116) Zhao, Y. *Macromolecules* **2012**, *45*, 3647.

(117) Jochum, F. D.; Theato, P. *Chem Commun* **2010**, *46*, 6717.

(118) Guo, M.; Yan, Y.; Zhang, H.; Yan, H.; Cao, Y.; Liu, K.; Wan, S.; Huang, J.; Yue, W. *J Mater Chem* **2008**, *18*, 5104.

(119) Aw, M. S.; Addai-Mensah, J.; Losic, D. *J Mater Chem* **2012**, *22*, 6561.

(120) Kim, H.; Jeong, S.-M.; Park, J.-W. *J Am Chem Soc* **2011**, *133*, 5206.

(121) Lee, H.-N.; Bai, Z.; Newell, N.; Lodge, T. P. *Macromolecules* **2010**, *43*, 9522.

(122) Mitsukami, Y.; Hashidzume, A.; Yusa, S.-i.; Morishima, Y.; Lowe, A. B.; McCormick, C. L. *Polymer* **2006**, *47*, 4333.

(123) Wang, D.; Wu, T.; Wan, X.; Wang, X.; Liu, S. *Langmuir* **2007**, *23*, 11866.

(124) Ma, N.; Li, Y.; Xu, H.; Wang, Z.; Zhang, X. *J Am Chem Soc* **2009**, *132*, 442.

(125) Convertine, A. J.; Lokitz, B. S.; Vasileva, Y.; Myrick, L. J.; Scales, C. W.; Lowe, A. B.; McCormick, C. L. *Macromolecules* **2006**, *39*, 1724.

(126) Moughton, A. O.; Hillmyer, M. A.; Lodge, T. P. *Macromolecules* **2011**, *45*, 2.

(127) Li, Z.; Kesselman, E.; Talmon, Y.; Hillmyer, M. A.; Lodge, T. P. *Science* **2004**, *306*, 98.

(128) Kubowicz, S.; Baussard, J. F.; Lutz, J. F.; Thünemann, A. F.; von Berlepsch, H.; Laschewsky, A. Angew. Chem. Int. Ed. **2005**, *44*, 5262.

(129) Lutz, J. F.; Laschewsky, A. *Macromol. Chem. Phys.* **2005**, *206*, 813.

(130) Pang, X.; Zhao, L.; Han, W.; Xin, X.; Lin, Z. *Nat Nanotech* **2013**, *8*, 426.

(131) Bednáî, B.; Edwards, K.; Almgren, M.; Tormod, S.; Tuzar, Z. *Makromol Chem Rapid Comm* **1988**, *9*, 785.

(132) Nishiyama, N.; Kataoka, K. *Pharmacol. Ther.* **2006**, *112*, 630.

(133) Liu, Y.; Wang, W.; Yang, J.; Zhou, C.; Sun, J. *Asian J. Pharmacol.* **2013**, *8*, 159.

(134) Yu, B.; Okano, T.; Kataoka, K.; Sardari, S.; Kwon, G. *J Control Release* **1998**, *56*, 285.

(135) Liu, M.; Kono, K.; Fréchet, J. M. *J Control Release* **2000**, *65*, 121.

(136) Jiang, J.; Qi, B.; Lepage, M.; Zhao, Y. *Macromolecules* **2007**, *40*, 790.

(137) Thurmond, K. B.; Kowalewski, T.; Wooley, K. L. *J Am Chem Soc* **1996**, *118*, 7239.

(138) Wooley, K. L. *J of Polym Sci Part A: Polym Chem* **2000**, *38*, 1397.

(139) Bronich, T. K.; Keifer, P. A.; Shlyakhtenko, L. S.; Kabanov, A. V. *J Am Chem Soc* **2005**, *127*, 8236.

(140) O'Reilly, R. K.; Hawker, C. J.; Wooley, K. L. *Chem Soc Rev* **2006**, *35*, 1068.

(141) Liu, S.; Weaver, J. V.; Tang, Y.; Billingham, N. C.; Armes, S. P.; Tribe, K. *Macromolecules* **2002**, *35*, 6121.

(142) Fujii, S.; Cai, Y.; Weaver, J. V.; Armes, S. P. *J Am Chem Soc* **2005**, *127*, 7304.

(143) Liu, S.; Weaver, J. V.; Save, M.; Armes, S. P. *Langmuir* **2002**, *18*, 8350.

(144) Li, Y.; Lokitz, B. S.; McCormick, C. L. *Macromolecules* **2006**, *39*, 81.

(145) Matsumoto, S.; Christie, R. J.; Nishiyama, N.; Miyata, K.; Ishii, A.; Oba, M.; Koyama, H.; Yamasaki, Y.; Kataoka, K. *Biomacromolecules* **2008**, *10*, 119.

(146) Jiang, X.; Luo, S.; Armes, S. P.; Shi, W.; Liu, S. *Macromolecules* **2006**, *39*, 5987.

(147) Lokitz, B. S.; Convertine, A. J.; Ezell, R. G.; Heidenreich, A.; Li, Y.; McCormick, C. L. *Macromolecules* **2006**, *39*, 8594.

(148) Zhang, L.; Bernard, J.; Davis, T. P.; Barner-Kowollik, C.; Stenzel, M. H. *Macromol. Rapid Commun.* **2008**, *29*, 123.

(149) Rijcken, C. J.; Snel, C. J.; Schiffelers, R. M.; van Nostrum, C. F.; Hennink, W. E. *Biomaterials* **2007**, *28*, 5581.

(150) Talelli, M.; Iman, M.; Varkouhi, A. K.; Rijcken, C. J.; Schiffelers, R. M.; Etrych, T.; Ulbrich, K.; van Nostrum, C. F.; Lammers, T.; Storm, G. *Biomaterials* **2010**, *31*, 7797.

(151) Jiang, X.; Zhang, J.; Zhou, Y.; Xu, J.; Liu, S. *J Polym Sci Part A: Polym Chem* **2008**, *46*, 860.

(152) Shuai, X.; Merdan, T.; Schaper, A. K.; Xi, F.; Kissel, T. *Bioconjugate chem* **2004**, *15*, 441.

(153) Wooley, K.; Remsen, E. *Chem Commun* **1998**, 1415.

(154) Yang, T.-F.; Chen, C.-N.; Chen, M.-C.; Lai, C.-H.; Liang, H.-F.; Sung, H.-W. *Biomaterials* **2007**, *28*, 725.

(155) Xiong, J.; Meng, F.; Wang, C.; Cheng, R.; Liu, Z.; Zhong, Z. *J Mater Chem* **2011**, *21*, 5786.

(156) Yusa, S.-i.; Sugahara, M.; Endo, T.; Morishima, Y. *Langmuir* **2009**, *25*, 5258.

(157) Zhao, Y.; Bertrand, J.; Tong, X.; Zhao, Y. *Langmuir* **2009**, *25*, 13151.

(158) Gohy, J.-F.; Zhao, Y. *Chem Soc Rev* **2013**, *42*, 7117.

(159) He, J.; Zhao, Y. *Dyes Pigm.* **2011**, *89*, 278.

(160) Li, Y.; Lokitz, B. S.; McCormick, C. L. *Macromolecules* **2006**, *39*, 81.

(161) van Nostrum, C. F. *Soft Matter* **2011**, *7*, 3246.

(162) Kaur, G.; Chang, S. L.; Bell, T. D.; Hearn, M. T.; Saito, K. *J Polym Sci Part A: Polym Chem* **2011**, *49*, 4121.

(163) Jin, Q.; Liu, X.; Liu, G.; Ji, J. *Polymer* **2010**, *51*, 1311.

(164) Choi, W. I.; Tae, G.; Kim, Y. H. *J Mater Chem* **2008**, *18*, 2769.

(165) Hales, M.; Barner-Kowollik, C.; Davis, T. P.; Stenzel, M. H. *Langmuir* **2004**, *20*, 10809.

(166) Bang, J.; Bae, J.; Löwenhielm, P.; Spiessberger, C.; Given-Beck, S. A.; Russell, T. P.; Hawker, C. J. *Adv Mater* **2007**, *19*, 4552.

(167) Yoo, M.; Kim, S.; Lim, J.; Kramer, E. J.; Hawker, C. J.; Kim, B. J.; Bang, J. *Macromolecules* **2010**, *43*, 3570.

(168) Li, Y.; Lokitz, B. S.; Armes, S. P.; McCormick, C. L. *Macromolecules* **2006**, *39*, 2726.

(169) Zhang, J.; Jiang, X.; Zhang, Y.; Li, Y.; Liu, S. *Macromolecules* **2007**, *40*, 9125.

(170) Xu, X.; Flores, J. D.; McCormick, C. L. *Macromolecules* **2011**, *44*, 1327.

(171) Li, Y.; Xiao, W.; Xiao, K.; Berti, L.; Luo, J.; Tseng, H. P.; Fung, G.; Lam, K. S. *Angew. Chem. Int. Ed.* **2012**, *124*, 2918.

(172) Gonzalez-Leon, J. A.; Ryu, S.-W.; Hewlett, S. A.; Ibrahim, S. H.; Mayes, A. M. *Macromolecules* **2005**, *38*, 8036.

(173) Ali, A. I.; Mayes, A. G. *Macromolecules* **2009**, *43*, 837.

(174) Chambon, S.; Schatz, C.; Sébire, V.; Pavageau, B.; Wantz, G.; Hirsch, L. *Mater. Horiz.* **2014**, *1*, 431.

(175) Lu, Y.; Wittemann, A.; Ballauff, M.; Drechsler, M. *Macromol. Rapid Commun.* **2006**, *27*, 1137.

(176) Perkin, K. K.; Turner, J. L.; Wooley, K. L.; Mann, S. *Nano lett.* **2005**, *5*, 1457.

(177) Huang, H.; Remsen, E. E.; Kowalewski, T.; Wooley, K. L. *J Am Chem Soc* **1999**, *121*, 3805.

(178) Sanji, T.; Nakatsuka, Y.; Ohnishi, S.; Sakurai, H. *Macromolecules* **2000**, *33*, 8524.

(179) Xie, M.; Zhang, L.; Liao, Y.; Ding, L.; Zeng, C.; You, Z. *J Polym Sci Part A: Polym Chem* **2011**, *49*, 4955.

(180) Sugihara, S.; Armes, S. P.; Lewis, A. L. *Angew. Chem. Int. Ed.* **2010**, *122*, 3578.

(181) Bridot, J.-L.; Faure, A.-C.; Laurent, S.; Rivière, C.; Billotey, C.; Hiba, B.; Janier, M.; Josserand, V.; Coll, J.-L.; Vander Elst, L.; Muller, R.; Roux, S.; Perriat, P.; Tillement, O. *J Am Chem Soc* **2007**, *129*, 5076.

(182) Hasegawa, U.; Nomura, S.-i. M.; Kaul, S. C.; Hirano, T.; Akiyoshi, K. *Biochem. Biophys. Res. Commun.* **2005**, *331*, 917.

(183) Wu, S.; Zhao, H.; Ju, H.; Shi, C.; Zhao, J. *Electrochem. Commun.* **2006**, *8*, 1197.

(184) Hifumi, H.; Yamaoka, S.; Tanimoto, A.; Citterio, D.; Suzuki, K. *J Am Chem Soc* **2006**, *128*, 15090.

(185) Park, J.-H.; von Maltzahn, G.; Ruoslahti, E.; Bhatia, S. N.; Sailor, M. J. *Angew. Chem. Int. Ed.* **2008**, *120*, 7394.

(186) Watson, K. J.; Zhu, J.; Nguyen, S. T.; Mirkin, C. A. *J Am Chem Soc* **1999**, *121*, 462.

(187) Hajji, P.; David, L.; Gerard, J.; Pascault, J.; Vigier, G. *J Polym Sci Part B: Polym Phys* **1999**, *37*, 3172.

(188) Sugimoto, H.; Daimatsu, K.; Nakanishi, E.; Ogasawara, Y.; Yasumura, T.; Inomata, K. *Polymer* **2006**, *47*, 3754.

(189) Rosenholm, J. M.; Peuhu, E.; Eriksson, J. E.; Sahlgren, C.; Lindén, M. *Nano lett.* **2009**, *9*, 3308.

(190) Kim, T.-W.; Slowing, I. I.; Chung, P.-W.; Lin, V. S.-Y. *ACS nano* **2010**, *5*, 360.

(191) Rosenholm, J. M.; Meinander, A.; Peuhu, E.; Niemi, R.; Eriksson, J. E.; Sahlgren, C.; Lindén, M. *ACS nano* **2008**, *3*, 197.

(192) Wu, T.; Zou, G.; Hu, J.; Liu, S. *Chem Mater* **2009**, *21*, 3788.

(193) Perruchot, C.; Khan, M.; Kamitsi, A.; Armes, S. v.; Von Werne, T.; Patten, T. *Langmuir* **2001**, *17*, 4479.

(194) Zhulina, E. B.; Borisov, O. V.; Priamitsyn, V. A. *J. Colloid Interface Sci.* **1990**, *137*, 495.

(195) Xu, H.; Yan, F.; Monson, E. E.; Kopelman, R. J Biomed Mater Res A **2003**, *66*, 870.

(196) Ow, H.; Larson, D. R.; Srivastava, M.; Baird, B. A.; Webb, W. W.; Wiesner, U. *Nano lett.* **2005**, *5*, 113.

(197) Wu, T.; Zhang, Y.; Wang, X.; Liu, S. *Chem Mater* **2007**, *20*, 101.

(198) von Werne, T.; Patten, T. E. *J Am Chem Soc* **2001**, *123*, 7497.

(199) Von Werne, T.; Patten, T. E. *J Am Chem Soc* **1999**, *121*, 7409.

(200) Mori, H.; Seng, D. C.; Zhang, M.; Müller, A. H. *Langmuir* **2002**, *18*, 3682.

(201) Pyun, J.; Jia, S.; Kowalewski, T.; Patterson, G. D.; Matyjaszewski, K. *Macromolecules* **2003**, *36*, 5094.

(202) Li, C.; Benicewicz, B. C. *Macromolecules* **2005**, *38*, 5929.

(203) Tissandier, C.; Diop, N.; Martini, M.; Roux, S.; Tillement, O.; Hamaide, T. *Langmuir* **2011**, *28*, 209.

(204) Du, J.; Chen, Y. *Macromolecules* **2004**, *37*, 6322.

(205) Du, J.; Chen, Y. *Macromol. Rapid Commun.* **2005**, *26*, 491.

(206) Wu, C.; Wang, X.; Zhao, L.; Gao, Y.; Ma, R.; An, Y.; Shi, L. *Langmuir* **2010**, *26*, 18503.

(207) Zhang, Y.; Luo, S.; Liu, S. *Macromolecules* **2005**, *38*, 9813.

(208) Koh, K.; Ohno, K.; Tsujii, Y.; Fukuda, T. *Angew. Chem. Int. Ed.* **2003**, *115*, 4326.

(209) Du, J.; Chen, Y. *Macromolecules* **2004**, *37*, 5710.

(210) Wei, H.; Cheng, C.; Cheng, C.; Chang, C.; Chen, W.-Q.; Cheng, S.-X.; Zhang, X.-Z.; Zhuo, R.-X. *Langmuir* **2008**, *24*, 4564.

(211) Du, J.; Chen, Y.; Zhang, Y.; Han, C. C.; Fischer, K.; Schmidt, M. *J Am Chem Soc* **2003**, *125*, 14710.

(212) Shi, J.; Votruba, A. R.; Farokhzad, O. C.; Langer, R. *Nano lett.* **2010**, *10*, 3223.

(213) Karnik, R.; Gu, F.; Basto, P.; Cannizzaro, C.; Dean, L.; Kyei-Manu, W.; Langer, R.; Farokhzad, O. C. *Nano lett.* **2008**, *8*, 2906.

(214) Duncan, R. *Nat. Rev. Cancer.* **2006**, *6*, 688.

(215) Torchilin, V. P. *J Control Release* **2001**, *73*, 137.

(216) Yokoyama, M.; Miyauchi, M.; Yamada, N.; Okano, T.; Sakurai, Y.; Kataoka, K.; Inoue, S. *Cancer Res* **1990**, *50*, 1693.

(217) Meng, F.; Zhong, Z.; Feijen, J. *Biomacromolecules* **2009**, *10*, 197.

(218) Upadhyay, K. K.; Bhatt, A. N.; Mishra, A. K.; Dwarakanath, B. S.; Jain, S.; Schatz, C.; Le Meins, J.-F.; Farooque, A.; Chandraiah, G.; Jain, A. K. *Biomaterials* **2010**, *31*, 2882.

(219) Lee, J. S.; Feijen, J. *J Control Release* **2012**, *161*, 473.

(220) Cheng, Y.; Wang, J.; Rao, T.; He, X.; Xu, T. *Front Biosci* **2007**, *13*, 1447.

(221) Gillies, E. R.; Frechet, J. M. *Drug discov today* **2005**, *10*, 35.

(222) Cao, W.; Zhou, J.; Mann, A.; Wang, Y.; Zhu, L. *Biomacromolecules* **2011**, *12*, 2697.

(223) Prabaharan, M.; Grailer, J. J.; Pilla, S.; Steeber, D. A.; Gong, S. *Biomaterials* **2009**, *30*, 5757.

(224) Gu, F.; Zhang, L.; Teply, B. A.; Mann, N.; Wang, A.; Radovic-Moreno, A. F.; Langer, R.; Farokhzad, O. C. *Proc Natl Acad Sci* **2008**, *105*, 2586.

(225) Prabaharan, M.; Grailer, J. J.; Pilla, S.; Steeber, D. A.; Gong, S. *Biomaterials* **2009**, *30*, 3009.

(226) Yang, X.; Grailer, J. J.; Pilla, S.; Steeber, D. A.; Gong, S. *Bioconjugate Chem* **2010**, *21*, 496.

(227) Chen, S.; Zhang, X.-Z.; Cheng, S.-X.; Zhuo, R.-X.; Gu, Z.-W. *Biomacromolecules* **2008**, *9*, 2578.

(228) Perrault, S. D.; Walkey, C.; Jennings, T.; Fischer, H. C.; Chan, W. C. *Nano Lett* **2009**, *9*, 1909.

(229) Jiang, W.; Kim, B. Y.; Rutka, J. T.; Chan, W. C. *Nat Nanotech* **2008**, *3*, 145.

(230) Thurmond, K. B.; Kowalewski, T.; Wooley, K. L. *J Am Chem Soc* **1996**, *118*, 7239.

(231) He, J.; Tong, X.; Tremblay, L.; Zhao, Y. *Macromolecules* **2009**, *42*, 7267.

(232) Hadjichristidis, N.; Pitsikalis, M.; Pispas, S.; Iatrou, H. *Chem. Rev.* **2001**, *101*, 3747.

(233) Rodriguez, M.; Figueruelo, J. E. *Macromol. Chem. Phys.* **1975**, *176*, 3107.

(234) Taton, D.; Saule, M.; Logan, J.; Duran, R.; Hou, S.; Chaikof, E. L.; Gnanou, Y. *J Polym Sci Part A: Polym Chem* **2003**, *41*, 1669.

(235) Feng, X.-S.; Taton, D.; Chaikof, E. L.; Gnanou, Y. *J Am Chem Soc* **2005**, *127*, 10956.

(236) Fischer, H. *Chem. Rev.* **2001**, *101*, 3581.

(237) Matyjaszewski, K. *Macromolecules* **2012**, *45*, 4015.

(238) Matyjaszewski, K.; Xia, J. H. *Chem. Rev.* **2001**, *101*, 2921.

(239) Moad, G.; Rizzardo, E.; Thang, S. H. *Polymer* **2008**, *49*, 1079.

(240) Vana, P.; Quinn, J. F.; Davis, T. P.; Barner-Kowollik, C. *Aust. J. Chem.* **2002**, *55*, 425.

(241) Chiefari, J.; Mayadunne, R. T. A.; Moad, C. L.; Moad, G.; Rizzardo, E.; Postma, A.; Thang, S. H. *Macromolecules* **2003**, *36*, 2273.

(242) Chong, Y. K.; Krstina, J.; Le, T. P. T.; Moad, G.; Postma, A.; Rizzardo, E.; Thang, S. H. *Macromolecules* **2003**, *36*, 2256.

(243) Yokozawa, T.; Yokoyama, A. *Chem. Rev.* **2009**, *109*, 5595.

(244) Iovu, M. C.; Sheina, E. E.; Gil, R. R.; McCullough, R. D. *Macromolecules* **2005**, *38*, 8649.

(245) Stefan, M. C.; Javier, A. E.; Osaka, I.; McCullough, R. D. *Macromolecules* **2009**, *42*, 30.

(246) Nakayama, M.; Okano, T. *Macromolecules* **2008**, *41*, 504.

(247) Shimizu, T.; Masuda, M.; Minamikawa, H. *Chem Rev* **2005**, *105*, 1401.

(248) Vriezema, D. M.; Comellas Aragonès, M.; Elemans, J. A.; Cornelissen, J. J.; Rowan, A. E.; Nolte, R. J. *Chem Rev* **2005**, *105*, 1445.

(249) Hayward, R. C.; Pochan, D. J. *Macromolecules* **2010**, *43*, 3577.

(250) Zhu, C.; Li, S.; Luo, M.; Zhou, X.; Niu, Y.; Lin, M.; Zhu, J.; Cao, Z.; Lu, X.; Wen, T.; Xie, Z.; Schleyer, P. v. R.; Xia, H. *Nat Chem* **2013**, *5*, 698.

(251) Gou, P.-F.; Zhu, W.-P.; Shen, Z.-Q. *Biomacromolecules* **2010**, *11*, 934.

(252) Gou, P.-F.; Zhu, W.-P.; Xu, N.; Shen, Z.-Q. *J Polym Sci Part A: Polym Chem* **2008**, *46*, 6455.

(253) Shanmugananda Murthy, K.; Ma, Q.; Clark Jr, C. G.; Remsen, E. E.; Wooley, K. L. *Chem Commun* **2001**, 773.

(254) Lemcoff, N. G.; Spurlin, T. A.; Gewirth, A. A.; Zimmerman, S. C.; Beil, J. B.; Elmer, S. L.; Vandeveer, H. G. *J Am Chem Soc* **2004**, *126*, 11420.

(255) Ding, Z. Y.; Aklonis, J. J.; Salovey, R. *J Polym Sci Part B: Polym Phys* **1991**, *29*, 1035.

(256) Allen, M. J.; Hud, N. V.; Balooch, M.; Tench, R. J.; Siekhaus, W. J.; Balhorn, R. *Ultramicroscopy* **1992**, *42*, 1095.

(257) Villarrubia, J. *J Res Natl Inst Stand Technol* **1997**, *102*, 425.

(258) Tsukruk, V. V.; Singamaneni, S. *Scanning probe microscopy of soft matter*; Wiley. com, 2012.

(259) Farokhzad, O. C.; Cheng, J.; Teply, B. A.; Sherifi, I.; Jon, S.; Kantoff, P. W.; Richie, J. P.; Langer, R. *Proc Natl Acad Sci* **2006**, *103*, 6315.

(260) Zhang, K.; Zha, Y.; Peng, B.; Chen, Y.; Tew, G. N. *J Am Chem Soc* **2013**, *135*, 15994.

(261) Vogt, T. C. B.; Bechinger, B. *J Biol Chem* **1999**, *274*, 29115.

(262) Zhang, Y.; Zhuo, R.-x. *Biomaterials* **2005**, *26*, 6736.

(263) Gaucher, G.; Dufresne, M.-H.; Sant, V. P.; Kang, N.; Maysinger, D.; Leroux, J.-C. *J Control Release* **2005**, *109*, 169.

(264) Kim, S. Y.; Lee, Y. M. *Biomaterials* **2001**, *22*, 1697.

(265) Feng, C.; Pang, X.; He, Y.; Li, B.; Lin, Z. *Chem. Mater.* **2014**, *26*, 6058.

(266) Gao, H.; Matyjaszewski, K. *Macromolecules* **2006**, *39*, 7216.

(267) Pang, X.; Feng, C.; Xu, H.; Han, W.; Xin, X.; Xia, H.; Qiu, F.; Lin, Z. *Polym Chem* **2014**, *5*, 2747.

(268) Matyjaszewski, K.; Tsarevsky, N. V. *J Am Chem Soc* **2014**.

(269) Yuan, J.; Xu, Y.; Walther, A.; Bolisetty, S.; Schumacher, M.; Schmalz, H.; Ballauff, M.; Müller, A. H. *Nat Mater* **2008**, *7*, 718.

(270) Müllner, M.; Yuan, J.; Weiss, S.; Walther, A.; Förtsch, M.; Drechsler, M.; Müller, A. H. *J Am Chem Soc* **2010**, *132*, 16587.

(271) Yijin, X.; Caiyuan, P. *Macromolecules* **2000**, *33*, 4750.

(272) Stenzel-Rosenbaum, M.; Davis, T. P.; Chen, V.; Fane, A. G. *J Polym Sci Part A: Polym Chem* **2001**, *39*, 2777.

(273) Pang, X.; Jing, R.; Huang, J. *Polymer* **2008**, *49*, 893.

(274) Zhao, L.; Pang, X.; Adhikary, R.; Petrich, J. W.; Lin, Z. *Angew. Chem. Int. Ed.* **2011**, *123*, 4044.

VITA

CHAOWEI FENG

Chaowei Feng was born in Jiujiang, Jiangxi, China on May 31, 1989 to Shaomao Feng and Qi Jiang. He attended the No.2 Middle School in Duchang County, Jiujiang, and graduated with a high school diploma. He received a B.S. in Materials Science and Engineering with specialization in Polymer Materials from East China University of Science and Technology (ECUST), Shanghai, China in 2010. He pursued a Ph.D. in Materials Science and Engineering at Georgia Institute of Technology with Prof. Zhiqun Lin. When he is not working on his research, Mr. Feng enjoys food, travel, movie, book, music and enjoying with friends.